T.C.
DOKUZ EYLUL UNIVERSITY
IZMIR INTERNATIONAL BIOMEDICINE AND GENOME INSTITUTE

GENERATION OF 3D MICROFLUIDIC SYSTEM FOR POLARIZATION OF IMMUNE CELLS

OLCAY BURÇİN AKBULUD

MOLECULAR BIOLOGY AND GENETICS

MASTER OF SCIENCES THESIS

İZMİR-2019

THESIS ID: DEU.IBG.MSc.2016850011

T.C.
DOKUZ EYLUL UNIVERSITY
IZMIR INTERNATIONAL BIOMEDICINE AND GENOME INSTITUTE

GENERATION OF 3D MICROFLUIDIC SYSTEM FOR POLARIZATION OF IMMUNE CELLS

MOLECULAR BIOLOGY AND GENETICS

MASTER OF SCIENCES THESIS

OLCAY BURÇİN AKBULUD

Supervisor: Assoc. Prof. Dr. Sinan GÜVEN

THESIS ID: DEU.IBG.MSc.2016850011

Dokuz Eylül Üniversitesi İzmir Uluslararası Biyotıp ve Genom Enstitüsü Genom Bilimleri ve Moleküler Biyoteknoloji Anabilim Dalı,
Moleküler Biyoloji ve Genetik Yüksek Lisans programı öğrencisi Olcay Burçin AKBULUD **'GENERATION OF 3D MICROFLUIDIC SYSTEM FOR POLARIZATION OF IMMUNE CELLS'** konulu Yüksek Lisans tezini 28/05/2019 tarihinde başarılı olarak tamamlamıştır.

Doç. Dr. Sinan GÜVEN
BAŞKAN

ÜYE
Doç. Dr. Duygu SAĞ WINGENDER
Dokuz Eylül Üniversitesi

ÜYE
Dr. Öğr. Üyesi H. Cumhur TEKİN
İzmir Yüksek Teknoloji Enstitüsü

YEDEK ÜYE
Dr. Öğr. Üyesi Yavuz OKTAY
Dokuz Eylül Üniversitesi

YEDEK ÜYE
Dr. Öğr. Üyesi Ozan KARAMAN
İzmir Kâtip Çelebi Üniversitesi

Dokuz Eylul University Izmir International Biomedicine and Genome Institute
Department of Genomics and Molecular Biotechnology,
Molecular Biology and Genetics graduate program Master of Science student Olcay Burçin AKBULUD has successfully completed her Master of Science thesis titled **'GENERATION OF 3D MICROFLUIDIC SYSTEM FOR POLARIZATION OF IMMUNE CELLS'** on the date of 28/05/2019.

Assoc. Prof. Sinan GÜVEN
CHAIR

MEMBER
Assoc. Prof. Duygu SAĞ WINGENDER
Dokuz Eylül University

MEMBER
Assist. Prof. H. Cumhur TEKİN
Izmir Institute of Technology

SUBSTITUTE MEMBER
Assist. Prof. Yavuz OKTAY
Dokuz Eylül University

SUBSTITUTE MEMBER
Asst. Prof. Ozan KARAMAN
Izmir Kâtip Çelebi Universit

TABLE OF CONTENTS

INDEX OF TABLES

INDEX OF FIGURES

LIST OF ABBREVIATIONS

2D	2-Dimension
3D	3-Dimension
CNS	Central Nervous System
DMSO	Dimethyl sulfoxide
ECM	Extracellular Matrix
FBR	Foreign Body Response
FBS	Fetal Bovine Serum
FTIR	Fourier transform infrared spectroscopy
GelMA	Gelatin Methacrylate
ICC	Immunocytochemistry
IFN-γ	Interferon-gamma
IL-4	Interleukin-4
IL-13	Interleukin-13
LPS	Lipopolysaccharide
MAA	Methacrylic Anhydride
PBS	Phosphate Buffered Saline
PDMS	Polydimethylsiloxane
PEG	Polyethylene glycol
PEGDA	Poly(ethylene glycol) diacrylate
PFA	Paraformaldehyde
PI	Photo-initiator
PMA	Phorbol 12-myristate 13-acetate
PMMA	Poly(methyl methacrylate)
Re	Reynold Number
RPMI 1640	Roswell Park Memorial Institute 1640 medium
SEM	Scanning Electron Microscopy
UV	Ultraviolet

ACKNOWLEDGMENT

First of all, I am grateful to my thesis advisor, Assoc. Prof. Sinan GÜVEN, for his continued guidance, endless support, patience, his great mentorship as well as shaping my scientific thinking. I will always feel exceedingly lucky to start my academic career in his lab.

I also would like to thank Assoc. Prof. Duygu SAĞ WINGENDER for her guidance, suggestions, valuable discussion and helpful comments made on my thesis.

I would like to thank Ali Kemal BAŞ, İbrahim ERBAY, Emine KAHRAMAN and Melis ASAL who are current members of Güven Lab. I am particularly grateful my dear friends Kübra Nur KAPLAN and Deniz KURŞUN who always supported me morally and scientifically for their contribution to my research. Also, I would like to thank all my friends in Izmir Biomedicine and Genome Center and Izmir International Biomedicine and Genome Institute to make the last three years unforgettable.

I would like to thank Erol GROSHA for his unconditional love, patience, motivation and always supporting me to follow my dreams. He always encourages me and always being there for me despite the long distance between us.

Last but not least, I would like to express my deepest love and dedicate this thesis to my father Ali İhsan AKBULUD, my mother Gülbin AKBULUD, and my sister Yüsra Gülçin AKBULUD for always supporting me to follow my dreams, their unconditional love and patience.

GENERATION OF 3D MICROFLUIDIC SYSTEM FOR POLARIZATION OF IMMUNE CELLS

Olcay Burçin AKBULUD, Izmir International Biomedicine and Genome Institute, Dokuz Eylul University Health Campus, Balcova, 35340, Izmir / Turkey

ABSTRACT

In tissue engineering and biomaterial applications, inflammation can occur as a result of affecting the immune mechanism of the implanted material or device. Such immune response is critical for the regeneration of the target tissue. Macrophages, immune system cells, play a critical role in regulating wound healing and tissue regeneration by changing their polarized state in response to stimuli from the microenvironment. Macrophage polarization and control of inflammation should be taken into account in order to prevent the rejection of the implant, failure of the graft and wound healing. While M1 macrophages, which have pro-inflammatory properties and fight with pathogens, M2 macrophages have anti-inflammatory properties and are involved in tissue regeneration and angiogenesis. Recent studies show that two-dimensional monolayer cell culture systems are insufficient to mimic the complex structure of the immune system.

Microfluidic systems are platforms designed to allow control of very small amounts of fluids and to investigate the response of tissue/disease models to external stimuli. The aim of this project is to provide the 3-dimensional (3D) dynamic microfluidic systems for the macrophage polarization of macrophages and microglial cells using tissue engineering approaches. Using these platforms, we investigate the

behavior of cells under stress conditions and when they are targeted by various microfluidic system designs.

In this study, a light-polymerizable biocompatible gelatin-based hydrogel is used like cellular 3D microenvironment. The 3D hydrogel exhibits tissue-like properties in terms of its mechanical properties and biodegradability and provides an artificial extracellular matrix function that provides the natural environment for macrophages. Microfluidic platforms are designed and developed using a variety of engineering software. After the cells are encapsulated in the 3D microfluidic chip, M1-M2 polarization is examined with qPCR and histological techniques under continuous flow.

Keywords: Tissue Engineering, Microfluidic System, GelMA, Immunomodulation, Polarization.

İMMÜN HÜCRELERİN POLARİZASYONUNA YÖNELİK 3-BOYUTLU MİKROAKIŞKAN SİSTEMLERİN GELİŞTİRİLMESİ

Olcay Burçin AKBULUD, İzmir Uluslararası Biyotıp ve Genom Enstitüsü, Dokuz Eylül Üniversitesi, Sağlık Kampüsü, Balçova, 35340, İzmir / Türkiye

ÖZET

Doku mühendisliği ve biyomalzeme uygulamalarında inflamasyon, implant edilen materyalin veya cihazın bağışıklık mekanizmasını etkilemesi sonucunda oluşabilmekte ve hedef dokunun rejenerasyonu açısından son derece önemlidir. Bağışıklık sistemi hücrelerinden olan makrofajlar, mikroçevrelerindeki uyaranlara yanıt olarak polarize durumunu değiştirerek yara iyileşmesini ve doku rejenerasyonunu düzenlemede kritik bir rol oynamaktadırlar. Makrofaj polarizasyonu, inflamasyonu kontrol etmek, implantın red edilmesini önlemek ve biyomateryalin entegrasyonunu hızlandırmak açısından dikkat edilmesi gereken bir konudur. M1 Makrofajları proinflamatuar özelliklere sahip olup aynı zamanda immün sisteme giren patojenlere karşı sitokin salgılamaktadırlar. M2 makrofajları ise anti-enflamatuar özelliklere sahiptirler ve doku rejenerasyonuyla beraber anjiyojenezde rol oynamaktadırlar. Yapılan son çalışmalar iki boyutlu tek tabaka hücre kültür sistemleri, immün sistemin karmaşık yapısını taklit etmede yetersiz kaldığını göstermektedir.

Mikroakışkan sistemler çok küçük miktardaki sıvıların kontrolüne izin veren ve doku/hastalık modellerinin dış uyaranlara karşı verdikleri tepkileri incelemek için tasarlanmış platformlardır. Bu proje kapsamında doku mühendisliği yaklaşımları kullanılarak 3-boyutlu (3B) dinamik mikroakışkan sistemler ile makrofaj ve mikroglia polarizasyonunun sağlanması ve kontrollü şekilde yönlendirilmesi amaçlanmaktadır. Bu

platformları kullanarak, dinamik kültür kaynaklı stres koşulları altında hücrelerin davranışını incelemeyi ve çeşitli mikroakışkan sistem tasarımları içerisinde analiz edilmesi hedeflenmektedir.

Bu çalışmada hücrelerin 3-boyutlu doğal ortamındaki gibi davranması için ışık ile polimerleşebilen jelatin bazlı biyouyumlu hidrojel kullanılmaktadır. 3B hidrojel, mekanik özellikleri ve biyobozunabilirliği açısından doku benzeri özellik göstermekte ve makrofaj hücreleri için doğal ortamı sağlayan yapay hücre dışı matris işlevini sağlamaktadır. Mikroakışkan platformlar çeşitli mühendislik yazılımları kullanılarak tasarlanmış ve üretilmiştir. Mikroakışkan çiplerin içerisine hücreler 3B enkapsüle edildikten sonra sürekli akış altında çeşitli sitokinlerle M1-M2 polarizasyonları mRNA ve histolojik düzeyde incelenmiştir.

Anahtar Sözcükler: Doku Mühendisliği, Mikroakışkan Sistem, GelMA, İmmünomodülasyon, Polarizasyon.

1. INTRODUCTION and GOALS

1.1. Statement and Importance of the Problem

Tissue engineering aims to artificially control and re-design new tissues and organs or tissue models by helping today's medical treatment tools (Güven et al., 2011). The approach to tissue engineering can be briefly summarized as follows: a biopsy is taken from the relevant healthy tissue of the patient and the cells are isolated. In addition, the stem/precursor cells can also be transformed into another type of cell line. The resulting cells are then loaded into the carrier scaffold or hydrogel, specifically prepared for the target tissue/organ and subsequent maturation steps are performed. Finally, the developed artificial tissue is implanted into the patient/damaged area. The most important benefits of this method are i) providing the most healthy and the correct dose of medication without harming the patient by using the patient's own cells ii) minimizing ethical concerns by reducing animal experiments iii) creating appropriate platforms for the development of new drugs and treatment modalities iv) to provide alternative and innovative techniques in addition to existing surgical methods to heal injured tissues and organs (Namkoong et al., 2016) .

In tissue engineering, inflammation would occur as a result of the implantation of the implanted material or the immune system of the device and inflammation is very important for target tissue regeneration. Macrophages and monocytes are one of the cells from the immune system, playing a critical role in modulating wound healing and tissue regeneration by altering the polarized state in response to stimuli in their microenvironment (B. H. Cha et al., 2017). Macrophage polarization is important to control inflammation, preventing the rejection of the implant and accelerating the integration of the biomaterial. Microglia is part of the immune system being the resident macrophages of the brain and central nervous system (CNS). Microglia have activation states similar to that of macrophages (Stansley, Post, & Hensley, 2012).

Also, human monocyte-derived macrophages THP-1 cell line has been widely used to study immune responses (Chanput, Mes, & Wichers, 2014). Microglia and monocytes-derived macrophages have very high plasticity and are capable of switching the polarization status against the inflammation in tissue (Forrester, Wassall, Hall, Cao, Heather, et al., 2018; Matias et al., 2017). Macrophages which are classically activated (M1), with stimulants such as Lipopolysaccharide (LPS) and Interferon-γ (IFN-γ), are proinflammatory and secrete cytokines against pathogens entering the immune system and alternatively activated macrophages (M2), stimuli such as interleukin-4 (IL-4) and interleukin-13 (IL-13) that are anti-inflammatory and are involved in tissue regeneration and angiogenesis (B. Cha et al., 2017).

Recent studies show that two-dimensional monolayer cell culture systems lack of the mimic the complex structure of the immune system. Microfluidic systems are designed platforms that allow to control of the very small amounts of liquids and also these systems are used to examine the response of tissue/disease models to external stimuli. Microfluidic systems can provide venues to observe the effect of external stimuli of a biological system (e.g., pH, temperature, signaling factors, and interstitial flow) on *in vitro* bioengineered platforms under well-controlled miniaturized volumes and microenvironments. These systems can be utilized to investigate the biological processes such as cell-cell and cell-material interaction, chemotherapeutic drug administration, single cell analysis, tumor metastasis. Microfluidic systems can also be incorporated with 3D hydrogels and tissue engineering approaches, so that mimicking the *in vivo* conditions can be achieved better than 2D cell culture systems while using a very low amount of reagents. In tissue engineering, natural and synthetic biopolymers have been successfully used as 3D cell culture platforms that mimic the extracellular microenvironment during disease development and progression (Bouyer et al., 2016; Calibasi Kocal et al., 2016).

1.2. Purpose of the Research

The aim of this thesis is to provide macrophage polarization of human monocytic THP-1 cells and a murine N9 cell line with 3D dynamic microfluidic systems and to control M1-M2 polarization in a controlled manner using tissue engineering approaches. Using such a platform, we aim to examine the behavior of the cells under various shear stress conditions and test the therapeutics with several microfluidic system designs.

1.3. Hypothesis of the Research

In our study, our hypothesis predicts that the polarization of the immune cells could affect the under the static and dynamic conditions.

2. GENERAL INFORMATION

2.1. Immune System

Vertebrates have an immune mechanism that defends and fights the body when the foreign pathogen enters the body and also can repair the wounded tissue. The immune system has two defense mechanisms that are innate and adaptive immunity (Calvo, Gonzalez-Yanes, & Maldonado, 2013; Warrington, Watson, Kim, & Antonetti, 2011).

2.1.1. *The Innate and Adaptive Immunity Cell Types*

Innate immunity, the first immunological response to fight against pathogens entering the body, is an antigen-independent mechanism. Due to their antigen-independent properties, innate immunity cannot remember if the body is exposed to the pathogen again. Another main function of innate immunity is to remove dead cells and foreign substances from tissues. Also, the innate immune system can be activated to an adaptive immune response by the ability to present antigen. This innate immune system contains various cell types. Innate immune cells contain both myeloid and innate lymphoid cells (ILC). Myeloid cell types are monocytes, macrophages, dendritic cells and granulocytes (neutrophils, basophils and eosinophils) (Calvo et al., 2013; Rivera et al., 2016; Warrington et al., 2011). In contrast to innate immunity, adaptive immunity is an antigen-dependent mechanism with memory capacity. Adaptive immunity compared to innate immunity is slower because of the adaptive immunity has the antigen-dependent mechanism. Whereby this memory ability of the adaptive immune cells, the immune response be constituted in a shorter period of time when the same pathogen is infected again. The adaptive cell types include T cells and B cells (Holleran, GrainneLopetuso et al., 2017; Warrington et al., 2011). Innate and adaptive immunity cell types shown in the Figure 1.

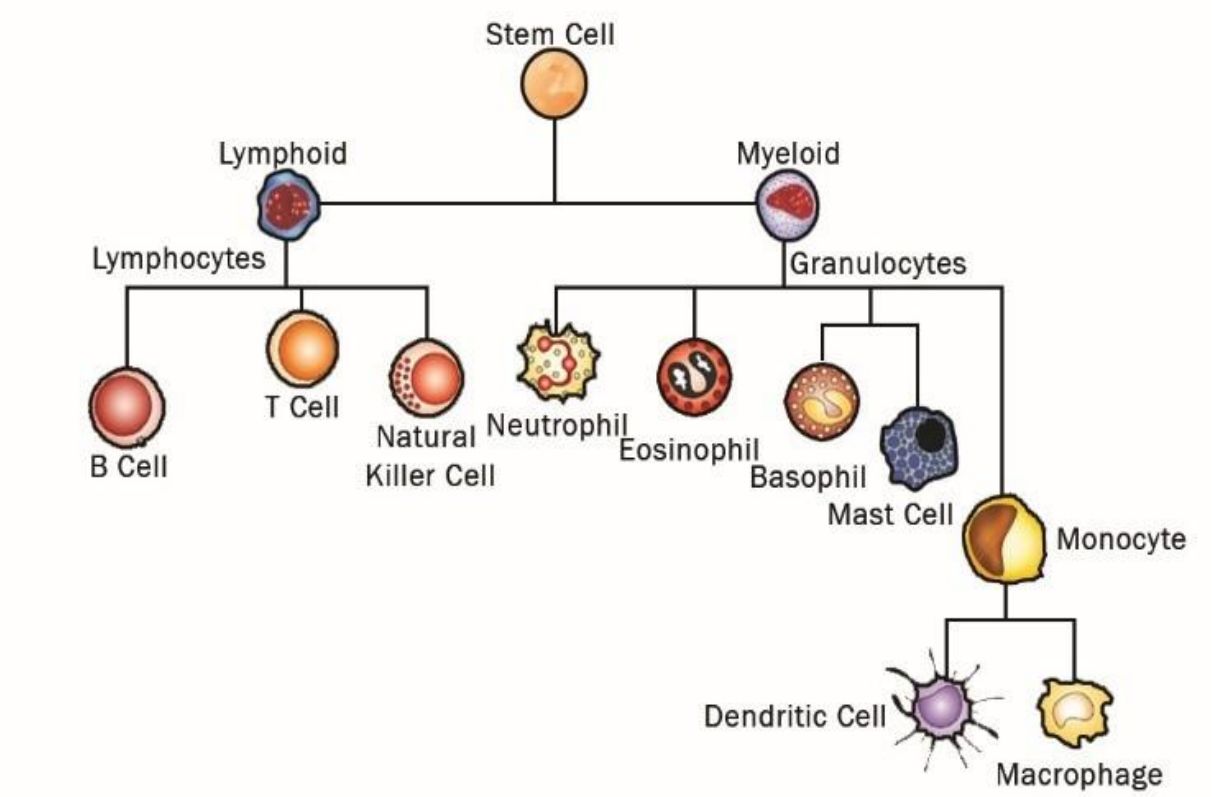

Figure 1: Schematic representation of the innate and adaptive immune system cells.

Monocytes and macrophages are innate immune system cells that can regulate the homeostasis, protect and respond to inflammation against the foreign pathogens. Dendritic cells, which are another functionary cell in response to infections, are derived from $CD34^{+}$ cells in the bone marrow and stimulants such as Granulocyte-macrophage colony-stimulating factor (GM-CSF) and Tumor necrosis factor-alpha (TNF-α) are effective in its development. Dendritic cells are located in tissues such as bone marrow, mucosa, blood, and lymphoid tissues and are important cells in the activation of the T cells. Dendritic cells are responsible for responding to infections and these cells act as a messenger between the innate and the adaptive immunity (Calvo et al., 2013; Dempsey, Vaidya, & Cheng, 2003; Warrington et al., 2011).

Granulocytes are multi-nuclei cells that have phagocytic properties and act against tissue damage and respond to pathogen attack. Granulocytes consist of bone

marrow-induced progenitors. Granulocytes responsible for innate immunity and also have antibacterial properties and granulocytes have three subclasses, which are neutrophils, basophils, and eosinophils. Neutrophils are immune cells capable of responding to bacterial infection. One of the important functions of neutrophils can be polarized like macrophages by various stimulant and they are an important source for other cells in the immune system by the reason of secreted cytokines and chemokines. Eosinophils are also bone marrow-derived cells like other granulocytes. Eosinophils are the cells that can be activated against bacterial stimuli and allergic reactions and are also involved in defense against parasites (Calvo et al., 2013; Rivera et al., 2016; Wen & Rothenberg, 2017). Basophils have a very small ratio (0.5-1%) of circulating blood cells and that cells are involved in antibacterial immunity. Basophils and mast cells together secrete heparin, histamine and IL-4 cytokines in allergic reactions or tissue repair. This secreted IL-4 cytokine induces M2 polarization of macrophages in the immune system (Calvo et al., 2013; Min, Brown, & Legros, 2012; Rivera et al., 2016).

Natural killer (NK) cells are different from other immune cells because they have the ability to directly kill without the need for differentiation. NK cells recognize the virus-infected cells by the virus-coded surface receptors and kill them. In addition to that, NK cells secrete proinflammatory cytokines to induce the M1 polarization of macrophages and dendritic cells (Calvo et al., 2013; Dempsey et al., 2003; Rivera et al., 2016).

T cells are derived from hematopoietic stem cells in the bone marrow and then migrate to the thymus to mature. T cells can recognize antigen presenting cells (APCs) with their TCR receptors in the membrane(Warrington et al., 2011). B cells are derived from hematopoietic stem cells in the bone marrow as like T cells. B cells can recognize free antigens without APCs on the contrary to the T cells. The main function of B cells is to produce antibodies against foreign antigens (Warrington et al., 2011).

2.1.2. *Monocytes and Macrophages*

Monocytes are immune cells containing the bean-shaped nucleus, which contain phagocytic vacuoles that originated from CD34+ myeloid progenitor cells in the bone marrow. Monocyte cells are heterogeneous and have two different subpopulations. One of these populations can be rapidly migrated from blood to inflamed tissue and is called inflammatory. Another population can be distinguished by cell surface proteins and is the tissue-resident macrophages. Macrophages are monocyte-derived cells that are responsible for the maintenance of life-long homeostasis since embryonic development (Calvo et al., 2013; Geissmann, Manz, Jung, Sieweke, & Ley, 2011; Kzhyshkowska et al., 2015; Martinez, Gordon, Locati, & Mantovani, 2006; Rivera et al., 2016; Shiratori et al., 2017; Zhang et al., 2018). Monocytes left from the bone marrow and enter the blood circulation system. After that, blood monocytes become macrophages that are recruited into the tissue. Macrophages are monocytes with high plasticity in be located all tissues such as lung, liver, and brain (Calvo et al., 2013; Genin, Clement, Fattaccioli, Raes, & Michiels, 2015; Mosser & Edwards, 2008; Rivera et al., 2016). Macrophages are named according to the tissue they are in. For example, macrophages found in the liver are called Kupffer cells, and macrophages found in the central nervous system are called microglia (Warrington et al., 2011).

Functions of Macrophages

One of the main functions of macrophages in the innate immune system cells is to induce an immune response to foreign pathogens (bacteria, virus or fungi) or to a foreign material (bioengineered scaffold, biomedical device or implant) (Alvarez Moisés et al., 2016; Chanput et al., 2014; Rivera et al., 2016). Macrophages that can be polarized by various stimulant so they produce an immune response after pathogen infection or implantation by secreting cytokines, chemokines, angiogenic molecules, and modulate their own phenotype and other cells around them and macrophages

provide an adaptive immune response (Alvarez Moisés et al., 2016; Kzhyshkowska et al., 2015; Rivera et al., 2016). Tissue-derived macrophages detect infection and injury and recruit circulating monocytes, neutrophils, and leukocytes into the damaged area by secreting chemokines (Forrester, Wassall, Hall, Cao, Wilson, et al., 2018; Rivera et al., 2016). Macrophages are also involved in tissue homeostasis by creating a microenvironment that encourages healing in injured tissue (Alvarez Moisés et al., 2016; Daigneault, Preston, Marriott, Whyte, & Dockrell, 2010; Forrester, Wassall, Hall, Cao, Wilson, et al., 2018)

2.1.3. *THP-1 Cell Line*

THP-1 cell line is an immortalized cell line that derived from peripheral blood of an acute monocytic leukemia patient in childhood (Bosshart & Heinzelmann, 2016). THP-1 cell lines exhibit both monocyte and macrophage-like phenotype and functions for example, they can be polarized by stimuli such as Lipopolysaccharide (LPS), Interferon-gamma (IFN-γ) (Chanput et al., 2014; Lund, To, Brien, & Donnelly, 2016; Tarique et al., 2015; Tedesco et al., 2018). Therefore, they are commonly used as a model instead of primary human monocyte cells to investigate the structure, functions of monocyte/macrophage cells, signaling pathways in both health and disease (Bosshart & Heinzelmann, 2016; Lund et al., 2016; Park et al., 2007). For activation of THP-1 cells and increasing the adherence, stimulant such as Phorbol 12-myristate 13-acetate (PMA), M-CSF, vitamin D or retinoic acid are used (Chanput, Mes, Savelkoul, & Wichers, 2013; Littlefield et al., 2014; Lund et al., 2016; Macrophages et al., 2010; Maeß, Wittig, Cignarella, & Lorkowski, 2014). THP-1 cells have many advantages over peripheral blood mononuclear cell (PBMC)-derived cells. One of these advantages is that THP-1 cells have a higher growth rate and they are easily proliferating. Also, PBMC access and culture of these cells are difficult and these cells cannot be stored for long periods. However, since the THP-1 cell line is immortalized, they allow for long-term storage. In PBMC studies cells are obtained from different donors, they indicate variability between in terms of reproducibility of experiments. Therefore, using the

THP-1 cell line is more advantageous in obtaining consistent results (Chanput et al., 2014; Forrester, Wassall, Hall, Cao, Wilson, et al., 2018; Maeß et al., 2014; Shiratori et al., 2017).

2.1.4. *Microglial Cells*

Microglia are first discovered and described in 1918 by Pio Del Rio Hortega, they are resident mononuclear phagocytes cells in the Central Nervous System (CNS) and innate immune cells of the brain (S. Hickman, Izzy, Sen, Morsett, & Khoury, 2018; Nakagawa & Chiba, 2015; Stansley et al., 2012; wang, 2018). According to Hortega's hypothesis, microglia are derived from mesoderm, myeloid, hematopoietic stem cells in the yolk sac. Nowadays, the origin of microglia found in CNS is known mesoderm origin to occur by the differentiation of macrophages produced in the yolk sac (Graeber & Streit, 2009; S. Hickman et al., 2018; Nakagawa & Chiba, 2015). Microglia are known as macrophages of the CNS and the brain, they show macrophage-like functions and characteristics. Microglia have similar function to macrophages because of their immunoregulatory and regenerative properties and they express the markers similar to macrophages such as CD11b, CD14, F4/80 , CX3C chemokine receptor 1 (CX3CR1: fractalkine receptor), and ionized calcium-binding adapter molecule (Iba-1) (S. Hickman et al., 2018; Kettenmann, Hanisch, Noda, & Verkhratsky, 2011; Ransohoff & Perry, 2009; Saijo & Glass, 2011; Xiong, Liu, & Yang, 2016). In the recent studies, new microglia-specific markers such as HexB, P2ry12, Tmem119, TREM2, and Olfml3 have been identified in the healthy brain by RNA-seq analysis (S. E. Hickman et al., 2013).

Functions of Microglia

Microglia have many functions in physiological and pathological processes. Most importantly, they regulate the homeostasis of the central nervous system and also detect and regulate the CNS microenvironment (Amadio, Ninno, Montilli, Businaro, & Gerardino, 2013). Microglia rapidly change their morphology and expression of cytokines or chemokines in response to changes in homeostasis and pathological processes in CNS. Microglial can be easily polarized by a various stimulant to protect the immune system or tissue regeneration (Perry, Nicoll, & Holmes, 2010). Because of their high plasticity, they are involved in many immunological processes such as neurogenesis and synaptogenesis. Due to phagocytic properties like macrophages, they are responsible for the elimination of apoptotic cells, removal of pathogens, and elimination of cell debris (Amadio et al., 2013; Cunha, Gomes, Vaz, & Brites, 2016; Xiong et al., 2016). In addition, microglia can be activated in cases of infection, degeneration, injury or ischemia. Activated microglia migrate to the site of damage and regulate the repair and regeneration processes by secreting anti-inflammatory or pro-inflammatory cytokines, chemokines and oxidative stress molecules (Amadio et al., 2013; Chhor et al., 2013; Xiong et al., 2016; Zhou et al., 2017).

2.1.5. *N9 Cell Line*

Nowadays, microglia studies also use immortal cell lines other than the primary cell culture. Primary microglial cell culture is used in neuroinflammatory studies because of they have in-vivo like properties. These primary cells are usually derived from the cortex of the mouse or rat just before or early after birth. Microglia were immortalized by the reason of insufficient cell number, difficulty in the culture of primary cells and time-consuming in primary cell culture studies. Murine BV2 and mouse N9 cell lines were immortalized by infecting the primary microglia cells with a retrovirus. Immortalized cell lines have been shown to have microglia specific surface

markers such as FcR, Mac-1, and F4/80. N9 microglia cells have similar properties to primary cells, however, due to the genetically modified N9 cell line, proliferation ability and surface adhesion properties increased compared to primary cells. N9 cell line used in this study was produced by Paola Ricciardi-Castagnoli by overexpression of c-myc oncogene (Graeber & Streit, 2009; Righi et al., 1989). Beside N9 and BV2 cell lines, genetically unmodified microglia cell lines which are also used in neuroinflammatory studies. These genetically unmodified cell lines are colony-stimulating factor-1 dependent EOC cells and Highly Aggressively Proliferating Immortalized (HAPI) cell lines. EOC and HAPI cell lines are also capable of secreting cytokine and reactive oxygen species such as primary cells. Human microglia cells are also used in neuroinflammation studies. But microglia from human embryos is difficult to produce due to ethical problems. To solve this problem, Nagai and his group developed the immortalized human microglia cell line (HMO6) by infecting primary human microglia cells with the retroviral vector (Stansley et al., 2012). Table 1 summarizes the basic characteristic of the microglia culture systems commonly used in neuroscience.

Table 1: Characteristic properties of microglial cells.

Characteristic	Primary Microglia		N9	BV2	EOC	HAPI	HMO6	MMGT12
Macrophages Antigen-1 (MAC-1)	+		+	+	+	+	+	+
LPS Stimulation	+		+	+	+	+	+	+
IL-1β release	+		+	-	N/A	+	-	+
TNF- release	+		+	+	N/A	+	+	+
Phagocytosis	+		+	+	+	+	+	+
•NO production	+		+	+	+	+	-	N/A

2.1.6. *Monocyte/Macrophage and Microglia Polarization*

Polarization of Macrophages

Macrophages are polarized to generate responses in the situation of any threat to the immune system (Alvarez Moisés et al., 2016; Kzhyshkowska et al., 2015). Macrophages with high plasticity are the cells that can rapidly change their phenotypes according to the stimuli they encounter (Barthes, Dollinger, Muller, Liivas, & Griffith, 2018; He & Carter, 2016). Macrophage polarization plays an important role in physiological conditions such as embryogenesis. Furthermore, macrophage polarization has an important role in pathological conditions such as infection, allergy, bacterial clearance, wound healing, tissue repair, response to foreign body and tumor progression (Barthes et al., 2018; Li, Levin, & Kaplan, 2016). Classically polarized M1 macrophages are pro-inflammatory, and alternatively polarized M2 macrophages are anti-inflammatory. These M1 and M2 states of macrophages are clinically important for controlling inflammation (B. Cha et al., 2017; Kzhyshkowska et al., 2015).

Th1 cells are responsible for the reaction against bacteria and virus and Th1 cells produce IFN-γ. M1 macrophages are obtained by activation of transcription factors such as STAT1, NF-kB and Interferon regulatory factor-5 (IRF-5), which are affected by stimulants such as LPS or IFN- γ (He & Carter, 2016; Kzhyshkowska et al., 2015). M1 macrophages are responsible for the defense of the immune system to bacterial and viral infection by secreting pro-inflammatory cytokines. In addition, M1 macrophages are cytotoxic and have important functions in tumor regression. M1 polarization of macrophages is characterized by high levels of expression to proinflammatory cytokines, such as TNF-α, IL-1β, IL-6, and IL-12 (Dollinger et al., 2017; Genin et al., 2015; Mantovani, Sica, & Locati, 2007). TNF-α and IL-1β is the main proinflammatory cytokine involved in chronic inflammation. IL-12 is a cytokine that promotes Th1 cell-mediated responses in the pathogenesis of autoimmune

diseases. These pro-inflammatory cytokines affect the activation of NK cells and lymphocytes and the uptake of neutrophils, provide the occurrence of the rapid inflammatory response (Kzhyshkowska et al., 2015). M1 macrophages also have a high antigen-presenting capacity and are characterized by high levels of effector molecules such as reactive oxygen species (ROS) and Nitric oxide (NO) production (Dollinger et al., 2017; Kzhyshkowska et al., 2015; LOCATI et al., 2004). The Inducible nitric oxide synthase (iNOS) enzyme, which is responsible for the NO production of M1 macrophages is specific only to murine macrophages, not human macrophages (Genin et al., 2015).

Th2 cells are responsible for the production of IL-4. M2 macrophages are obtained by activation of transcription factors such as STAT3, STAT6, PPAR, and IRF-4, which are affected by stimulants such as IL-4, IL-13 or IL-10 (He & Carter, 2016; Jablonski et al., 2015). M2 macrophages are responsible for generating anti-inflammatory responses in case of parasitic infection or inflammation. They also have an important function in the pathogenesis of allergy and cancer. Other important functions of M2 macrophages are provide wound repair, angiogenesis, tissue remodeling, and immunoregulation (Dollinger et al., 2017; Genin et al., 2015; Knopf-Marques et al., 2016; Kzhyshkowska et al., 2015; Mantovani et al., 2007). M2 macrophages are divided into three subclasses; M2a macrophages are obtained by stimulation of IL-4 and IL-13, M2b macrophages are obtained by a combination of immune complexes and Toll-like receptor (TLRs) and M2c macrophages deactivated with IL-10, TGF-β, and glucocorticoids (Forrester, Wassall, Hall, Cao, Wilson, et al., 2018; Mantovani, Martinez, & Gordon, 2004; Saleh & Bryant, 2017). M2 polarized macrophages produce a high level of anti-inflammatory cytokines such as IL-10 and IL-1Rα. IL-1Rα is involved in the treatment of autoinflammatory diseases such as rheumatoid arthritis (Dollinger et al., 2017). Furthermore, M2 macrophages are characterized by the expression high level of arginase-1 (Arg-1), chitinase-like 3 protein (YM-1), Fizz-1, mannose receptor (CD206), the scavenger receptors (CD163) and various chemokines (CCL1,16,17,18,22, and 24) (Barthes et al., 2018; Dollinger

et al., 2017; Genin et al., 2015; Mantovani et al., 2007). CCL18 is produced by myeloid cells and promotes collagen deposition in fibroblasts. IL-4 induces collagen release in fibroblasts and induces angiogenesis. Thus, IL-4 cytokine is an effective agent in the development of the Extracellular matrix (ECM) and 3D bioengineered tissues and their implantation (Barthes et al., 2018; Vrana, 2016).

Polarization of Microglial Cells

Microglia are found in both healthy and injured brain and modulate neurogenesis (Ekdahl, 2012). Microglia that are affected by the introduction of foreign antigen/pathogens into the brain or changes in brain homeostasis are activated to act as protective or regenerative by changing the resting state. As a result of the microglia being exposed to a foreign antigen or by stimulation with LPS or IFN-γ, M1 Polarization which is classically active to maintain natural immunity occurs. Microglia in the M1 phenotype characterized by producing proinflammatory cytokines such as IL-1a, IL-1β, IL-6, IL-12, IL-23, TNF-α, and increasing the expression of inducible NO (iNOS). M2 polarization occurs in tissue regeneration, allergies, angiogenesis or immunoregulation. M2 phenotype which is an alternative polarization in microglia is activated by stimuli such as IL-4, IL-13 or IL-10. As in macrophages, microglia also have a subpopulation of M2 polarization (Ekdahl, 2012; Hu et al., 2014; Orihuela, McPherson, & Harry, 2016; Ransohoff & Perry, 2009). In the activation of M2a, microglia are stimulated with IL-4 and IL-13 to response the allergy and the anti-parasite, in M2b activation Fcγ receptor is induced by the induction of TLR and immune complexes to response the immunoregulation. Activation of M2c is achieved by stimulation of microglia with IL-10 to response the immunoregulation and tissue repair (Colton & Wilcock, 2012; Hu et al., 2014; Orihuela et al., 2016).

2.2. Tissue Engineering

Cell culture practices are traditionally performed in 2-dimension (2D) *in vitro*. However, the human body is a dynamic system consisting of various cell types and 3-dimension (3D) structures. 2D cell cultures are inadequate to mimic the complex structure and cellular behaviors of *in vivo* tissues as shown in Table 2. Therefore, nowadays, tissue engineering studies have gained importance for understanding the 3D structures of the tissues (Asghari, Samiei, Adibkia, Akbarzadeh, & Davaran, 2017; CHo, Erbridge, Avalos, & Ee, 2018; Geckil H, Xu F, Zhang X, Moon S, 2010; Mogosanu, Verplancke, Dubruel, & Van, 2016; Namkoong et al., 2016). Tissue engineering is an interdisciplinary field that enables the 3D modeling of a tissue or organ *in vitro* by combining life sciences such as chemistry, physics, and biology with the engineering approaches (Langer & Vacanti, 1993). Researchers can obtain more accurate information about the microenvironment, cell-cell, and cell-ECM interactions of the tissue by mimicking *in vivo*-like structures with 3D *in vitro* cell culture systems. In addition, scaffolds used in 3D cell culture systems provide a larger surface area for the growth and migration of cells than in 2D culture methods. Cho et al. have done the first study comparing traditional *in vitro* 2D, *in vitro* 3D model, and *in vivo* of brain inflammation modeling. In this research, they have developed an *in vitro* 3D modeling by encapsulating the microglia cells in hydrogel and the physiological and molecular responses of the cells were compared by stimulating with pro-oxidative and pro-inflammatory stimuli. Compared to 2D and 3D cell culture systems, 3D systems provide close resemblance of experimental *in vivo* models (CHo et al., 2018).

Table 2: A Comparison of cell/behavior under 2D and 3D Cell culture conditions (Geckil H, Xu F, Zhang X, Moon S, 2010).

Feature/function	In 2D	In 3D	Ref.
Tissue-specific architecture	Poor	Rich	[220]
Cell morphology	Flat, extended	Round, contracted	[17,221]
Interactions	Limited	Multiple	[38]
Cell motility	Fast, free	Slow, restricted	[6]
Cell adhesion	Weak	Strong	[222]
Cell growth	Directional	In all directions	[6,223]
Cell proliferation	High	Low	[5,6]
Apoptosis	Induced	Tissue-like	[223,224]
Intracellular stiffness	An order-of-magnitude higher in 3D		[4]
Cell polarization	Partly	Full	[6]
extracellular matrix remodeling	Absent or poor	Present	[5]
Fluid perfusion	1D	3D	[170]
Signaling and diffusion	Asymmetric	Nearly symmetric	[225]
Metabolic rate	High	Low	[223]
Cell survival when exposed to cytotoxic agents	Low	High	[226]

The main aim of tissue engineering is to mimic the *in vivo* structural and functional properties of the tissue in *in vitro* and assisting in today's medical treatment methods to treat damaged tissue or artificially remodeling new tissues that can replace damaged tissue (Güven et al., 2011). The approach to tissue engineering can be briefly summarized as follows: a biopsy is taken from the relevant healthy tissue of the patient and the cells are isolated. In addition, the stem/precursor cells can also be transformed into another type of cell line. The resulting cells are then loaded into the carrier scaffold, or hydrogel, specifically prepared for the target tissue/organ, and subsequent maturation steps are performed. Finally, the developed artificial tissue is implanted into the patient/damaged area (Figure 2). The most important benefits of this method are 1) providing the healthiest and correct dose of medication without harm to the patient by using the patient's own cells, 2) minimizing ethical concerns by reducing animal experiments, 3) creating appropriate platforms for the development of new

drugs and treatment modalities, 4) to provide alternative and innovative techniques in addition to existing surgical methods to heal injured tissues and organs.

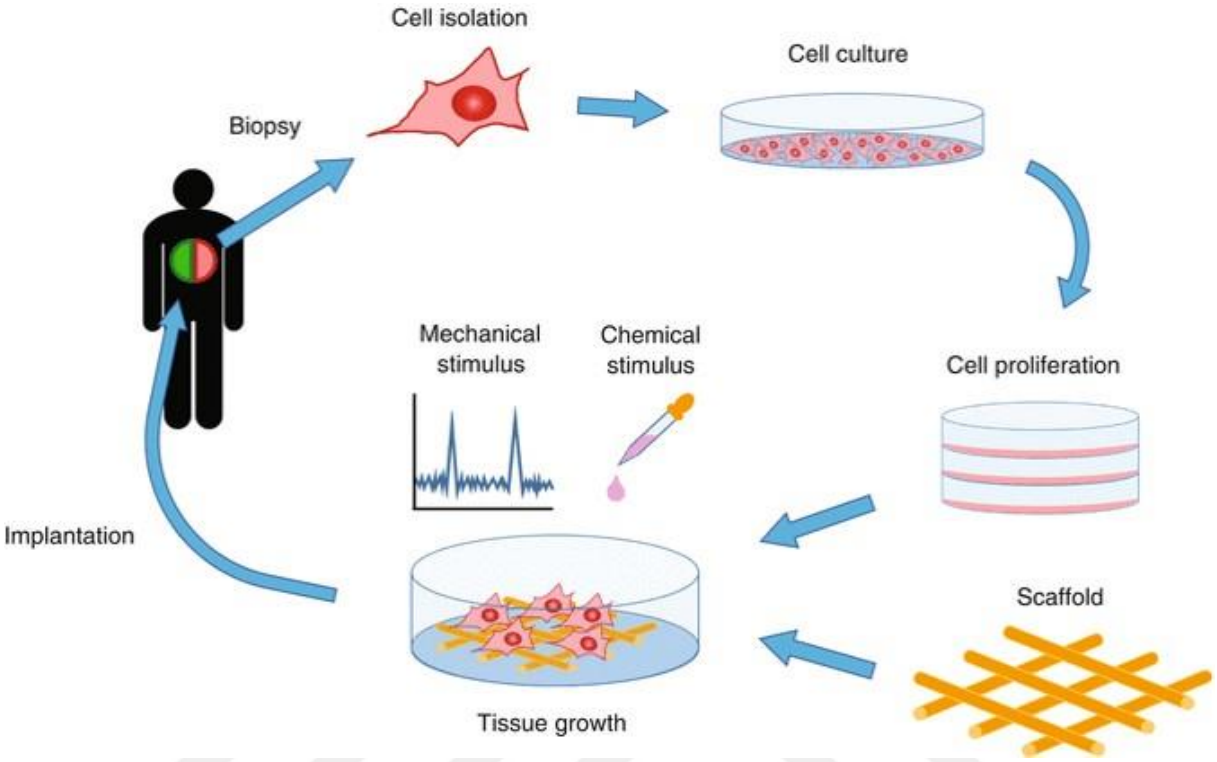

Figure 2: Schematic representation of tissue engineering. (Noh S. et al., 2018)

There are some limiting factors in mimicking the complex architecture of natural tissues in *in vitro*. One of these factors is the use of biomaterials with appropriate mechanical, chemical and biological properties to allow the cell to adhere, proliferate and migrate. The stiffness and strength of the material used affect cell differentiation and phenotype. In addition, oxygen and nutrient intake and removal of waste are very essential for the cell to maintain its presence. Appropriate porous and permeable material should be used for these needs of the cell. Another limiting factor is that the artificial tissues produced for the damaged tissue should be biocompatible with the body. They should show minimal immunological reactions with the body upon implantation and afterward (Khademhosseini & Langer, 2016).

2.3. Biomaterials

Biomaterials are natural or synthetic materials that are capable of treating, repairing or replacing any tissue, organ or function of the body (Dziki & Badylak, 2018). Biomaterials, which have long been used in the clinical field, are used as a scaffold in tissue engineering applications and 3D cell culture studies. Scaffold are models of natural or synthetic biomaterials designed to mimic the native ECM structure and biological functions of the tissue. There are many parameters that should be considered in the selection of the appropriate scaffold material. These parameters include the porosity, mechanical stiffness and strength, biocompatibility, biodegradability, and surface adhesion for the cell attachment (Geckil H, Xu F, Zhang X, Moon S, 2010).

Synthetic biomaterials such as metals, fabrics, and polymers are used in areas such as wound healing and implants. Examples of synthetic polymers that are used in tissue engineering include polyester, Polyglycolic acid (PGA), Polylactic acid (PLA), poly (lactic-co-glycolic acid) (PLGA), Polycaprolactone (PCL), and Polyethylene glycol (PEG). Synthetic polymers are biologically compatible and degradable materials. Synthetic biomaterials are commercially available and have a very advantageous use for reproducible production with a highly controlled chemical structure (Asghari et al., 2017; Chung, Maestas, Housseau, & Elisseeff, 2017). PEG is a non-toxic, non-immunogenic, mechanically stable synthetic polymer used in 3D cell culture studies. The disadvantage of using PEG is that cells cannot directly bind to the PEG biopolymer and the cell cannot show its natural morphology and functions (Hutson, Tunable, Liebert, & Link, 2019).

In mammals, ECM provides structural support to the cell and also plays an important role in the interaction of cells with various cells and tissues. The ECM is a complex structure that comprises of proteins, proteoglycans, and other soluble

molecules as shown in Figure 3. Natural polymers are biomaterials obtained from biological organisms such as microorganisms, plants or animals. Natural polymers can be originated from polysaccharide, protein or obtained from the tissue itself by decellularization techniques. Chitin, chitosan, and alginate are polysaccharide-originated polymers and collagen and gelatin are protein-originated polymers. The use of natural polymers in tissue engineering studies has several advantages. It has the advantages of being metabolically compatible with the body, non-toxic, showing biological functions similar to the host tissue and being degradable by enzymatic reactions over time. Nonetheless, due to plant and animal origin, there is a possibility of transmission of disease from other species to the host organism and natural polymers are mostly temperature sensitive materials. (Asghari et al., 2017; Chung et al., 2017; Geckil H, Xu F, Zhang X, Moon S, 2010).

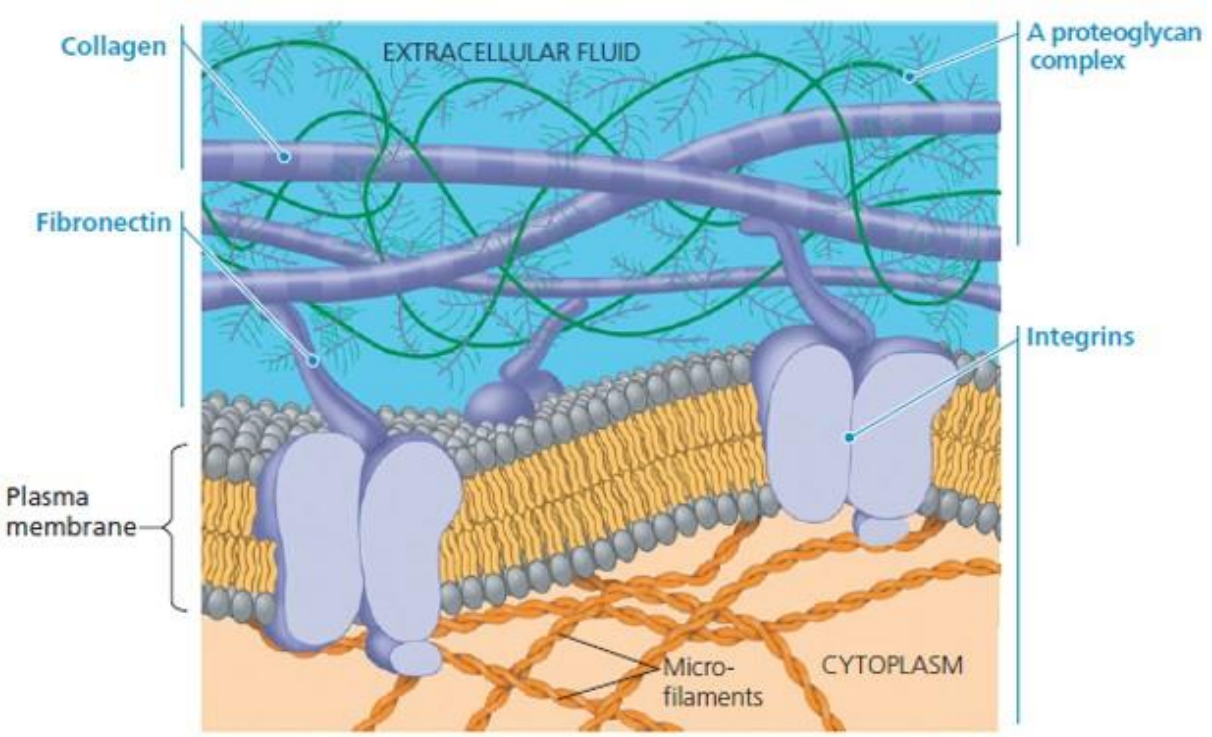

Figure 3: Schematic representation of extracellular matrix (Bassler BL, 2011).

The immune system is the constitutive first reaction to the tissue injuries, defense against the foreign bodies entering to the body, wound healing or the biomaterial implant. After the implant of the biomaterial, foreign body response (FBR) occurs with the fusion of macrophages and neutrophils around the foreign body. Following cytokine secretion of macrophages and neutrophils, the wound healing process continues with adaptive immune cells. However, when the biomaterial is used which is not suitable for the tissue, FBR is formed and this FBR can cause tissue damage with excessive inflammation of the tissue and failure of the implant function. ECM remodeling, a part of tissue homeostasis, has an important role in wound repair. By designing biomaterials with immunoregulatory properties suitable for tissue, FBR formation can be prevented or reduced, thereby accelerating the wound healing process. Recent studies have shown that hydrogels are more successful in mimicking native ECM (Chung et al., 2017; Dziki & Badylak, 2018; Sharifi et al., 2019).

2.3.1. *Hydrogel*

Appropriate scaffold selection is very important for mimicking the complex functional structure of tissues, cell-cell or cell-tissue interactions, as well as the mechanical and chemical functions of the cell to function similar to the native microenvironment in tissue engineering applications. The hydrogels are mostly used in 3D tissue engineering studies because they are similar to the mechanical and physicochemical properties of the native ECM. Hydrogels are water-swollen, hydrophilic, polymeric structures formed by crosslinking one or more monomers. Various natural and synthetic biomaterials are used in the production of hydrogels. Examples of natural polymers such as collagen, fibrin, fibronectin, alginate, and agarose are used in wound healing, artificial blood vessel, and tissue regeneration. Synthetic materials such as PEG, PLA, and PGA are also used for tissue engineering studies (Vrana, N. E., Biomaterials and Immune Response: Complications, Mechanisms and Immunomodulation: CRC Press 2018)(Geckil H, Xu F, Zhang X, Moon S, 2010; Wang, Ma, Wang, & Zhang, n.d.).

Collagen is the most abundant structural protein in the ECM of animal tissues. Collagen is obtained by extracting from the animal's skin, bone, cartilage or tendons. Collagen has a triple polypeptide structure, biocompatible, can easily be degradable by enzymes in the body and has a high cell binding capacity, therefore, it is widely used in tissue engineering studies (Asghari et al., 2017; Chaubaroux et al., 2012).

Gelatin, a hydrolysis product of collagen, has chemical and mechanical properties similar to that of collagen. The triple helix structure of the collagen is degraded by denaturation and the gelatin becomes a biodegradable, non-immunogenic product. Gelatin is a product comprising the RGD sequence and MMP sequences used for cell binding and reconstruction of the cell microenvironment. Owing to these sequences, gelatin has a high capacity to bind cells (Choi, Yong, Choi, & Cowie, 2019; Lee et al., 2019; Nichol et al., 2010). Due to this property, gelatin is an excellent alternative to tissue engineering applications. The gelatin becomes liquid in aqueous solutions and must be crosslinked for use in 3D cell culture studies. The gelatin could be crosslinked physically or chemically. Therefore, it has recently been used as photocrosslinkable form namely, gelatin methacrylate (GelMA) in 3D cell culture applications (Asghari et al., 2017; Journal, Modaresifar, Hadjizadeh, & Niknejad, 2018).

2.3.2. *Gelatin-Methacrylate (GelMA)*

Photocrosslinkable hydrogels are polymers that are used in a wide variety of biomedical areas, which must be exposed to light to have the desired structure. GelMA is a photocurable hydrogel obtained by chemically modifying gelatin with Methacrylic Anhydride (MAA) (Choi et al., 2019; Shirahama, Lee, Tan, & Cho, 2016). Gelatin-based photocrosslinkable GelMA was first synthesized by Van Den Bulcke et al in 2000 (Bulcke et al., 2000). GelMA is a biologically compatible, hydrophilic, biodegradable, low cytotoxicity, and a great photocrosslinkable hydrogel (Hutson et al., 2019; Oktay & Alemdar, 2019; Paula et al., 2018; Wang et al., n.d.). They can be crosslinked with

visible light (400-800 nm) or Ultraviolet (UV) light (200-400 nm). GelMA is more advantageous than gelatin with its ability to gelation under UV light and maintains its physical form and structure stability at body temperature (Shirahama et al., 2016). GelMA is a biomaterial with high cell binding capacity as it contains the RGD sequence in the structure of gelatin. GelMA, a suitable platform for biomedical applications, is widely used in regenerative medicine and therapeutic studies, tissue engineering, drug delivery system, cancer modeling and *in vitro* 3D healthy and disease biomimetic tissue modeling. Another advantage of using GelMA as a scaffold is that the stiffness and porosity of GelMA can be controlled by the MAA concentration and the light exposure process (Journal et al., 2018; Lee et al., 2019; Nichol et al., 2010) (Geckil H, Xu F, Zhang X, Moon S, 2010).

Photosensitive hydrogels usually require photoinitiator, pre-polymer and other components to crosslink. Choosing an appropriate photoinitiator is very important for tissue engineering. The choice of suitable photoinitiator for tissue should be water-soluble and low cytotoxicity. Because the free radicals in the photoinitiator can react with the nucleic acids and proteins, it can affect the cell viability and even cause damage to the DNA structure. (2-hydroxy-1- (4- (hydroxyethoxy) phenyl) -2-methyl-1-propanone) is water-soluble, has low cytotoxicity and low immunogenic properties, which is the reason that it is the most widely used photo-initiator in the tissue engineering field (Choi et al., 2019).

2.4. Microfluidic System

Cells are constantly exposed to shear stress and dynamic conditions in natural 3D micro-environments where fresh nutrients and gases are provided. Understanding the physical, chemical, mechanical and biological aspects of the 3D complex and dynamic microenvironment of the cell and understanding of its cellular behavior is very important for tissue engineering (Barthes et al., 2014; Duinen, Trietsch, Joore, Vulto,

& Hankemeier, 2015). Therefore, recently researchers have developed the microfluidic technologies to mimic the *in vitro* functions of dynamic 3D tissues. Microfluidic technology is a multidisciplinary field intersecting engineering, physics, chemistry, biochemistry, nanotechnology, and biotechnology. Microfluidic systems are designed platforms that allow the control of very small amounts of liquids and also these systems are used to examine the response of tissue/disease models to external stimuli (Bang, Na, Jang, Kim, & Jeon, 2016; Huh, 2010).

Microfluidic systems can provide venues to observe the effect of external stimuli of a biological system (e.g., pH, temperature, signaling factors, and interstitial flow) on *in vitro* bioengineered platforms under well-controlled miniaturized volumes and microenvironments. These systems can be utilized to investigate the biological processes such as cell-cell and cell-material interaction, chemotherapeutic drug administration, single cell analysis, tumor metastasis, artificial microvascular tissue engineering, cell viability testing, and stem cell researches. Microfluidic systems can also be incorporated with 3D hydrogels and tissue engineering approaches so that mimicking the *in vivo* conditions can be achieved better than 2D cell culture systems while using a very low amount of reagents (Bouyer et al., 2016; Calibasi Kocal et al., 2016). The use of microfluidic platforms in tissue engineering studies has many advantages over traditional cell culture methods. These advantageous: (i) miniaturized the 3D dynamic structures and functions onto a chip size, (ii) integration of multiple biological functions in a single system, (iii) design flexibility according to tissue or disease model, (iv) replace the animal testing, (v) optically transparency, (vi) low production cost and a small amount of nutrients, sample, and chemical requirement (Barthes et al., 2014; Convery & Gadegaard, 2019; Kong et al., 2017; Yanagawa, Sugiura, & Kanamori, 2016).

Microfluidic systems are commonly produced from Polydimethylsiloxane (PDMS) or Poly(methyl methacrylate) (PMMA). PDMS is a biocompatible, gas-permeable,

transparent and easy to manufacture material, but due to its hydrophobic properties, microfluidic chips produced from PMMA are more useful for tissue engineering studies than PDMS microfluidic chips. PMMA is optically transparent, biocompatible, easy to manufacture, low cost and rigid than PDMS (Convery & Gadegaard, 2019; Harink, Gac, Truckenmüller, Blitterswijk, & Habibovic, 2013).

Reynold number which is dimensionless number is used in the fluidic systems to determine the flow regime.

$$\mathrm{Re} = \frac{\rho v l}{\mu}$$

Where, ρ=density of the fluid, V=velocity of the fluid, μ=viscosity of fluid, L=length or diameter of the fluid. If the Reynold number is less than 2000, flow is defined as the laminar flow, if greater than 4000, flow is defined as the turbulence flow. The flow in the microfluidic chip channels is in the laminar flow regime. Molecular transfers in the laminar flow regime are carried out by diffusion. Microfluidic chips have been developed by the engineers, in which the two fluids can flow side by side in one channel with the effect of this diffusion-based transport of the fluids and the surface tension forces. These microfluidic chips are called 'H-filter' (Convery & Gadegaard, 2019).

H-filter microfluidic systems are developed to generally separate small molecules within heterogeneous mixtures such as saliva based on diffusion of laminar flow without membrane in the channel (Breslauer, Lee, & Lee, 2006; Osborn et al., 2010). Two Non-Newtonian laminar flows at the same volumetric velocity and equivalent viscosity in the microchannel remain constant over time (Helton & Yager, 2007). Therefore, without the need for a membrane between two fluids, controlled diffusion can be achieved without interfering the surface tension forces between the liquids with each other in the center of the channel. H-filter platforms that can be controlled by

the design of the microfluidic channel geometry, the flow rate of the fluids and the controlled diffusion as shown in Figure 4. Using two different reagents in the H-filter microfluidic channel, it is possible to create chemical gradient models with no barrier, adjacent perfusion (Helton, Nelson, Fu, & Yager, 2008).

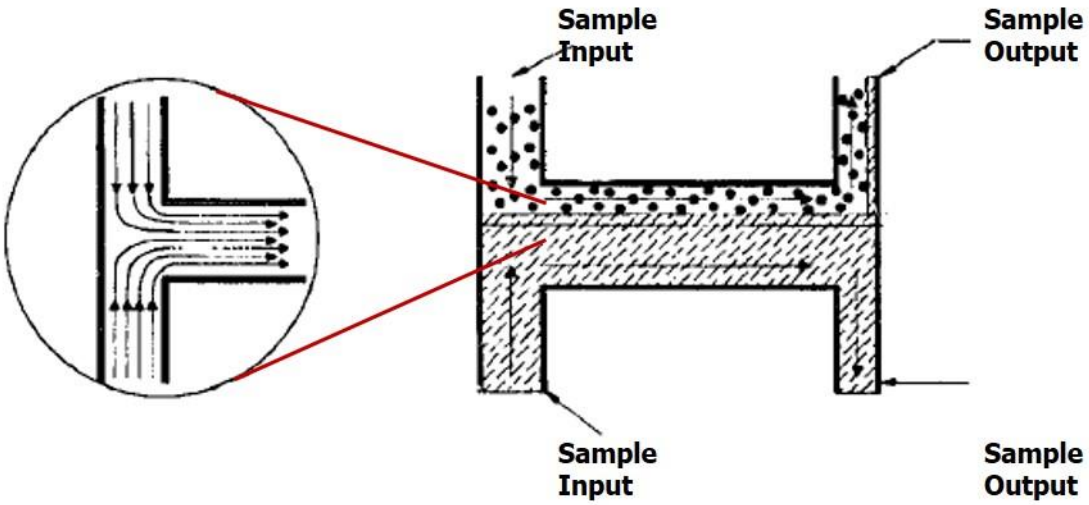

Figure 4: Schematic design of H-filter microfluidic system.

3. MATERIALS & METHODS

3.1. Type of Research

This study is an *in vitro* experimental study.

3.2. Time and Location of Research

All of the research was conducted in September 2016 - May 2019 at Izmir Biomedicine and Genome Institute.

3.3. The Universe and Sample of Research

In this thesis scope, primary human samples were not used.

3.4. Materials of Research

In this study, N9 mouse cell line and THP-1 human monocytic cell line were used. N9 mouse cell line on 26.07.2016 and THP-1 human monocytic cell line on 06.09.2018 was provided from Prof. Dr. Şermin Genç. Biopolymer used in the study is synthesized in IBG.

3.5. Variables of the Research

Independent variables: RPMI medium, the ratio of FBS and Pen-Strep.

Dependent variables: Flow rate in a microfluidic system, cell seeding density, stiffness of the GelMA based artificial matrix, the concentration of induction stimulant such as LPS, IFN- γ, IL-4, IL-13 and PMA, duration of the induction, level of RNA.

3.6. Data Collection Methods

3.6.1. *Cell Culture*

3.6.1.1. N9 Mouse Microglial Cell Culture

Roswell Park Memorial Institute (RPMI) 1640 medium is used in cell culture for N9 microglia cells. RPMI 1640 (Gibco, 21875034) medium was prepared for cell culture to complete medium by adding 10% heat-inactivated Fetal Bovine Serum (v/v) (FBS, Gibco, 10500064) and 1% Penicillin-Streptomycin (v/v) (Pen-Strep, Gibco, 15140-122). N9 microglia cells were seeded in a cell culture plate with complete RPMI 1640 medium.

Adherent N9 cells were subcultured when the confluency reached about 80-90%. For subculturing the adherent cells, firstly cell culture media was removed and aspirated from the culture plate using the Pasteur glass pipette and then washed the culture plate with 1X Phosphate Buffered Saline (PBS, Gibco, 10010023) to remove cell debris and residues of the serum. PBS was slowly added to the opposite side of the cells where the cells are seeded to avoid the remove the cells from the surface and the cell surface is washed thoroughly by shaking back and forth several times. And then aspirated the PBS from the culture plate. After that Trypsin-EDTA (0.25%) (Gibco, 25200056) was added to remove cells from the plate surface, used enough amount of trypsin to get complete coverage of the surface (approximately 1 ml per 25 cm^2) and culture plate was incubated at 37°C incubator for 2-10 minutes. The cells were observed under a microscope to see if cells were completely removed from the plate surface. If the majority of the cells have not been removed from the surface, gently tapped the plate from the side with the palm of your hand. After ensuring that all cells were removed from the surface, two volumes of medium were added to inactivate the Trypsin-EDTA, so that the cells were suspended. After that, the cell suspension was transferred to the 15 ml conical-falcon tube and centrifuge at 1500 rpm for 5 minutes.

And then the supernatant was aspirated and cells were resuspended with fresh complete medium. To calculate the total number of cells and percent of viability, 100-200 µl of cell suspension was taken, stained with Trypan Blue (Biological Industries, 03-102-1B) and were counted using the hemocytometer. The recommended amount of cells were seeded into the new labeled cell culture plate and incubated at 37°C, 5% CO2. These processes were repeated when confluency about 80-90%.

For freezing the cells, as in the cell sub-culturing process, the confluency of the cells was about 80-90 % were removed from the plate surface, counted and centrifuged. After that, a freezing medium was prepared to contain 10% Dimethyl sulfoxide (DMSO, Sigma-Aldrich, D2650) and 90% FBS. After centrifugation, the supernatant was removed by vacuum and cells resuspended with the freezing medium at a concentration of approximately 1-2 x 10^6 cells per vial. The cell suspension was transferred to the vials as 1 ml. In order to avoid damaging the cells during freezing, the vials were placed at Mr. Frosty Freezing Container (Nalgene, 5100-0001) which is reduce the temperature by 1 °C per minute, and stored at -80 °C overnight. After that, vials were transferred to the liquid nitrogen tank.

Thawing of frozen cells is a step that needs to be done quickly in contrast to the cells freezing protocol because DMSO is cytotoxic for cells and can damage the cell membrane. For thawing the cells, firstly RPMI was heated to 37 °C in a water bath and then frozen vial was removed from the liquid nitrogen tank and quickly placed it into a 37 °C water bath. After that, the vial was wiped with 70 % ethanol and then was transferred into the laminar flow cabinet. After that, the cells in the vial were transferred to a sterile falcon tube, 5 ml of pre-warmed complete medium was added to the falcon tube and the cell suspension was centrifuged to remove DMSO at 1500 rpm for 3 minutes. The supernatant was removed by vacuum and then cells were resuspended with fresh complete growth medium. Finally, the cells were seeded on a culture plate accordingly recommended cell density.

3.6.1.2. THP-1 Human Monocytic Cell Culture

RPMI 1640 containing 10% FBS and 1% Pen-Strep was used for suspension culture of human monocytic THP-1 cell culture. The subculture of suspension cell culture protocol is different from the adherent cells subculture. Trypsin-EDTA was not used in subculture because of THP-1 cells do not adhere to the surface of the culture plate. The recommended cell passage time is 2 days for the THP-1 cell line. Suspension cells in the cell culture plate were taken into a 15 ml conical-falcon tube using a sterile pipette and to calculate the total number of cells and percent of viability, 100-200 µl of cell suspension was taken, stained with Trypan Blue and were counted using the hemocytometer. The cell suspension was centrifuged at 1000 rpm for 5 minutes, and then the supernatant was aspirated and cells were resuspended by the addition of fresh medium according to the total cell number. The recommended amount of cells (approximately 2-4 x 10^5 viable cells/ml) were seeded into the new labeled cell culture plate and incubated at 37°C, 5% CO2. These processes were repeated when cell concentration reaches 8x10^5 cells/ml.

Cell freezing and thawing protocols were performed as same in adherent cell culture methods.

3.6.2. *Monolayer Differentiation of THP-1 into Macrophages-like with PMA*

Phorbol 12-myristate 13-acetate (PMA, Sigma-Aldrich, P8139) was used to the differentiation of suspended human monocytic THP-1 cells to the adherent macrophage-like state (M0). The cells were treated with different concentrations of PMA to determine the optimal PMA concentration to be used in the experiment. After cells were counted with the hemocytometer, the cells were seeded in 24-well plates at a density of 2 x 10^5 cells/well in 1 ml complete RPMI at a concentration of 10, 50, 150 and 200 ng/ml for 24 hours and 48 hours incubation. After 24 hours and 48 hours, the

cells adhered in the bottom of the 24-well plate were examined under a phase-contrast microscope and images were obtained. We used 10 ng/ml, the lowest concentration in the differentiation of THP-1 cells, in experiments. After 24h differentiation, PMA medium was removed and added the complete medium on THP-1 cells and they were incubated for 48h.

3.6.3. *Hydrogel Synthesis*

Gelatin-based photocrosslinkable hydrogel, Gelatin-methacryloyl (GelMA), used in the thesis study has been prepared in three steps.

3.6.3.1. Reaction Step

In order to achieve a final hydrogel concentration of 10% (wt/v), 50 ml of 1X PBS was heated to 50 °C in a heated magnetic stirrer and 5 grams of gelatin from porcine skin Type A (Sigma-Aldrich, G6144-100G) or gelatin from bovine skin Type B (Sigma-Aldrich, G9382-100G) was weighed on a precision scale. The gelatin was added slowly into the PBS on the stirrer to dissolve completely, and the solution was stirred for about 1 hour until the solution became clear. After this step, for each 1 gram of gelatin, 2 ml of methacrylic anhydride (MAA, Sigma-Aldrich, 276685-100ML) was used, in total 10 ml of methacrylic anhydride were added dropwise into the solution, the addition of MAA was divided into 5 different times with an average of 10 min between each addition. And then the solution was stirred for 4 hours at 40 °C. As the organic solvents such as methacrylate is cytotoxic and could be dissolved plastic pipettes, so glass pipette was used in the addition step and was worked in a fume hood to minimize inhalation damage. After the methacrylate reaction step, preheated to 40 °C 200 ml of Ultrapure water or PBS was added to the solution to the ratio of dilution 1:5. The

solution was then transferred to 50 ml falcon tubes and centrifuged at 3500 g for 10 min at RT to remove unreacted methacrylate.

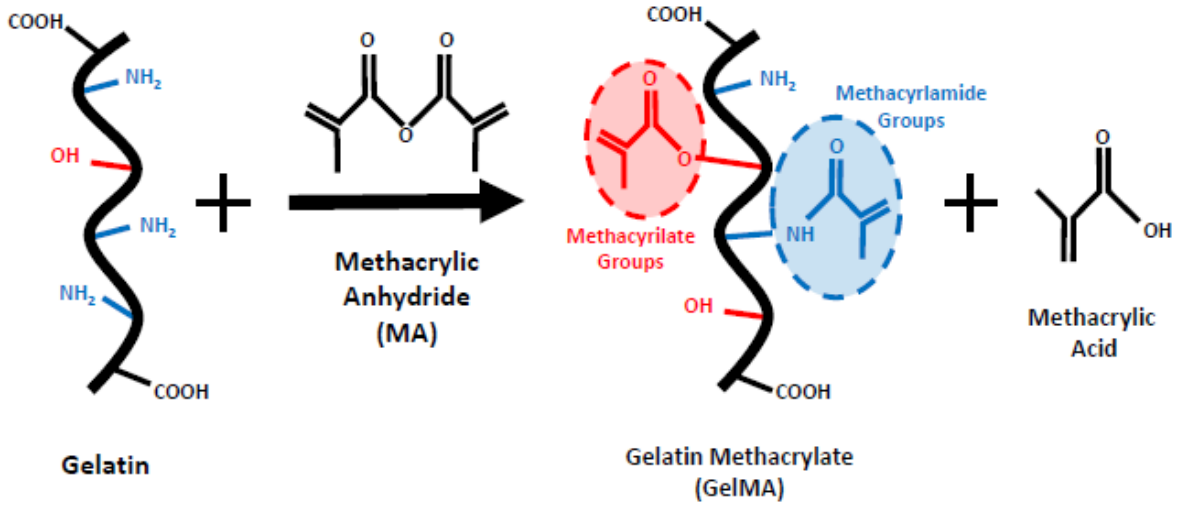

Figure 5: GelMA synthesis reaction step.

3.6.3.2. Dialysis Step

After centrifugation, the supernatant was transferred to the dialysis membrane (Membra-Cel, 14-kDa MWCO). Dialysis process was performed in a plastic bucket with 5L Ultrapure water at 85 rpm at 40 °C on shaker as shown in the Figure 6 and the process was continued until no methacrylate was present in the solution. The ultrapure water in the plastic bucket was changed every day. Aluminum foil was used as an indicator to see extra unreacted methacrylate in dialysis. If the color of the aluminum foil during dialysis turns brownish-blackish, there is still too much methacrylate in solution (Figure 7). Dialysis continued until the color of the aluminum foil remained unchanged and the pH of the solution was 7-8.

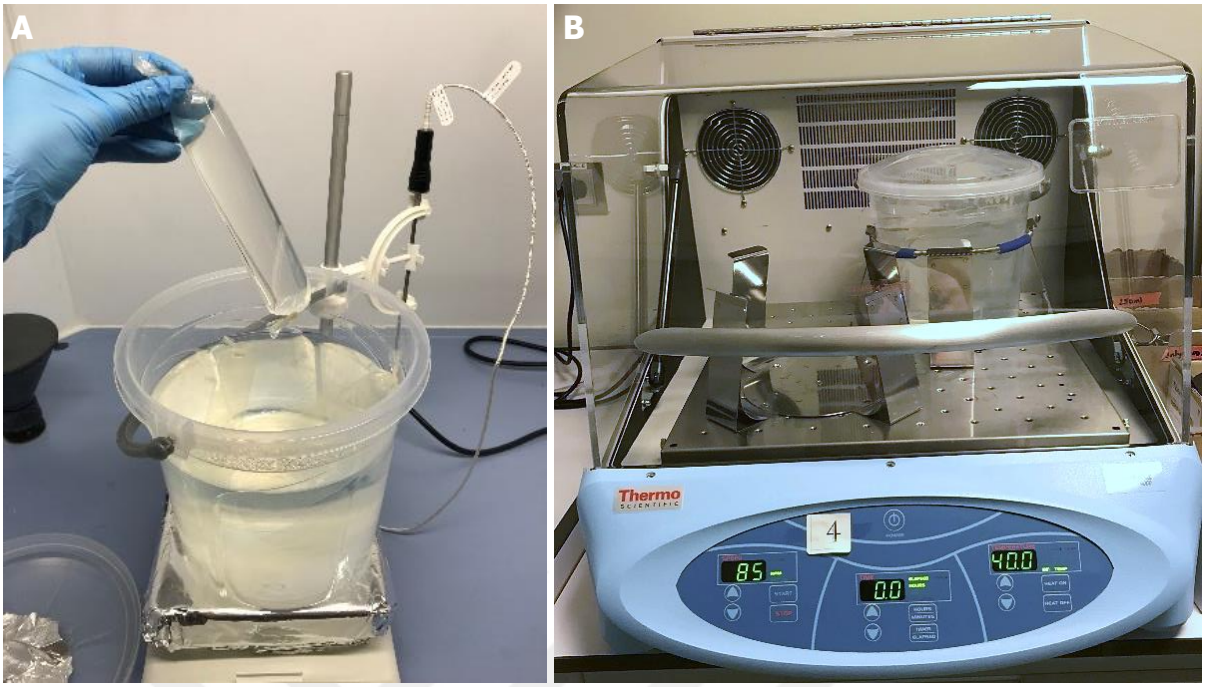

Figure 6: Dialysis step of GelMA. A) Hydrogel filled in dialysis membrane in Ultrapure water. B) Dialysis of GelMA in the plastic bucket on the shaker at 85 rpm, 40 °C.

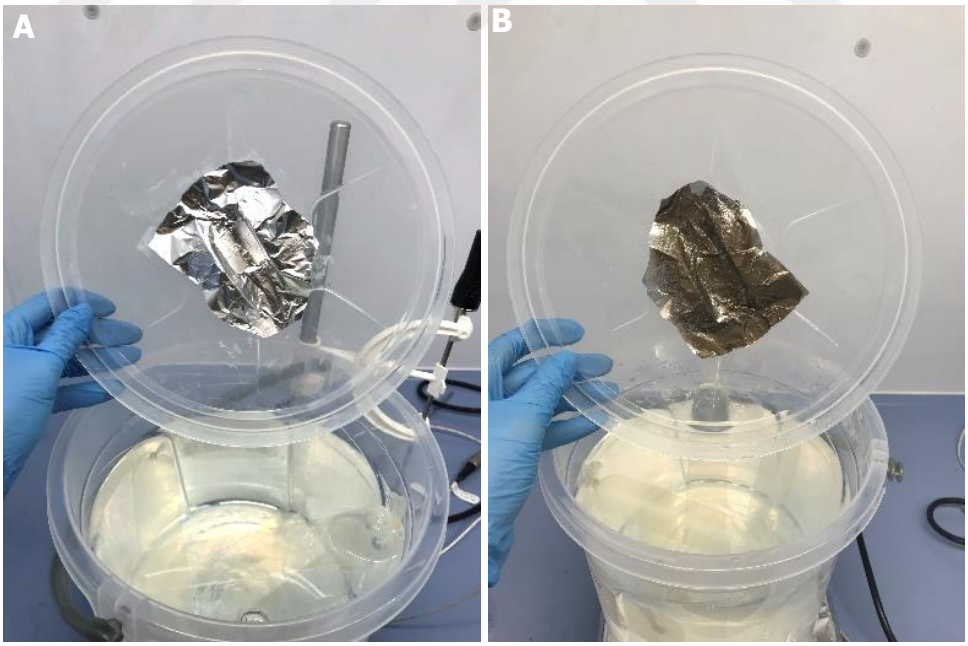

Figure 7: Changing the color of aluminum foil during the dialysis process. A) The color of the aluminum foil after changing the water of GelMA. B) The color of aluminum foil when excess methacrylate in GelMA.

3.6.3.3. Lyophilization Step

After the dialysis step was completed, the GelMA solution was aliquoted into 50 ml falcon tubes and frozen at -80 °C for 2 days. And then, these falcon tubes were transferred to the freeze-dryer and lyophilized them until the GelMA is fully dehydrated (approximately 5-7 days) (Figure 8). Lyophilized GelMA was stored at -20 °C until used.

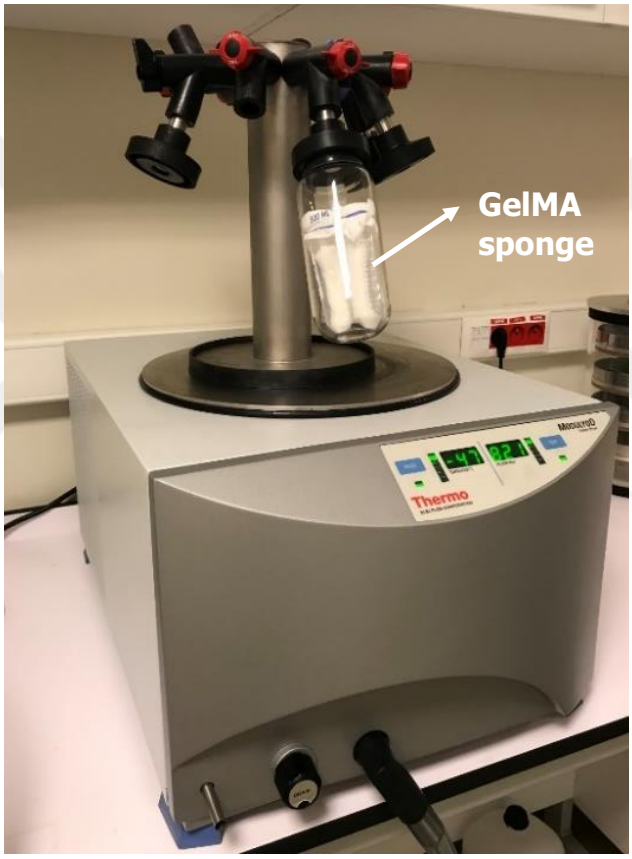

Figure 8: Lyophilization step of GelMA.

3.6.4. *Fabrication of Photomasks and Microfluidic Systems*

Based on the principles of fluid mechanics, microfluidic chips were designed that allows two different liquids to flow through the same channel without mixing each other. Microfluidic chips were designed using engineering software such as Corel Draw. Poly(methyl methacrylate) (PMMA) sheets and double-sided adhesive tape with a thickness of 0.13 mm (3M™ High-Performance Acrylic Adhesive Transfer Tape 468MP) were cut to designed size with a high-resolution laser cutter (Epilog Mini 18 Laser 30-Watt). When assembling the microfluidic chip pieces, reference holes were designed and opened at the edges of the chip to prevent any errors. The microfluidic chip pieces were sterilized before assembling. After cutting in the laser cutter as shown in the Figure 9, the white protective gelatin on the PMMA was removed in the laminar flow cabinet. Then these pieces were washed with 70% ethanol, allowed to dry and then allowed to stand for 20 minutes under Ultraviolet (UV) light to sterilize. After that, the pieces were manually assembled on the platform which is prepared with syringe needles (Figure 10). In order to validate that there was no leakage in the microfluidic chips before the use in the experiment, the leakage test was performed by using food dye.

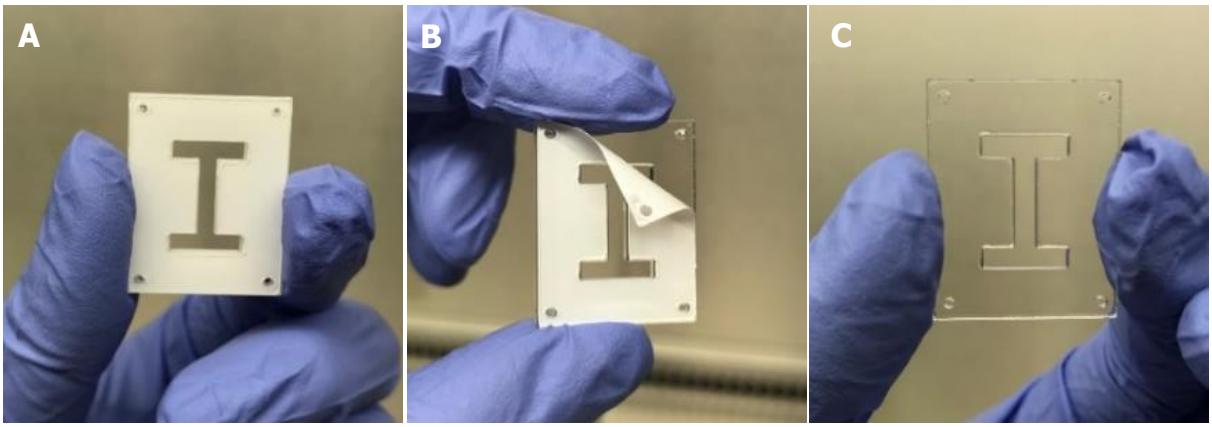

Figure 9: Microfluidic chip sterilization.

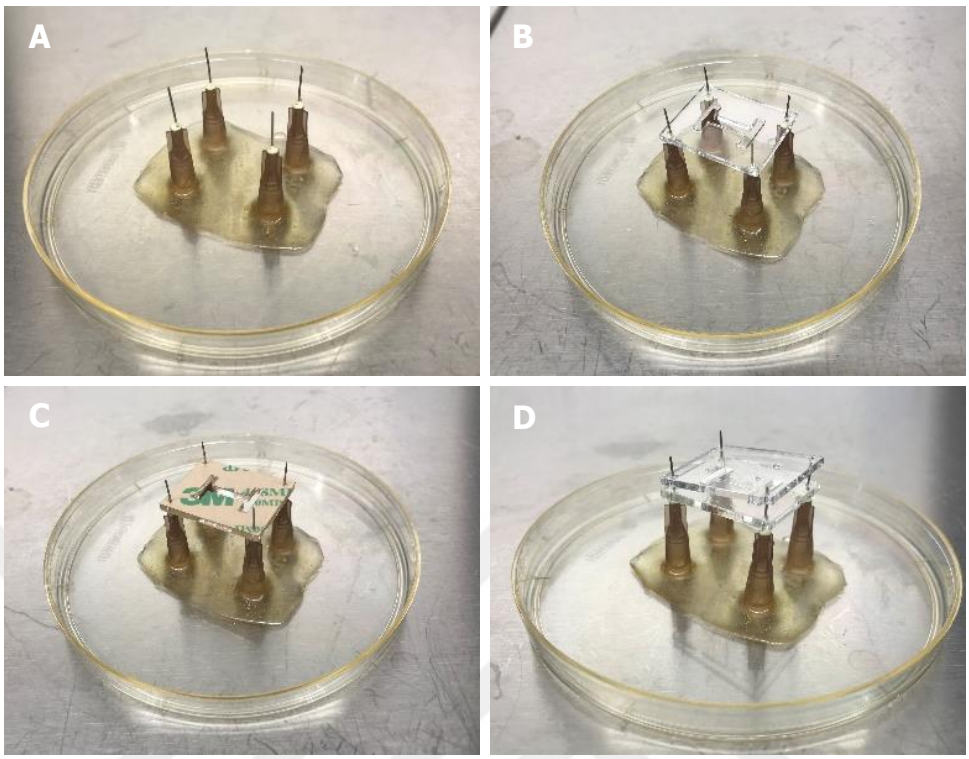

Figure 10: Microfluidic chip assembly. A) The platform which is allows to precise assembling for the microfluidic chip. B-D) Assembling the chip parts one by one.

Photomasks were also designed using engineering software Corel Draw. Different type of photomasks such as vertical lines, small squares or circles, nested frames, and circles or zigzag shape were designed to be 22x22 mm in sizes. After designing, the photomasks were printed on acetate paper (Figure 11).

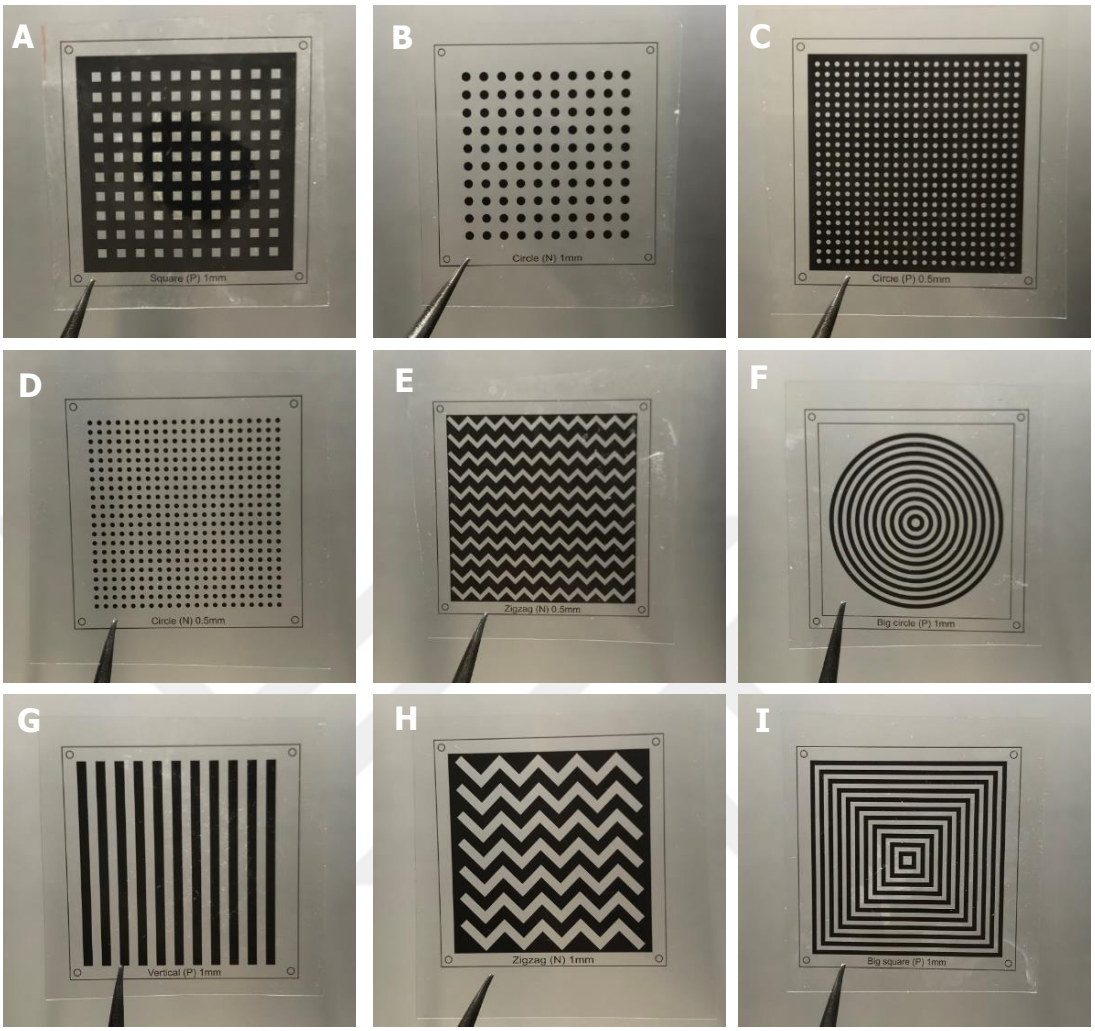

Figure 11: Various designed photomasks. A) Square 1 mm. B) Circle 1 mm. C) Circle 0,5 mm. D) Circle 0,5 mm. E) Zigzag 0,5 mm. F) Big circle 1 mm. G) Vertical 1 mm. H) Zigzag 1 mm. I) Big square 1 mm.

3.6.5. *Encapsulation of Cells and 3D Cell Culture*

3.6.5.1. 3D Static Culture

Firstly, a photo-initiator (PI) solution was prepared for GelMA to be crosslinked under UV light. The photo-initiator (2-hydroxy-1- (4-(hydroxyethoxy) phenyl)-2-methyl-1-propanone photo-initiator) (Sigma, 480896 - 10G) was weighed in a precision balance of 0.5% (wt/v) and dissolved in pre-warmed 1X PBS. Vortex was used to completely dissolve the solution. After this, the lyophilized GelMA was weighed on the precision balance and mixed with the photo-initiator solution to be 5% (wt/v). Thus, the precursor solution was prepared to give the cells a 3D structure. The precursor solution was sterilized using a 0.22 µm syringe filter before mixing with the cells. N9 cell density was counted as $7x10^6$ cells/ml and THP-1 cell density was counted $7x10^6$ cells/ml and they were centrifugated. After centrifugation, the supernatant was vacuumed and the cells mixed and resuspended with the precursor solution in a laminar flow cabinet. In 3D static cell culture, the cells were encapsulated onto the coverslip. As shown in the Figure 12, firstly two 150 µm thick coverslips were glued on the sterile petri dish with a distance of less than 22 mm to each other to give a 150-µm height to the cells. The coverslip was placed on these two spacers and the mixture of the cell-precursor solution was placed in the space between the coverslip and the petri dish. Preferred Photomask was placed on the coverslip and was cross-linked under UV light (1 mW/cm^2) for 60 seconds. Coverslip was taken over the spacer with tweezers, and the non-cross linked cell-precursor solution remaining on the photomask's opaque side was washed with PBS. Finally, cells encapsulated onto the coverslip were placed in the well-plate and medium or stimulating medium was added to the wells.

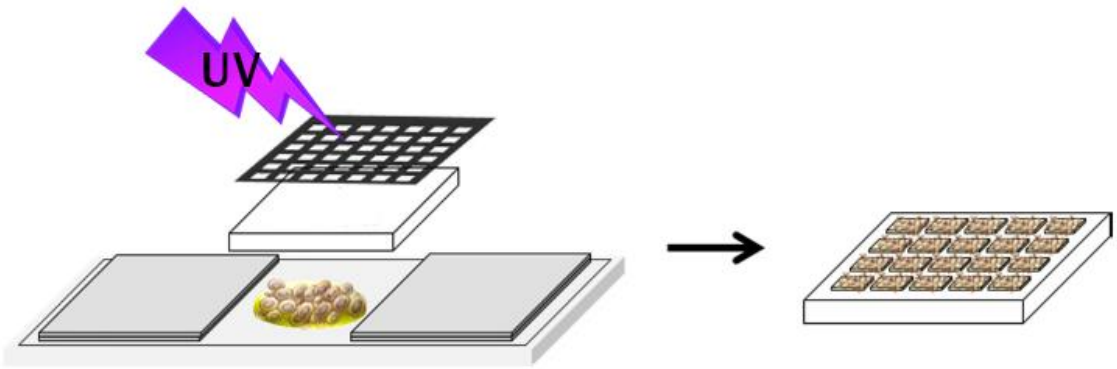

Figure 12: Schematic representation of encapsulation with using a spacer.

3.6.5.2. 3D Dynamic Culture

In the same way, as in 3D static cell encapsulation, photo-initiator, cell-precursor solutions, and cell density were prepared. The cells were encapsulated into the microfluidic chip. The cell-precursor solution was encapsulated in a 100 µl volume of H-filter microfluidic channel and a single channel for 60 seconds under UV light (1 mW/cm^2). After encapsulation, the tubing (Cole-Parmer Tygon, AAD0291-CP) used to provide continuous flow to the microfluidic chips were glued to the inlet and outlet with epoxy (Diall, 1000195195). After the epoxy dried, the microfluidic chips were ligated to the syringes using the insulin needle tip and continuous flow was achieved in the syringe pump (Figure 13). Firstly, the flow rate was set for 100 µl/min to test the flow and leakage, and then the flow rate was set up for 10 µl/min for 4 hours polarization and 0.5 µl/min for 24 hours polarization.

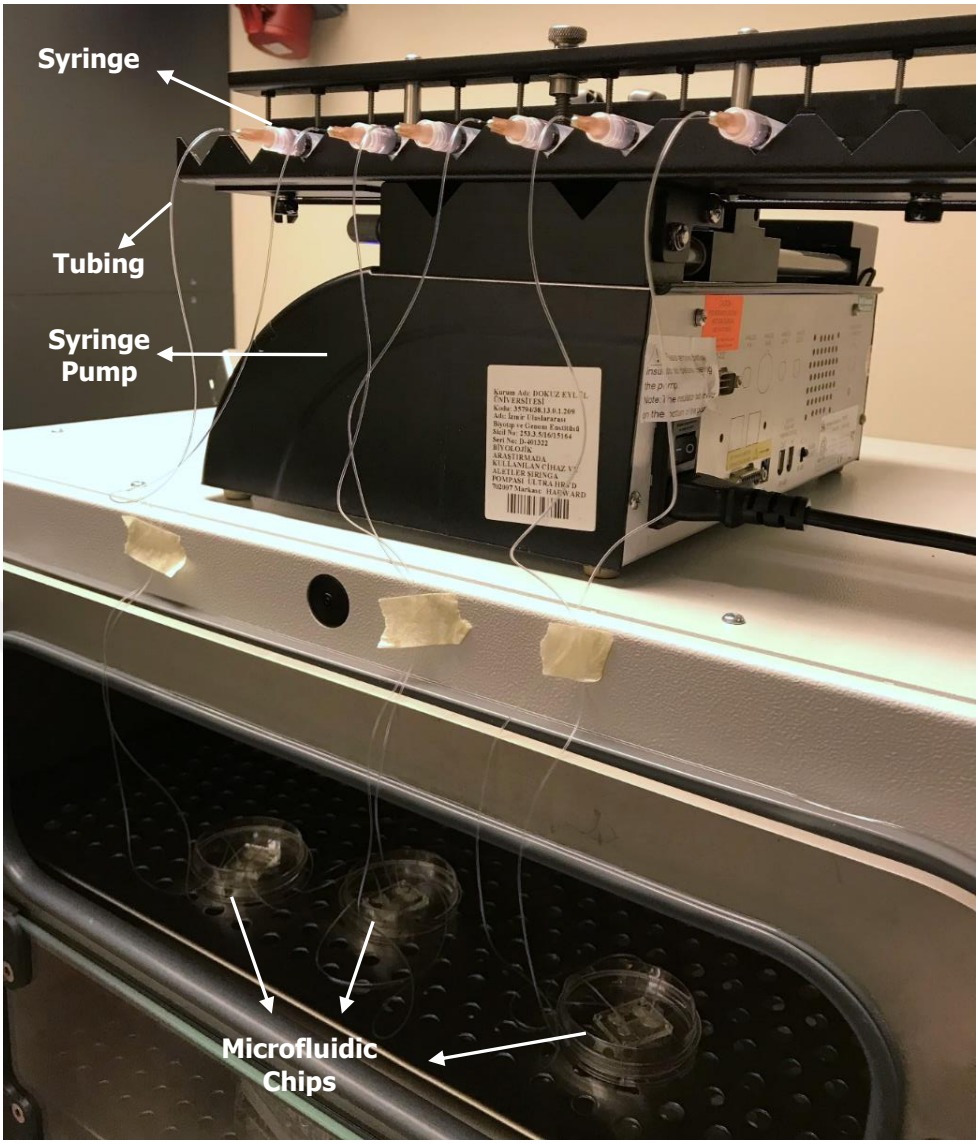

Figure 13: Microfluidic/tubing/ Syringe pump.

3.6.6. *Polarization of Cells*

3.6.6.1. The Polarization of N9 Cells to M1 and M2

Mouse microglia N9 cells were seeded on a 2D cell culture plate to be 1.6 x 10^5 cell/cm^2 and stimulated with Lipopolysaccharides (LPS, Escherichia coli O111:B4, Sigma-Aldrich, L4391) at a concentration of 100 ng/ml for 4 hours and 24 hours to generate M1 polarization. To generate M2 polarization, cells were seeded on a 2D cell

culture plate and stimulated with Interleukin-4 (IL-4, Peprotech, 200-04) at a concentration of 10 ng/ml for 4 hours and 24 hours.

For polarization of 3D static culture, N9 cells were resuspended in the hydrogel to be 7 x 10^6 cells/ml and printed on the coverslip with using photomask. Cells were stimulated with LPS at a concentration of 100 ng/ml for 4 hours and 24 hours to generate M1 polarization. To generate M2 polarization, cells were encapsulated on a coverslip and stimulated with IL-4 at a concentration of 10 ng/ml for 4 hours and 24 hours.

For polarization of 3D dynamic culture in a microfluidic chip, N9 cells were resuspended in the hydrogel to be 7 x 10^6 cells/ml and they encapsulated in a microfluidic channel. The polarization of M1 and M2 were provided by syringe pump flow. Cells were stimulated with LPS at a concentration of 100 ng/ml for M1 polarization and IL-4 at a concentration of 10 ng/ml for M2 polarization, with at a flow rate of 10 µl/min for 4 hours and with at a flow rate of 0.5 µl/min for 24 hours.

3.6.6.2. The Polarization of THP-1 Cells to M1 and M2

Human monocytic THP-1 cells firstly turn into a macrophage-like state with 10 ng/ml PMA containing medium, cells were seeded on a 2D cell culture plate to be 1.6 x 10^5 cell/cm^2 and incubated for 24 hours. After that, the supernatant was vacuumed and we added the complete medium on M0 THP-1 cells and incubated for 24 hours. stimulated with LPS at a concentration of 100 ng/ml and Interferon-gamma (IFN-γ, Peprotech, 500-P32) at a concentration of 20 ng/ml for 4 hours and 24 hours to generate M1 polarization. To generate M2 polarization, cells were seeded on a 2D cell culture plate and stimulated with IL-4 at a concentration of 20 ng/ml and Interleukin-13 (IL-13, Peprotech, 200-13) at a concentration of 20 ng/ml for 4 hours and 24 hours.

M0 THP-1 cells were resuspended in the hydrogel to be 7 x 10^6 cells/ml and printed on the coverslip with using photomask for the polarization of 3D static culture. Cells were stimulated with LPS at a concentration of 100 ng/ml and IFN-γ at a concentration of 20 ng/ml for 4 hours and 24 hours to generate M1 polarization. To generate M2 polarization, cells were printed and stimulated with IL-4 at a concentration of 20 ng/ml and IL-13 at a concentration of 20 ng/ml for 4 hours and 24 hours.

For polarization of 3D dynamic culture in a microfluidic chip, M0 THP-1 cells were resuspended in the hydrogel and they encapsulated in a microfluidic channel. The polarization of M1 and M2 were provided by syringe pump flow. Cells were stimulated with LPS at a concentration of 100 ng/ml and IFN-γ at a concentration of 20 ng/ml for M1 polarization and IL-4 at a concentration of 20 ng/ml and IL-13 at a concentration of 20 ng/ml for M2 polarization, with at a flow rate of 10 µl/min for 4 hours and with at a flow rate of 0.5 µl/min for 24 hours.

3.6.7. *Characterization of Hydrogel and Cells*

3.6.7.1. Hydrogel Characterization

In this thesis study, scanning electron microscopy (SEM) was used for the characterization of the morphological properties and Fourier transform infrared (FTIR) spectroscopy was used for the characterization of the chemical bonds of the synthesized hydrogel.

Scanning Electron Microscopy (SEM)

We used the SEM analysis to show that the GelMA has a porous structure. Firstly, we mixed the synthesized GelMA with 0.5 % PI solution and crosslinked under UV light for 60 seconds. Then the crosslinked hydrogel was frozen at -80 °C for 24 hours. The frozen hydrogel was then lyophilized for 24 hours. We divided Freeze-dried GelMA into small pieces to fit into the platform of the SEM with the help of a sterile surgical blade. The porous surface of the samples was placed facing upwards on the platform with double-sided carbon band and the surface was covered with a thin layer of gold (platinum). The process of placing on the platform, covering the surface with gold and taking the images was done by the electron microscope core facility specialist.

Fourier transform infrared spectroscopy (FTIR)

We used the FTIR spectroscopy to characterized the specific chemical bonds in the hydrogel which is synthesized by our team and composition of samples before and after photocrosslinking. We have four different samples. Control group is Bovine gelatin in powder form used in the hydrogel synthesis, the other group is sponge form synthesized GelMA, another group is GelMA and the photoinitiator mixture solution, and the final group is the freeze-dried form of GelMA after photocrosslinking under the UV light. The freeze-dried form after the crosslinking was prepared as same in the SEM analysis and divided into appropriate sizes on the rack of FTIR device. FTIR analysis was performed by Perkin Elmer Spectrum AUTR Two Spectrometer. the spectra were collected at in the wavelength range of between 400-4000 cm^{-1} after 4 scans.

3.6.7.2. Cell Characterization

In this thesis, we used the qPCR method to perform nucleic acid amplification and gene expression analysis. We performed gene expression analysis in four steps which are RNA isolation, cDNA synthesis, primer design, and qPCR analysis. Also, we used the immunocytochemistry techniques to cell characterization.

RNA Isolation

We used both the Trizol (Invitrogen, 15596026) and RNA isolation kit (Macherey-Nagel, NucleoSpin RNA XS, 740955.50) in the RNA isolation protocol. First, we aspirated the medium in the culture plate and washed the cells by adding cold 1X PBS. After the PBS was aspirated, we added Trizol (about 1 ml for 106 cells) to lysate the cells and scraped the monolayer cell or the 3D cells from the culture platform surface by using a cell scraper. After that, the cells were transferred to the 2 ml eppendorf and the cell lysate was thoroughly pipetted and vortexed to homogenize the cells and then incubated at RT for 5 min to allow the complete dissociation of nucleoprotein complexes. After that, we added 0.2 ml of chloroform per 1 ml of Trizol and shook the eppendorf vigorously for about 20 seconds and incubated them at the RT for 2-3 min. After the incubation step, we centrifuged the sample at 12000 g for 15 min at 4 °C to phase separation. After centrifugation, the mixture was separated into three phases as shown in Figure 14 which are an organic phase, interphase, and an aqueous phase. The red-pink colored bottom layer phase is the organic phase containing proteins and lipids. The middle white layer is the interphase which is containing the DNA and the colorless top layer is an aqueous phase that is containing the RNA. We transferred the RNA in the aqueous phase to a new DNase, RNase-free eppendorf. At this step, we care was taken to remove the RNA in the aqueous phase without interfering with the DNA in the middle phase. Because if the pipette tip is white, RNA is contaminated with DNA. We transferred the RNA in the aqueous phase to a new eppendorf using a 200

µl pipette. At this step, we carefully transferred the RNA in the aqueous phase avoiding the touch the DNA in the middle white phase. Because if the pipette tip touched the white phase, RNA is contaminated with DNA. We measured the volume of the aqueous phase and added the 70 % ethanol the same volume of the aqueous phase to wash the RNA. We mixed the samples by pipetting up and down and incubated at RT for 10 min.

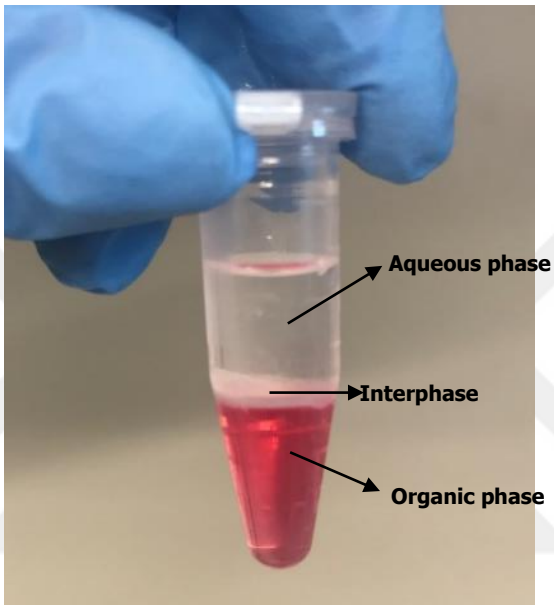

Figure 14: Phases of RNA isolation.

From this step, we used the RNA isolation kit protocol. We placed the NucleoSpin RNA XS Column (Light blue ring) in the collection tube and loaded the lysate to the column and then centrifugated for 30 s at 11000g to binding the RNA. Column maximum loading capacity is 600 µl so when we had larger volumes of samples, we repeated the binding RNA step. To desalt the silica membrane, we added the 100 µl Membrane Desalting Buffer and centrifuged at 11000g for 1 min. After this step, we prepared the rDNase reaction mixture in a new sterile eppendorf and we added 25 µl mixture directly onto the center of silica membrane of the column and then was incubated at RT for 15 min to digest the DNA. To wash and dry the silica membrane, we added buffer solutions and centrifuged at 11000 g for 30 s. These processes were repeated 3 times. Finally, in order to obtain pure RNA, we added 60 µl RNase-free

water into the column and centrifuged at 11000 g for 30 s. Thus we have obtained a total of 60 µl RNA. After the isolation protocol was completed, we quantified the RNA quality and concentration by spectrophotometry with the Nanodrop apparatus. The ratio of the absorbance at 260 and 280 nm (A260/280) and (A260/230) are used to assess the purity of RNA. The A260/280 ratio of pure RNA is about 2. Values of less than 1.8 indicate DNA or protein contamination. The A260/230 ratio should also be above 2.

Complementary DNA (cDNA) Synthesis

We used the cDNA kit (ABM, OneScript Plus cDNA Synthesis Kit, G236) protocol in cDNA synthesis. The isolated RNA and all reagents of kit were thawed on ice. Firstly, we made calculations based on the concentration of RNA isolated. If the RNA concentration is too low, the calculation is made so that the lowest suitable amount of the cDNA is 100 ng. According to the calculations, 1 µl Random Primers (10 µM), 1 µl dNTP Mix (10 mM), the calculated amount of RNA, and Nuclease-free water were added until the total was completed to 14.5 µl into the PCR tube. We set up the thermal cycler 65 °C and this mixture heated for 5 minutes and then immediately incubated on ice for 1 minute. After incubation, we added to the mixture 4 µl of 5X RT Buffer, 0.5 µl of RNaseOFF Ribonuclease Inhibitor and 1 µl of OneScript® Plus RTase. Thus, we have obtained a total of 20 µl mixture. We spin-down the mixture in a mini-centrifuge and then we set up the thermal cycler and incubated the mixture respectively 25 °C for 10 minutes, 50 °C for 50 minutes and finally to stop reaction 85 °C for 5 minutes. The newly synthesized cDNA was stored at -20 °C.

Primer Design

Primers used in this thesis for evaluation of cell polarization are based on published literature and several parameters have been considered during their design. One of these parameters is the primer length. Primer length generally was chosen 18-25 bp. Because it affects the annealing temperature of the primers in the longer or shorter base pairs. Another parameter is the primer melting temperature which is important for hairpins. The melting temperature should be lower than the annealing temperature range between 55°C and 65°C. Primer pairs should have similar Tm's. The other parameter is the GC content, which is the ratio of the number of G and C in the primer sequence to the total bases. Ideal GC content should be between 40 % and 60 %. Another issue is avoiding primer dimers. We used the Primer-BLAST and UCSC in-silico PCR database to verify the designed primers. For mouse and human cells housekeeping gene is Glyceraldehyde 3-phosphate dehydrogenase (GAPDH). For mouse cells, M1 polarization markers are TNF-α, IL-6, iNOS, and IL-1β, and M2 markers that are Arg-1, Ym-1, CD206, and IL-10. For the human cells, M1 markers are IRF5, TNF-α, IL-6, and iNOS, and M2 markers are CD206, IL-10, CCL17, and CCL22. All primers shown in Table 3 are synthesized by Oligomer Biyoteknoloji, Ankara. Primers were diluted to 100 µM using nuclease-free H2O in the amounts recommended by the company and they were stored at -20 °C after dilution.

Table 3: Primer Sequences for M1/M2 Polarization in mouse and human.

Gene	Organism	Forward Sequence (5′→3′)	Reverse Sequence(3′→5′)
IL-6	mouse	CCCCAATTTCCAATGCTCTCC	CGCACTAGGTTTGCCGAGTA
TNF- α	mouse	GTGCCACTTCATACCAGGAGAA	TCACAGACGAATGACTCCAA
iNOS(NOS2)	mouse	CCCTTCAATGGTTGGTACATGG	ACATTGATCTCCGTGACAGCC
IL-1β	mouse	CACAGCAGCACATCAACAAG	GTGCTCATGTCCTCATCCTG
Arg1	mouse	CTTGGCTTGCTTCGGAACTC	GGAGAAGGCGTTTGCTTAGTTC
Ym1	mouse	AGAAGGGAGTTTCAAACCTGGT	GTCTTGCTCATGTGTGTAAGTGA
CD206 (MMR/Mrc1)	mouse	CAGGTGTGGGCTCAGGTAGT	TGTGGTGAGCTGAAAGGTGA
IL-10	mouse	AAGGGTTACTTGGGTTGCCA	CCTGGGGCATCACTTCTACC
IRF5	human	CCAGCCAGGACGGAGATAAC	CATCCACGCCTTCGGTGTAT
IL-6	human	ACTCACCTCTTCAGAACGAATTG	CCATCTTTGGAAGGTTCAGGTTG
iNOS(NOS2)	human	ATTCACTCAGCTGTGCATCG	TCAGGTGGGATTTCGAAGAG
TNF- α	human	GAGGCCAAGCCCTGGTATG	CGGGCCGATTGATCTCAGC
IL-10	human	TACGGCGCTGTCATCGATTT	TAGAGTCGCCACCCTGATGT
CD206(MMR/MRC1)	human	CTACAAGGGATCGGGTTTATGGA	TTGGCATTGCCTAGTAGCGTA
CCL22	human	ATTACGTCCGTTACCGTCTG	TAGGCTCTTCATTGGCTCAG
CCL17	human	CGGGACTACCTGGGACCTC	CCTCACTGTGGCTCTTCTTCG
GAPDH	human & mouse	ACCACAGTCCATGCCATCAC	TCCACCACCCTGTTGCTG TA

Quantitative Polymerase Chain Reaction (qPCR)

SYBR-Green protocol has been used to perform the qPCR. We prepared the white 96well-plate to be 10 µl per well (5 µl mastermix (Promega, GoTaq A6001), 2 µl nuclease-free H2O, 1 µl forward primer, 1 µl reverse primer, 1 µl cDNA). For each condition, three repetitive experimental plans are prepared. For example, to detect the TNF-alpha gene the plate was prepared three wells contain control cDNA and 3 wells contain M1 cDNA, 3 wells contain M2 cDNA. The prepared plate was detected in Roche Lightcycler 480. The protocol used is shown in Table 4.

CT values obtained from each reaction were analyzed according to the ΔΔCT method. First, the ΔCT values of the CT_{mRNA} - CT_{GAPDH} formula were calculated using Excel (Microsoft, USA). Average $\Delta CT_{control}$ values were calculated and in order to determine the change in expression ΔΔCT values, $\Delta CT_{control}$ - ΔCT_{M1}, $\Delta CT_{control}$ - ΔCT_{M2} values were calculated according to the formula and $2^{-\Delta\Delta CT}$ formula was used to calculate fold change rates.

Table 4: qPCR run protocol.

Program	**Cycle**	**Temperature (°C)**	**Time (s)**
Pre-incubation	1	95	120
PCR	40	95	10
		60	10
		72	30
Melting	1	95	10
		65	30
Cooling	1	40	30

Immunocytochemistry Assay (ICC)

Immunocytochemistry assay is a commonly used technique to detect the expression of a target protein or antigen in cells by using a combination of specific primary and secondary antibodies. We used the Mouse-iNOS Monoclonal Antibody (4E5) (Invitrogen, MA5-17139) unconjugated antibody and Rabbit-Cyclooxygenase 2 Polyclonal (COX2) unconjugated antibody (Bioss-USA, BS-0732R) to characterize the M1 phenotype cells. Also, we used the Rabbit-CD163/M130 Polyclonal (Bioss-USA, BS-0732R) unconjugated antibody and Mouse-CD206 (MMR) (Santa Cruz, sc-58986) unconjugated antibody to characterize the M2 phenotype cells. We diluted the COX2 and CD163 primary unconjugated antibodies in staining buffer at a ratio of 1:100. The primary antibody binds to a secondary antibody conjugated to the fluorophore so that is allowing the target molecule to be seen under a fluorescence microscope. We dissolved the conjugated secondary antibody Alexa Fluor® 594 AffiniPure Donkey Anti-Rabbit IgG (H+L) (Jackson Immunoresearch, 711-585-152) was dissolved in sterile 400 µl dH20 and aliquoted. We diluted the Donkey Anti-Rabbit antibody in staining buffer PBS at a ratio of 1:500.

After stimulation of the cells, we fixed the cells at room temperature for 20-30 minutes with 4% paraformaldehyde (PFA). Then, the PFA was withdrawn by vacuum, and we washed the fixed cells 3 times with PBS. For permeabilization of the cell membrane, we added the staining buffer containing 1% BSA (w/v) and 0.3% Triton-X100 (v/v) in PBS and incubated overnight at +4 °C. Again we washed the cells 3 times with PBS. After that, we added the primary antibody and they were incubated overnight. The target molecule is recognized by the primary antibody. The primary antibody solution was withdrawn with vacuum and we washed the cells 3 times with 0.1% BSA solution in PBS to remove unbound primary antibody. After that, we added the diluted secondary antibody to the cells and were incubated 2 hours at room temperature or overnight at +4 °C.

3.7. Research Plan

	September 2016 - December 2017	January 2018 – December 2018	January 2019 – May 2019
Literature Review	X	X	X
Planning the Experiment		X	X
Data Collection and Experiments		X	X
Evaluation of data			X
Thesis Writing			X

3.8. Evaluation of Data

Within the scope of this thesis study, GraphPad Prism 7.1 program was used to analyze the findings. Results are presented in the mean ± standard error format. Mann-Whitney U test and ANOVA (two way) were used for statistical analysis. $P < 0.05$ was accepted to be statistically significant.

3.9. Limitation of Research

In case of that, the gelatin-based hydrogel cannot be produced properly; Poly (ethylene glycol) diacrylate (PEGDA), alginate or agarose will be used as an alternative biopolymer. In case of a leakage in PMMA microfluidic chips, Polydimethylsiloxane (PDMS) silicon-based microfluidic system will be used as an alternative system.

3.10. Ethics Committee Approval

Ethics committee approval is not required for this thesis.

4. RESULTS

4.1. SEM Imaging of GelMA Hydrogel

GelMA hydrogels prepared from %5 GelMA in 1X PBS mixed with a 0.5% photoinitiator were crosslinked with UV light, power of 4, for 60 seconds. After crosslinking, the gels were lyophilized for 24 hours, coated with gold and imaged with, SEM at 600X magnification Figure 15.

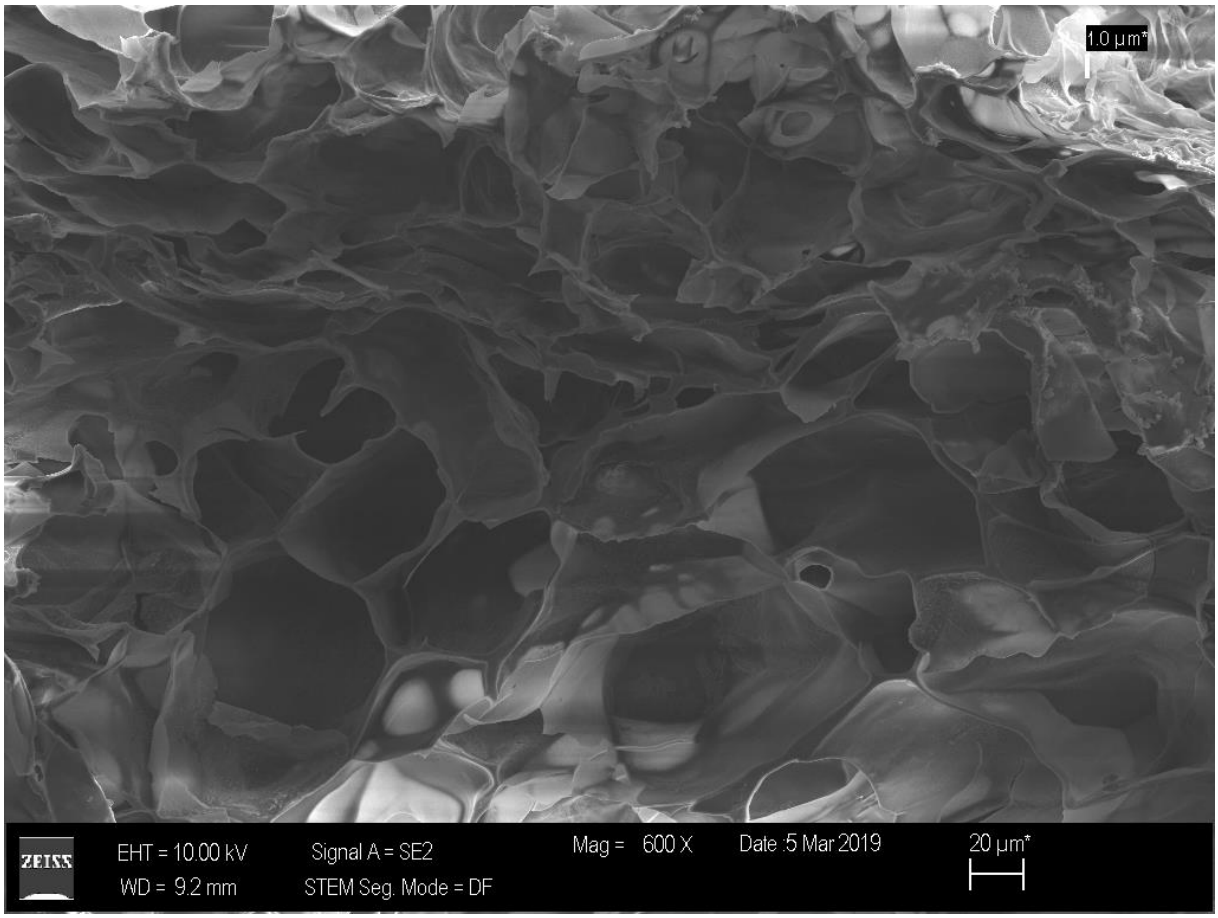

Figure 15: SEM image of 5% GelMA under UV light for 60 seconds.

4.2. FTIR Spectrum of GelMA

Chemical structure of gelatin and GelMA were characterized by FTIR analysis and their spectra were shown in Figure 16 and 17.

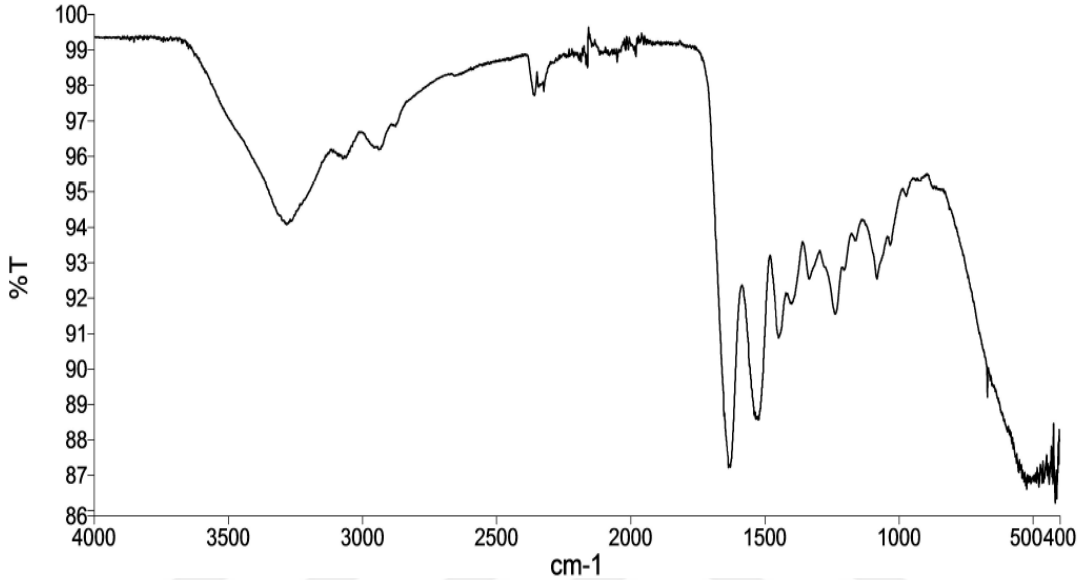

Figure 16: Standard powder gelatin FTIR spectrum.

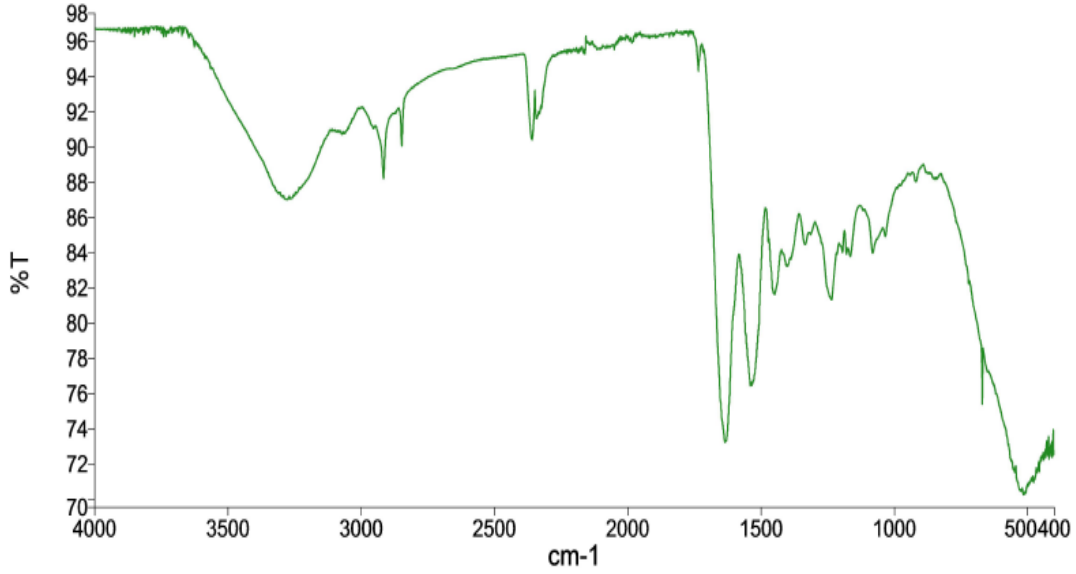

Figure 17: Crosslinked GelMA (%5) FTIR spectrum.

4.3. Fabrication and Validation of the Microfluidic Systems

Microfluidic system pieces were cut from the PMMA layers with high precision laser cutter according to the dimensions specified in Figure 18 and Figure 19. After pieces of the chip were cut and sterilized they were assembled using the double-sided adhesive tape. Before cell encapsulation into the microfluidic channels, chips were tested for leakage and proper H-filter function using food dyes. In Figure 20, the red and blue food dyes flow through the channel without a membrane in the channel and without mix each other.

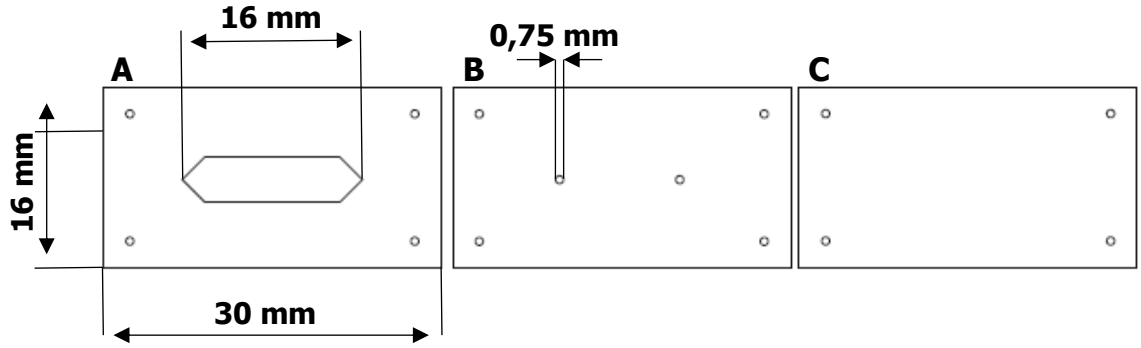

Figure 18: Schematic representation of Single Channel microfluidic platform.

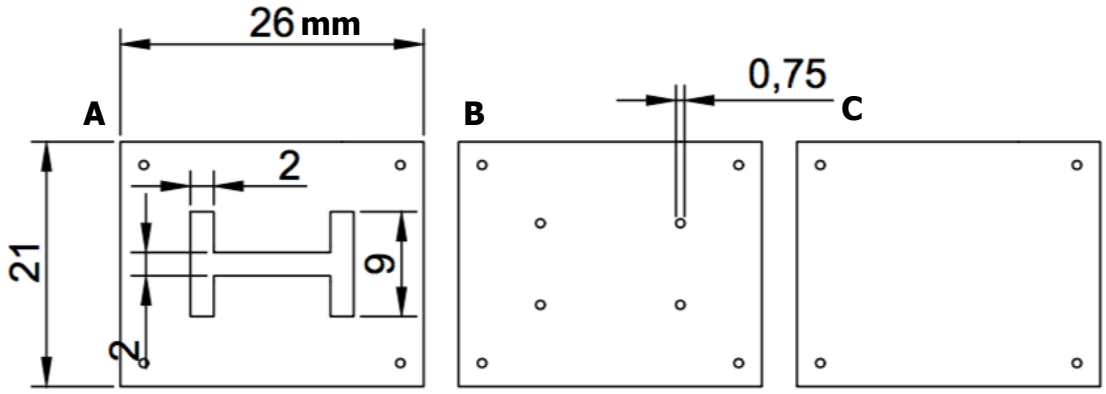

Figure 19: Schematic representation of H-filter microfluidic platform.

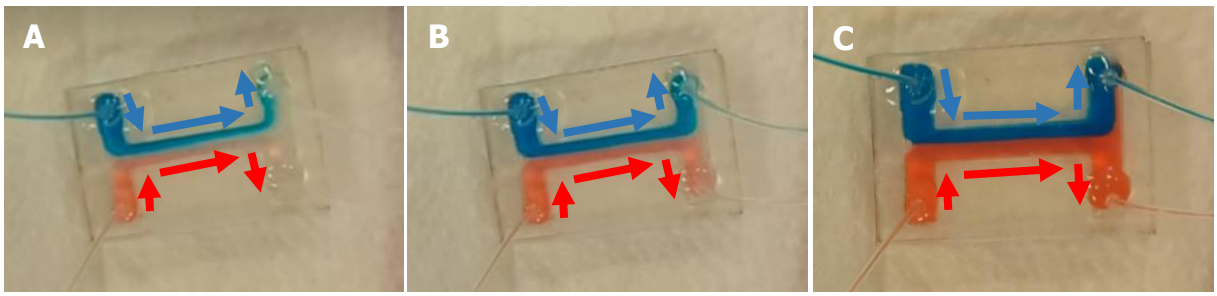

Figure 20: Time-laps photos of H-filter microfluidic chip. A) 5 seconds image B) 10 seconds image C) 15 seconds image.

4.4. Encapsulation of the Cells

Cells were encapsulated into GelMA hydrogel, that we synthesized to give cells a 3D structure, through UV crosslinking. We first encapsulated different cell types onto the coverslip using various photomask designs for 3D static controls of study and evaluated for long term culture. Further, for 3D dynamic culture, we encapsulated the cells into the microfluidic channel.

4.4.1. Encapsulation of the Cells for 3D Static Culture

The spacer and hydrogel prepared as described in Section 3.5.6.1 were mixed with various cell lines and encapsulated onto the coverslip under UV light. Spacer preparation and 3D static cell encapsulation are shown in Figure 25.

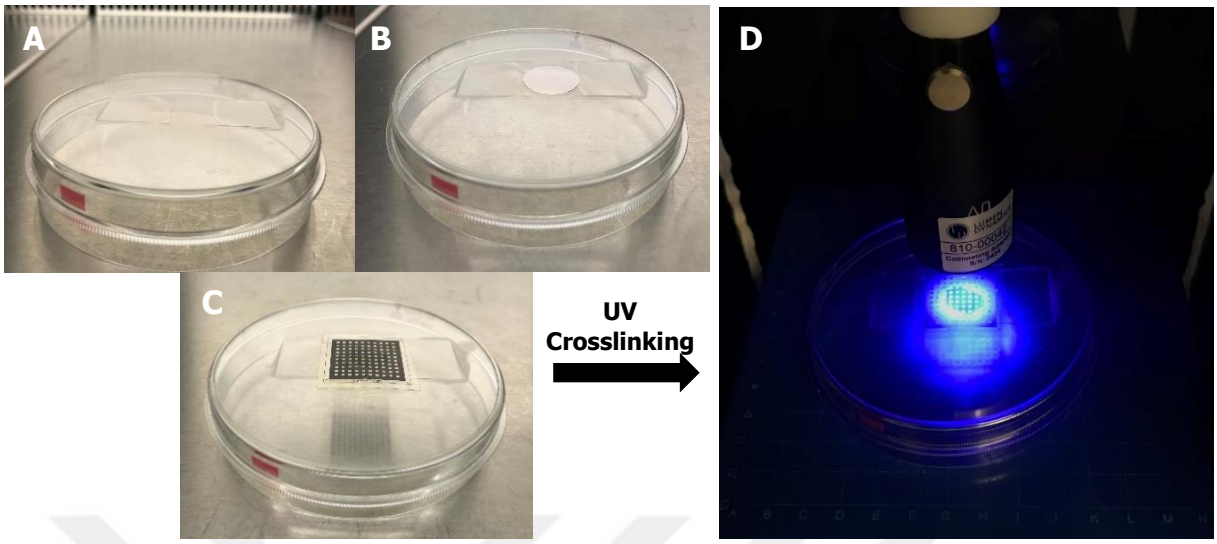

Figure 21: Spacer preparation and encapsulation of cells under UV light.

SH-SY5Y Cell Line

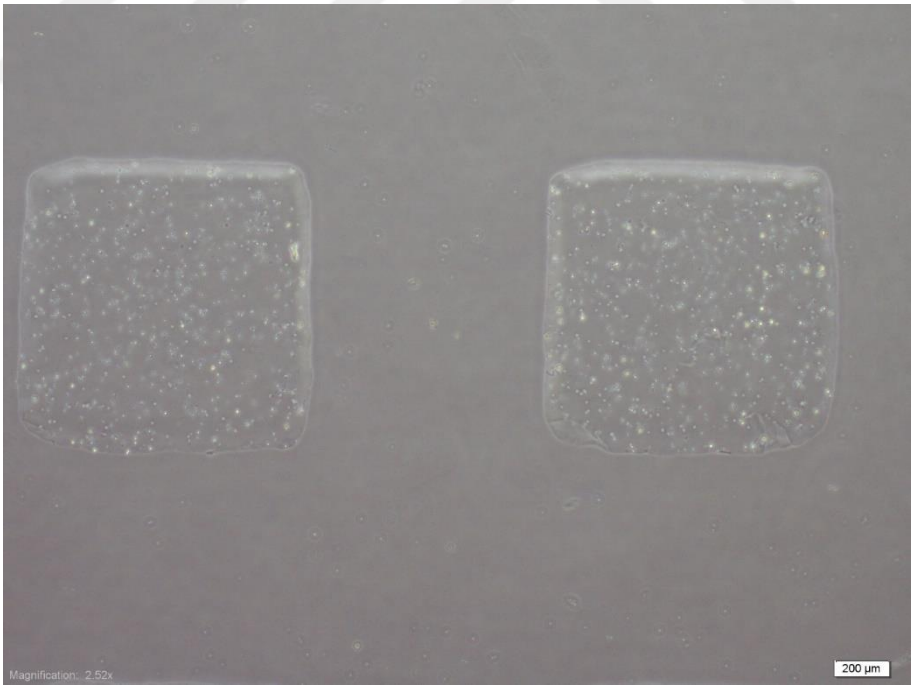

Figure 22: Encapsulation of SH-SY5Y cells in GelMA with using square photomask onto the coverslip.

U251 Cell Line

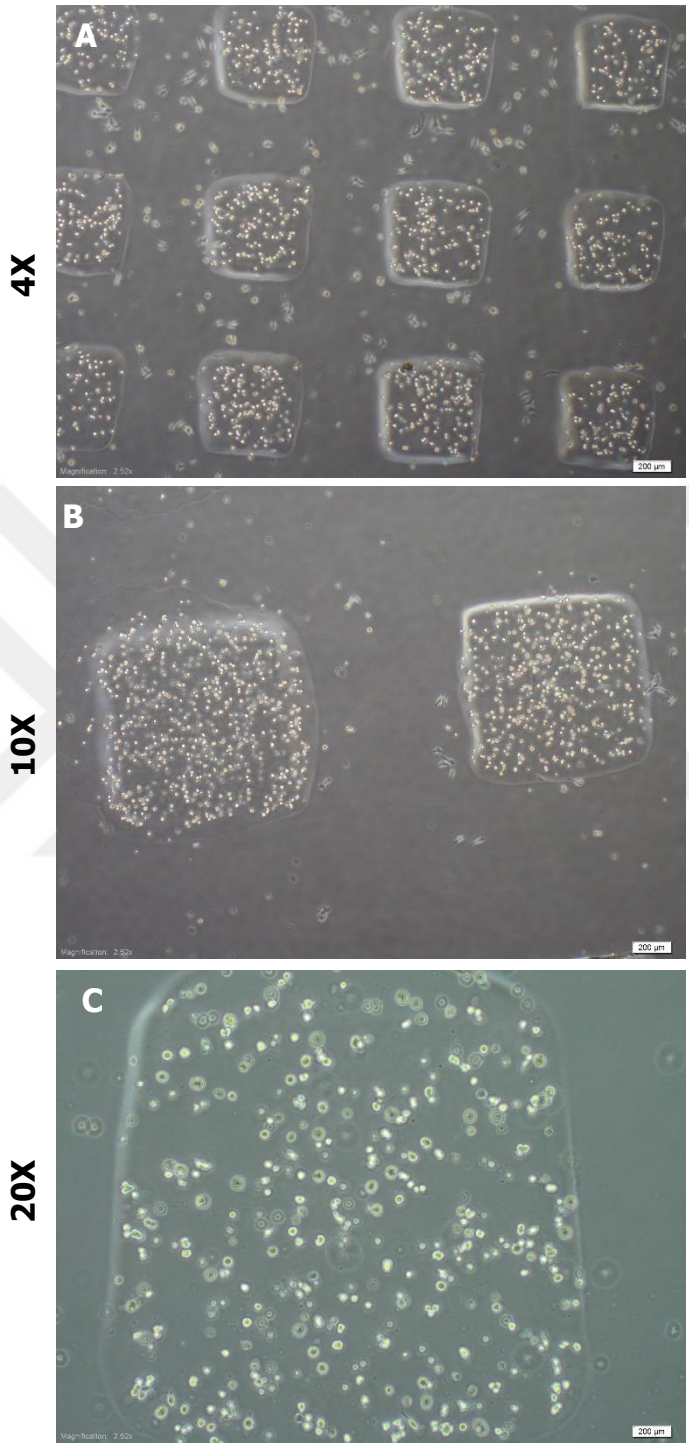

Figure 23: Encapsulation of U251 cells in GelMA with using square photomask onto the coverslip Day 1 images. A) 4X B) 10X C) 20X.

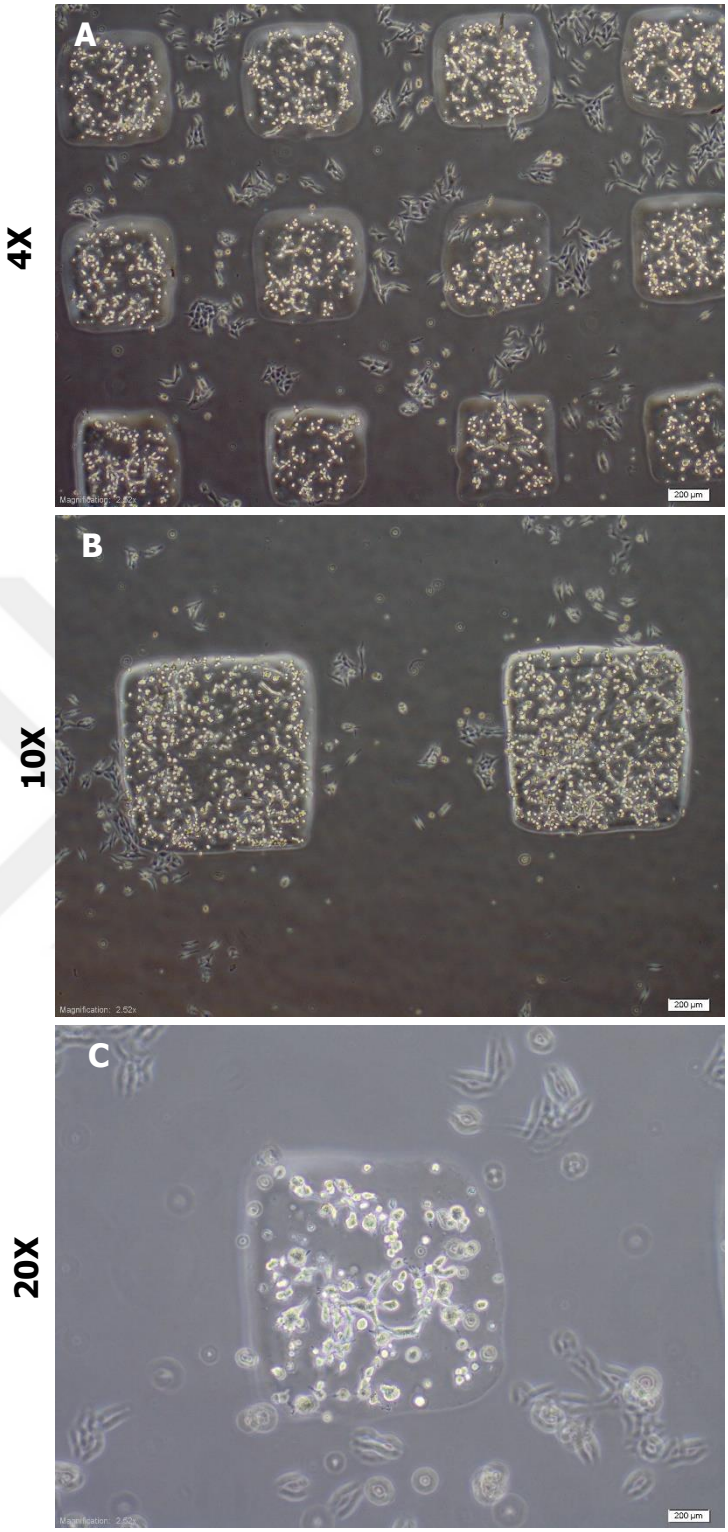

Figure 24: Encapsulation of U251 cells in GelMA with using square photomask onto the coverslip Day 3 images. A) 4X B) 10X C) 20X.

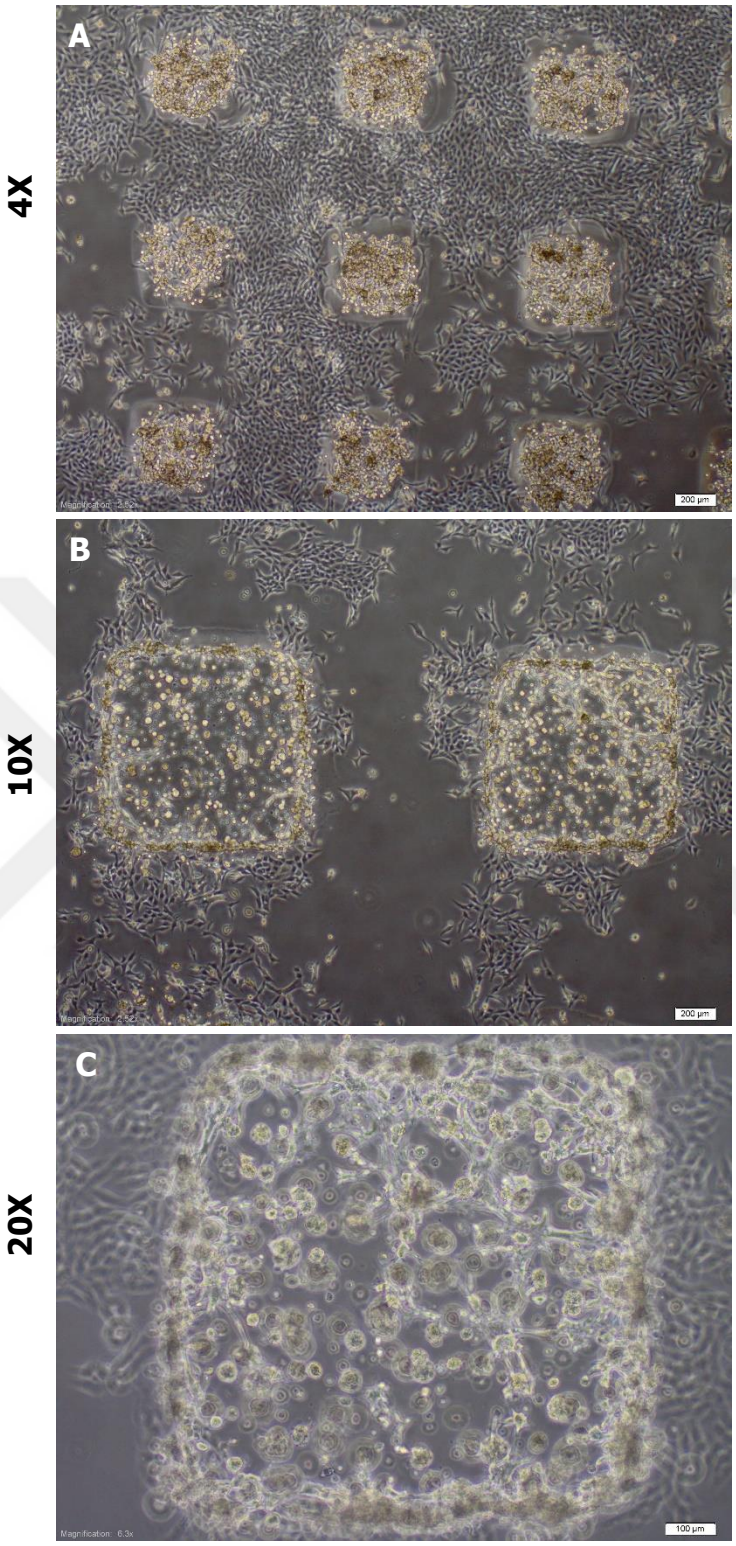

Figure 25: Encapsulation of U251 cells in GelMA with using square photomask onto the coverslip Day 6 images. A) 4X B) 10X C) 20X.

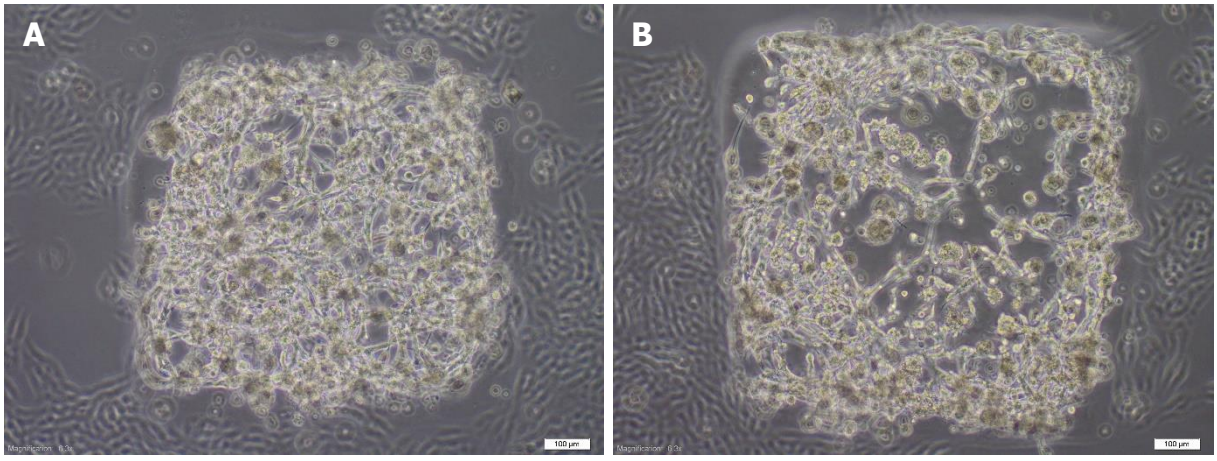

Figure 26: Encapsulation of U251 cells in GelMA with using square photomask onto the coverslip Day 6 images. A-B) 20X images.

U87 Cell Line

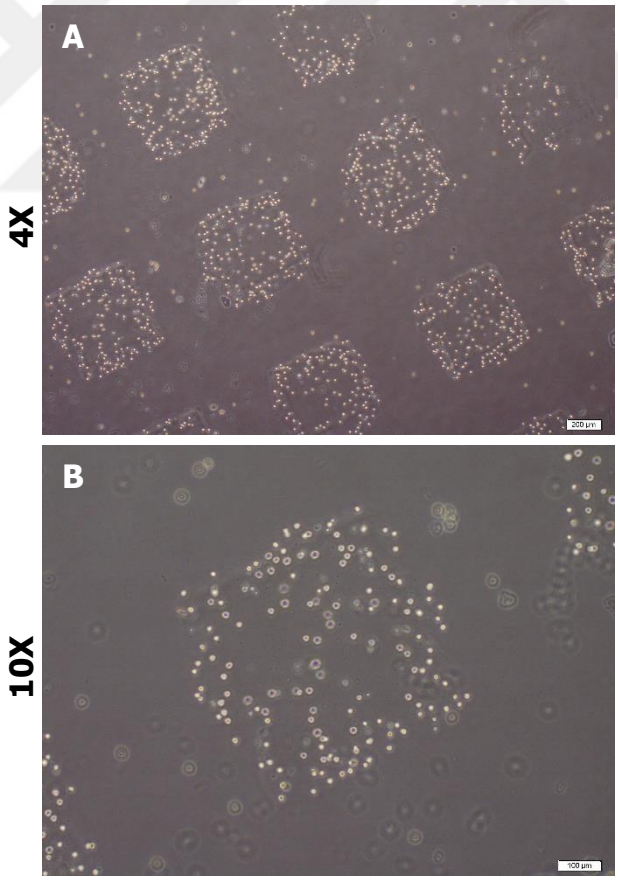

Figure 27: Encapsulation of U87 cells in GelMA with using square photomask onto the coverslip Day 0 images. A) 4X B) 10X.

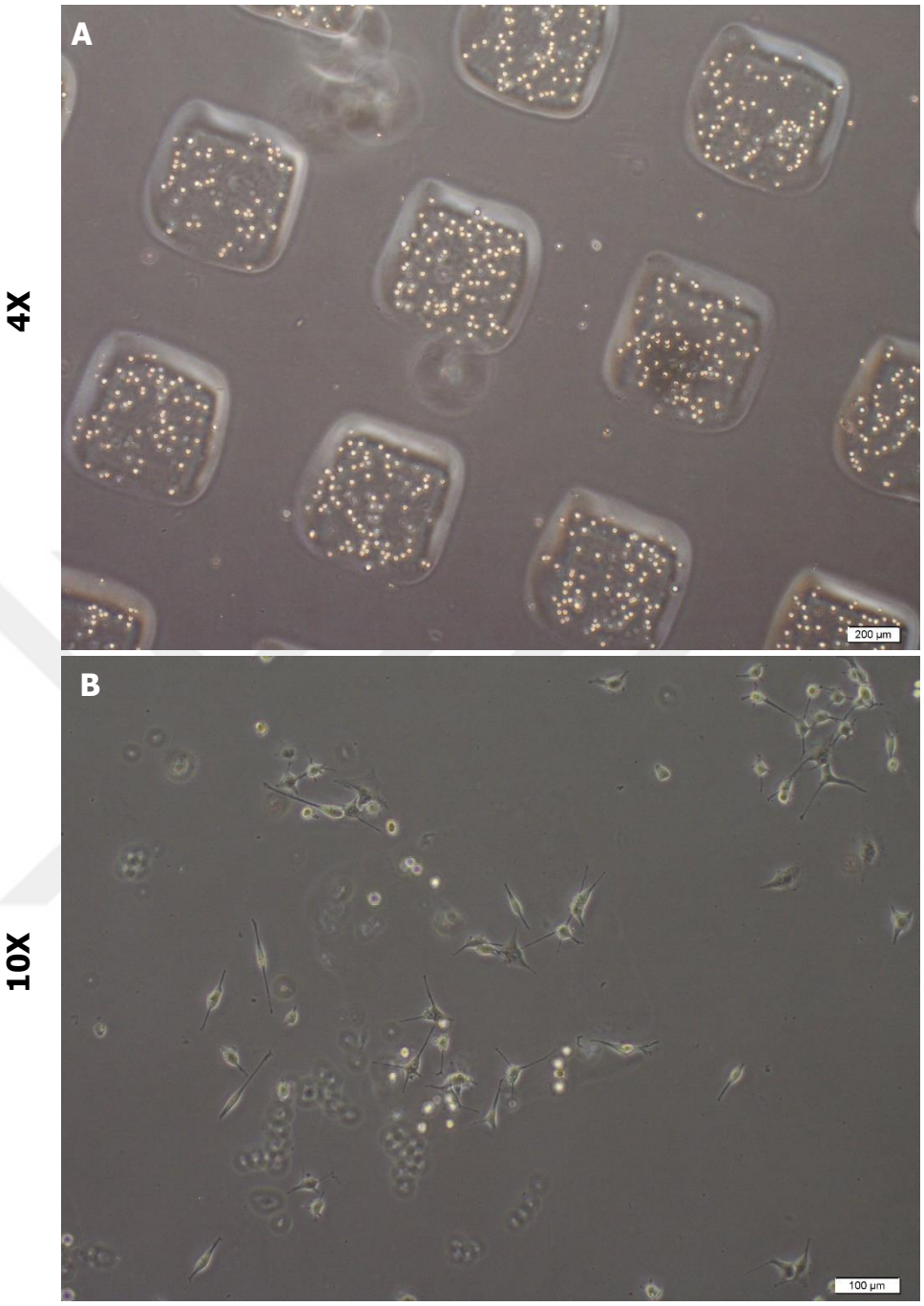

Figure 28: Encapsulation of U87 cells in GelMA with using square photomask onto the coverslip Day 1 images. A) 4X B) 10X.

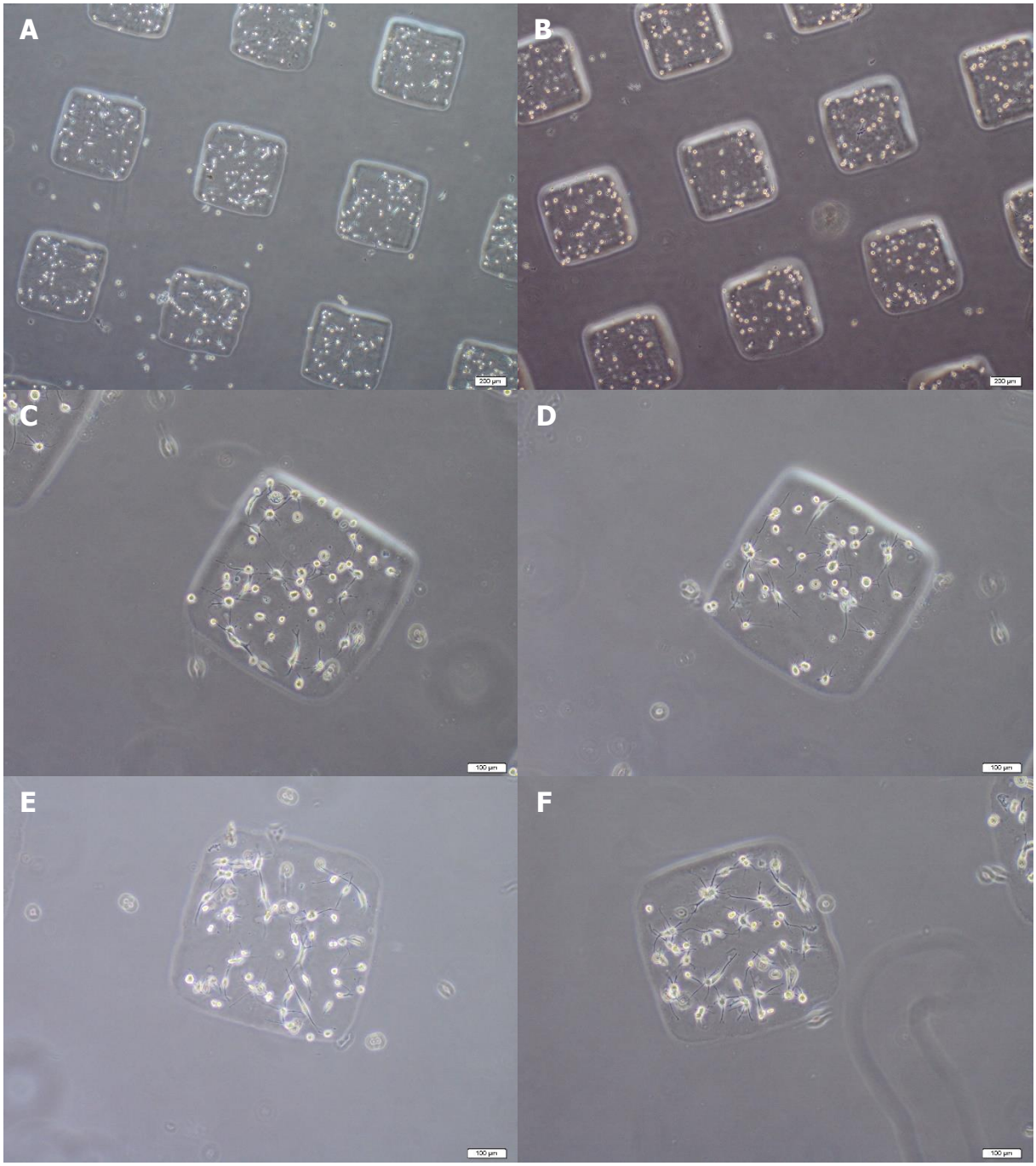

Figure 29: Encapsulation of U87 cells in GelMA with using square photomask onto the coverslip Day 2 images. A-B) 4X C-F) 10X image.

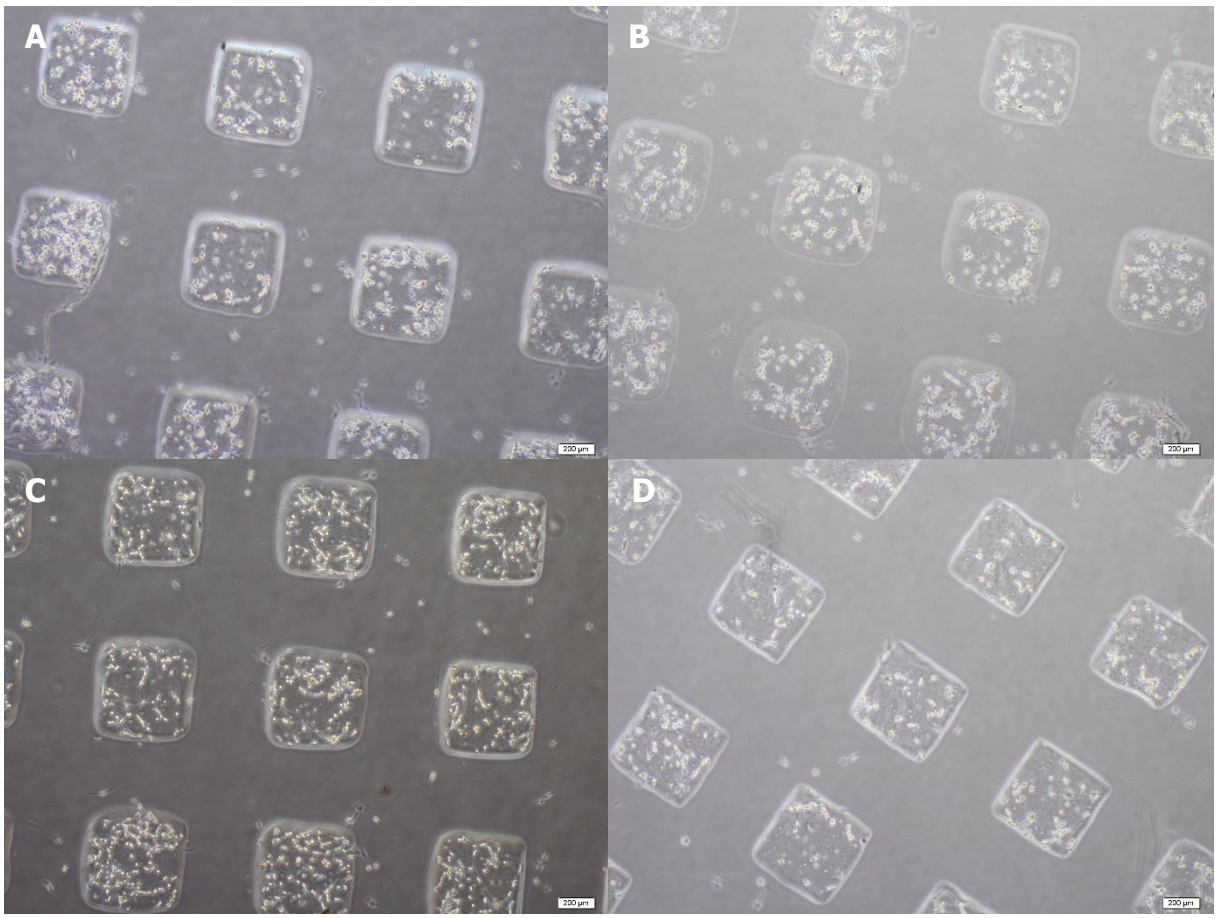

Figure 30: Encapsulation of U87 cells in GelMA with using square photomask onto the coverslip Day 4 images. A-D) 4X image. Scale bar: 200 µm.

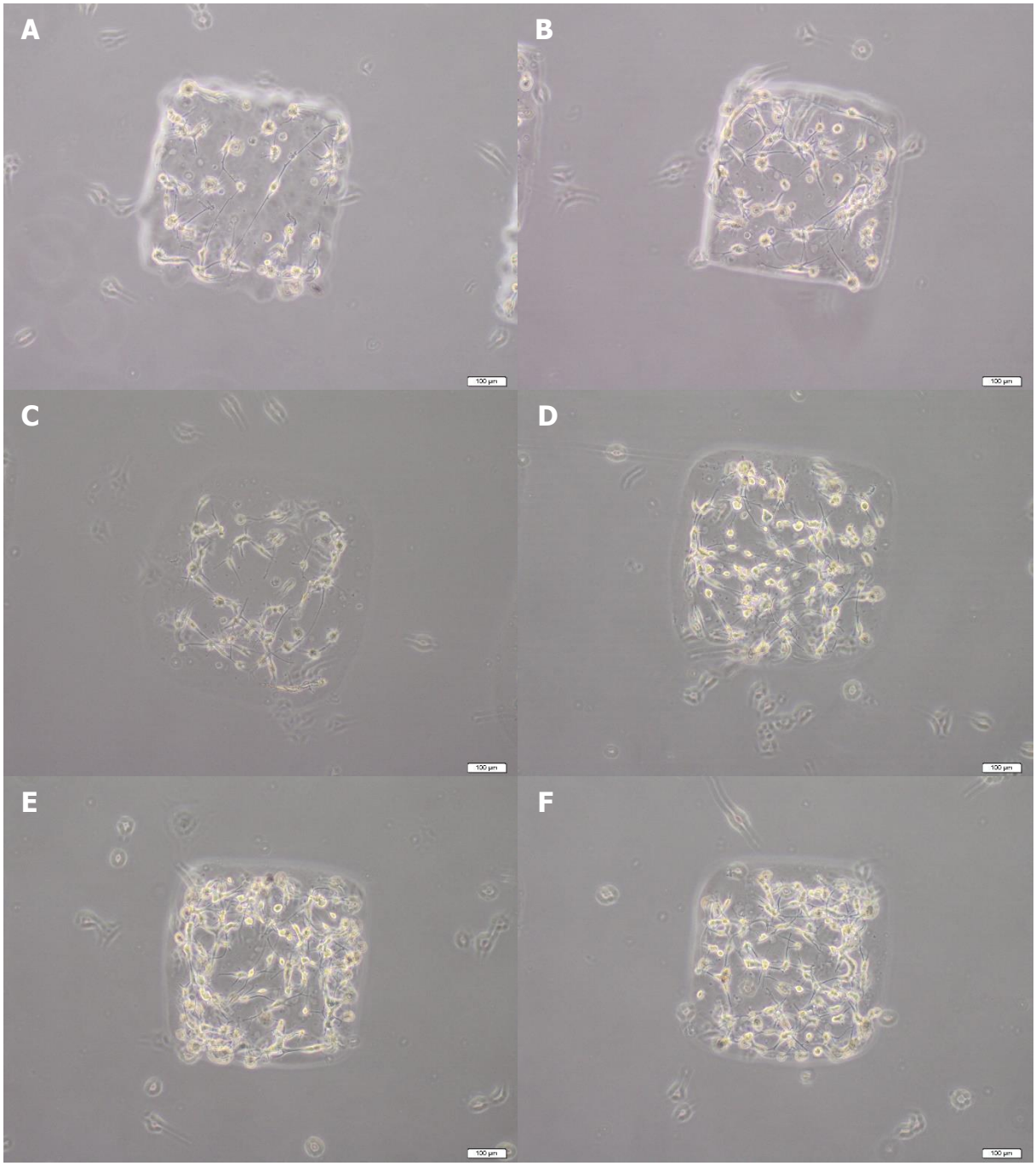

Figure 31: Encapsulation of U87 cells in GelMA with using square photomask onto the coverslip Day 4 images. A-F) 4X image. Scale bar: 100 µm.

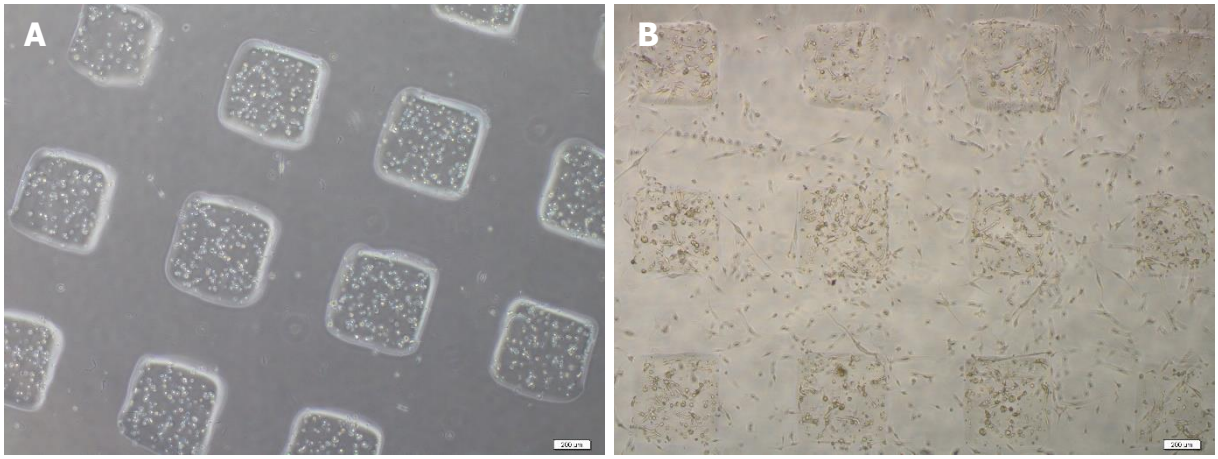

Figure 32: Another encapsulation of U87 cells in GelMA with using square photomask onto the coverslip 4X images. A) Day 0 B) Day 5 image. Scale bar: 200 µm.

N9 Cell Line

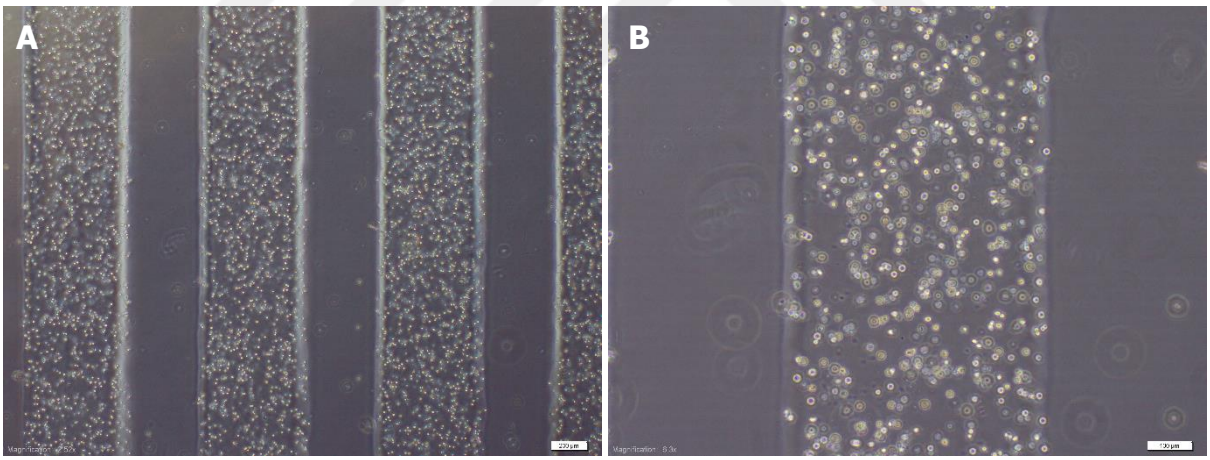

Figure 33: Encapsulation of N9 cells in GelMA with using strip photomask onto the coverslip Day 0 images. A) 4X B) 10X image.

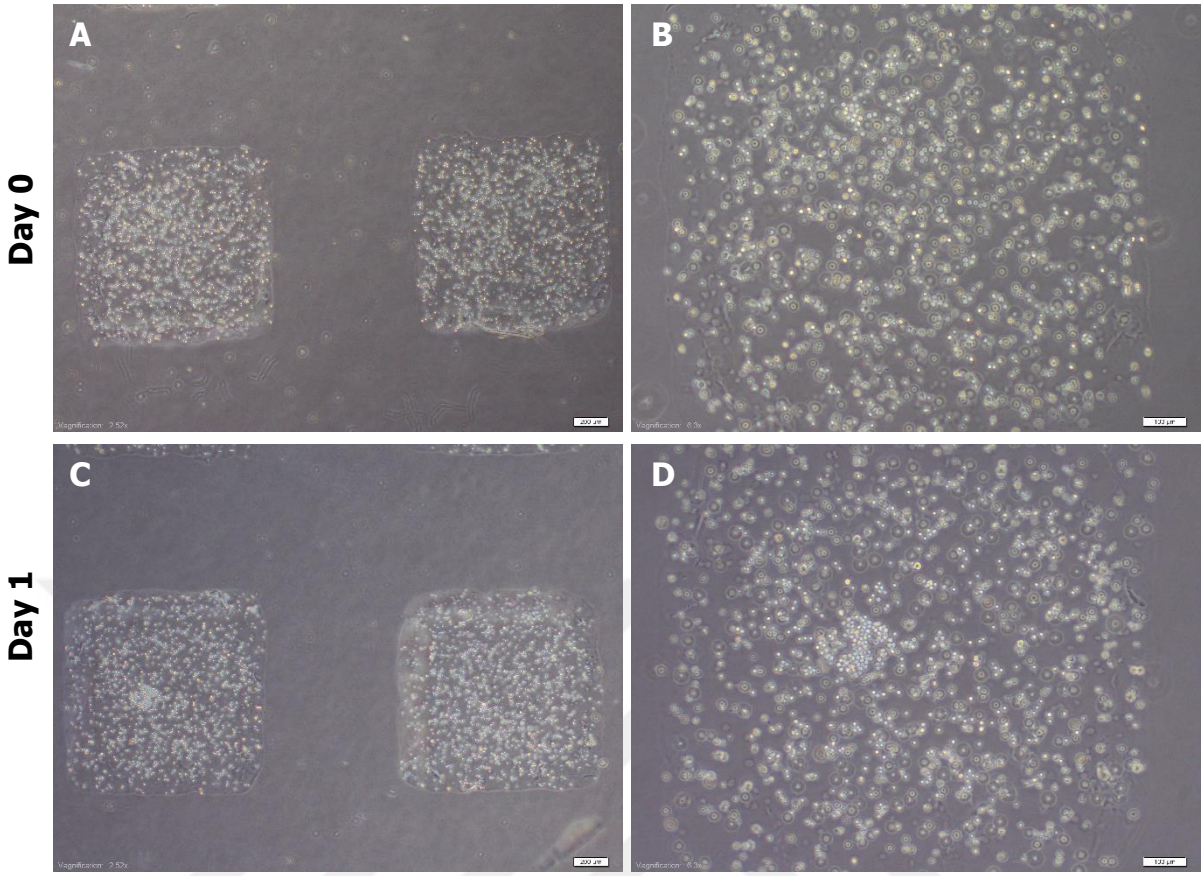

Figure 34: Encapsulation of N9 cells in GelMA with using square photomask onto the coverslip Day 0 and Day1 images. A-C) 4X, B-D) 10X image.

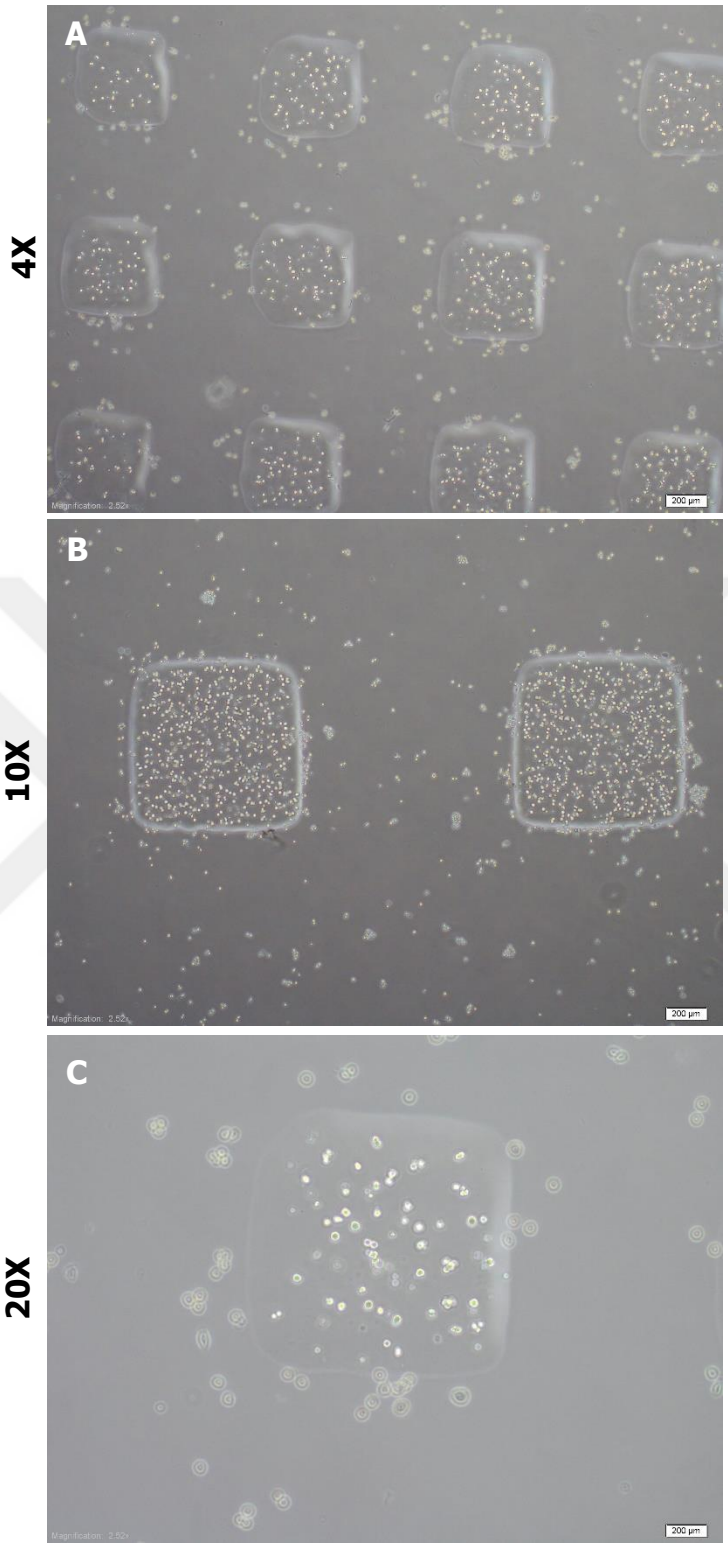

Figure 35: Encapsulation of N9 cells in GelMA with using square photomask onto the coverslip Day 0 images. A) 4X B) 10X C) 20X.

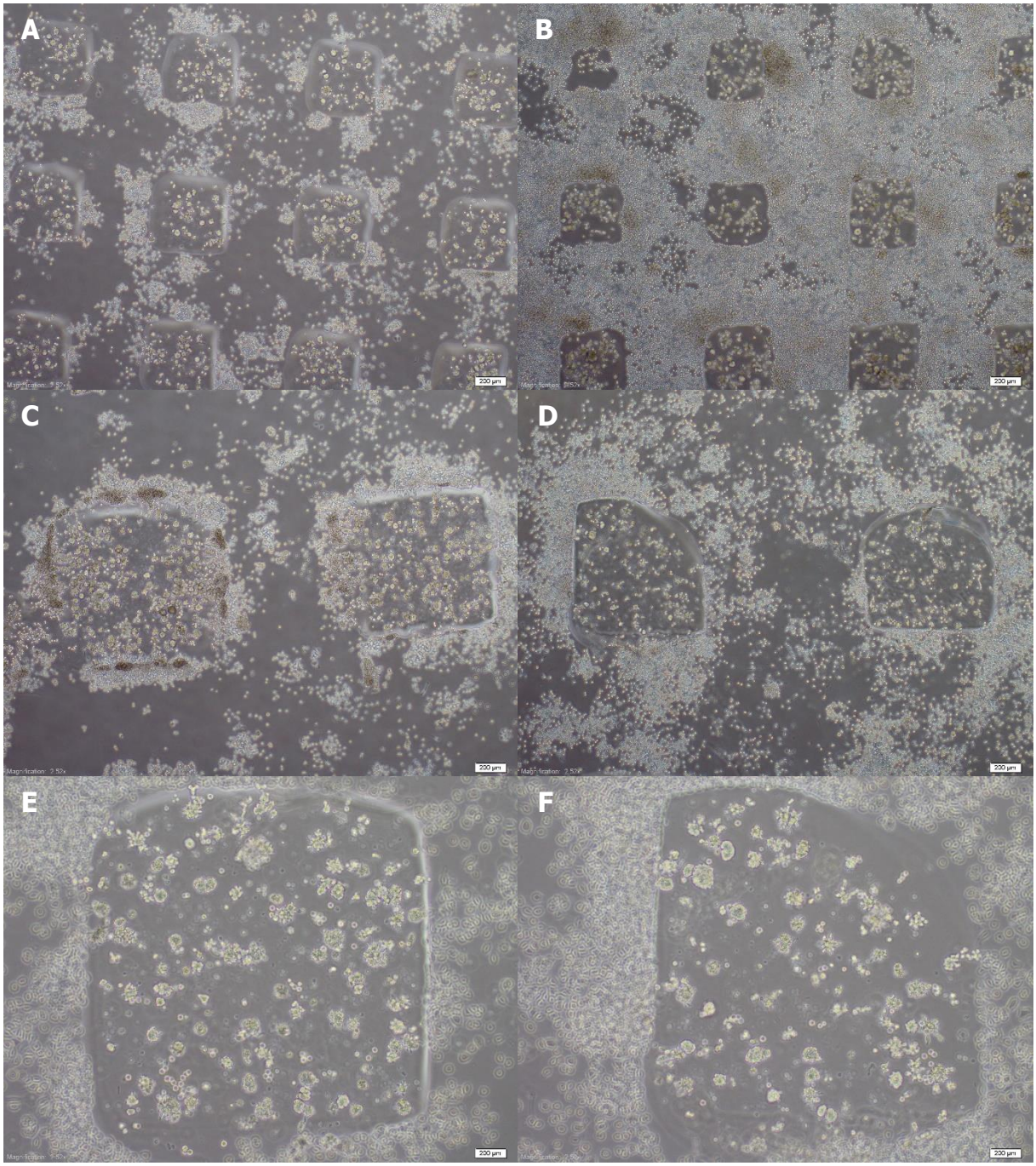

Figure 36: Encapsulation of N9 cells in GelMA with using square photomask onto the coverslip Day 3 images. A-B) 4X image, C-D) 10X image and E-F) 20X image.

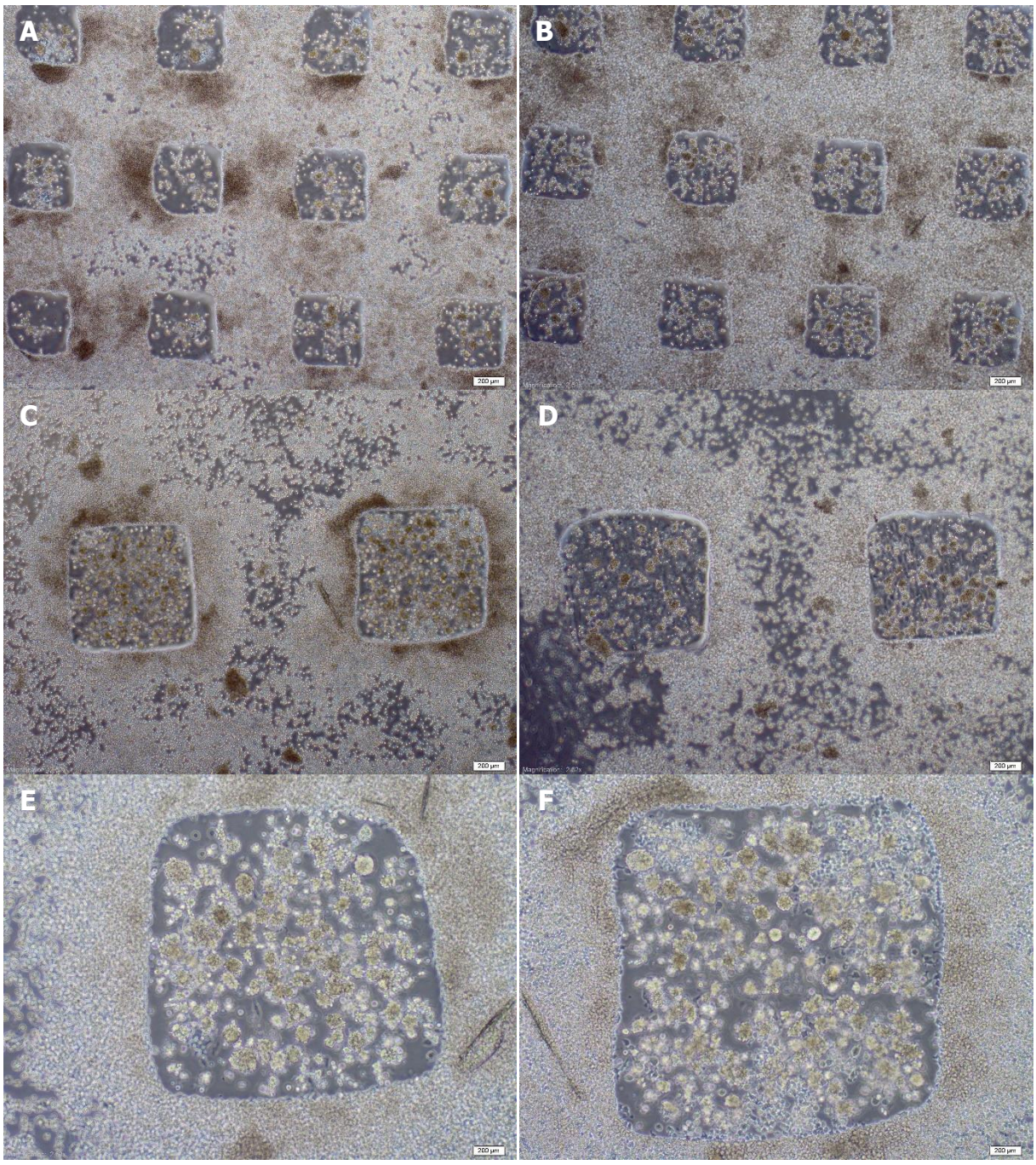

Figure 37: Encapsulation of N9 cells in GelMA with using square photomask onto the coverslip Day 3 images. A-B) 4X image, C-D) 10X image and E-F) 20X image.

THP-1 Cell Line

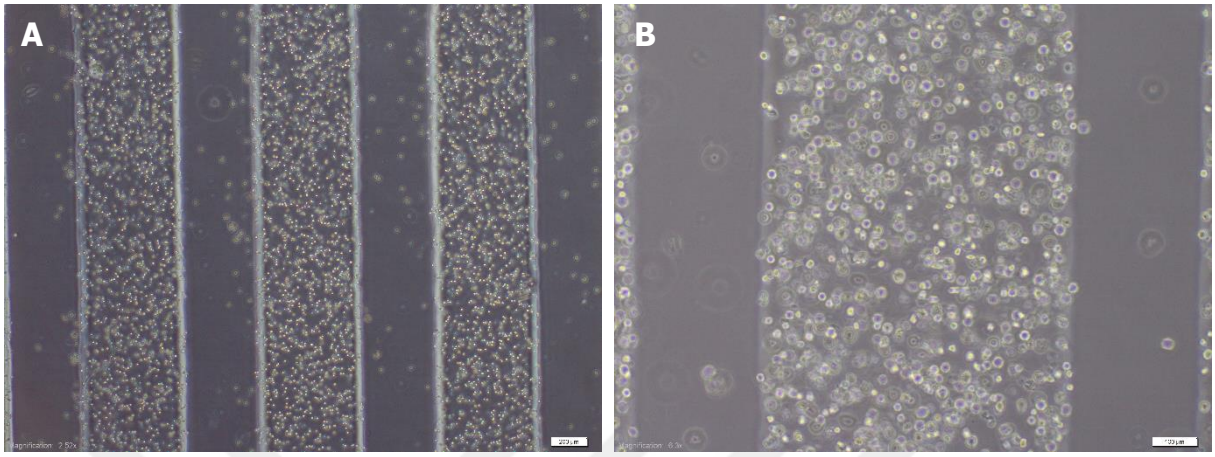

Figure 38: Encapsulation of THP-1 cells in GelMA with using strip photomask onto the coverslip Day 0 images. A) 4X B) 10X image.

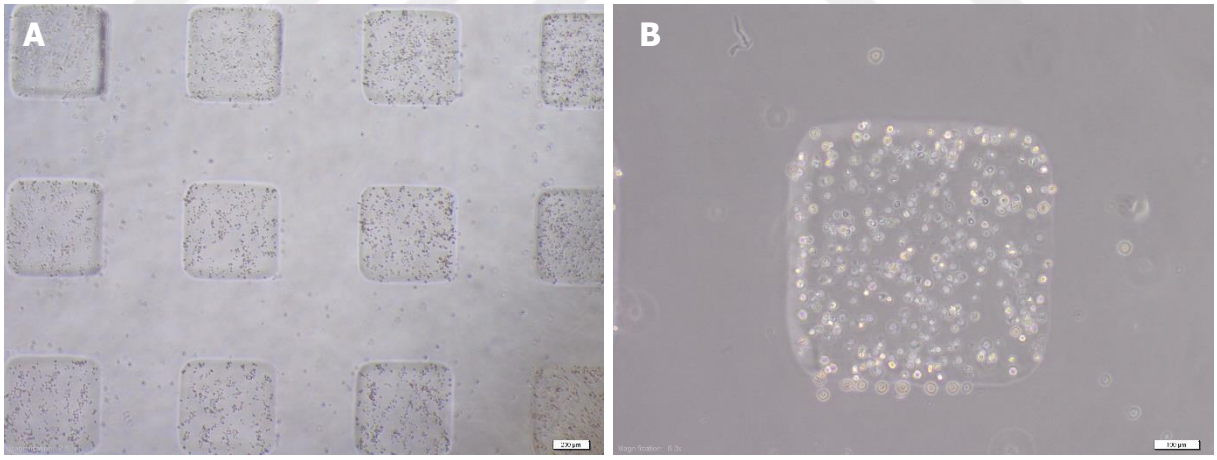

Figure 39: Encapsulation of THP-1 cells in GelMA with using square photomask onto the coverslip Day 0 images. A) 4X B) 10X image.

4.4.2. Encapsulation of the Cells for 3D Dynamic Culture

Various cell lines mixed with the GelMA as described in Section 3.6.5.2 were crosslinked into the microfluidic channel under UV light. After encapsulation, the microfluidic channel was connected to the continuous flow.

U251 Cell Line

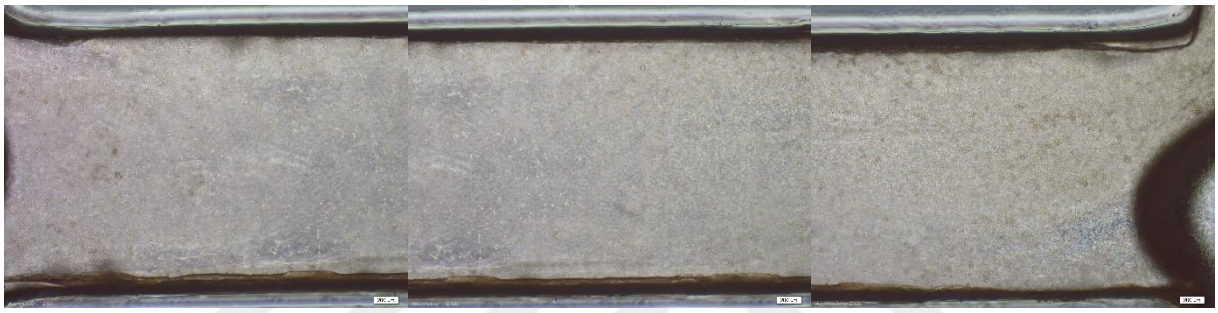

Figure 40: Encapsulation of U251 cells in GelMA into the single channel microfluidic chip Day 0 images. Flow rate: 2 µl/min. Scale bar: 200 µm.

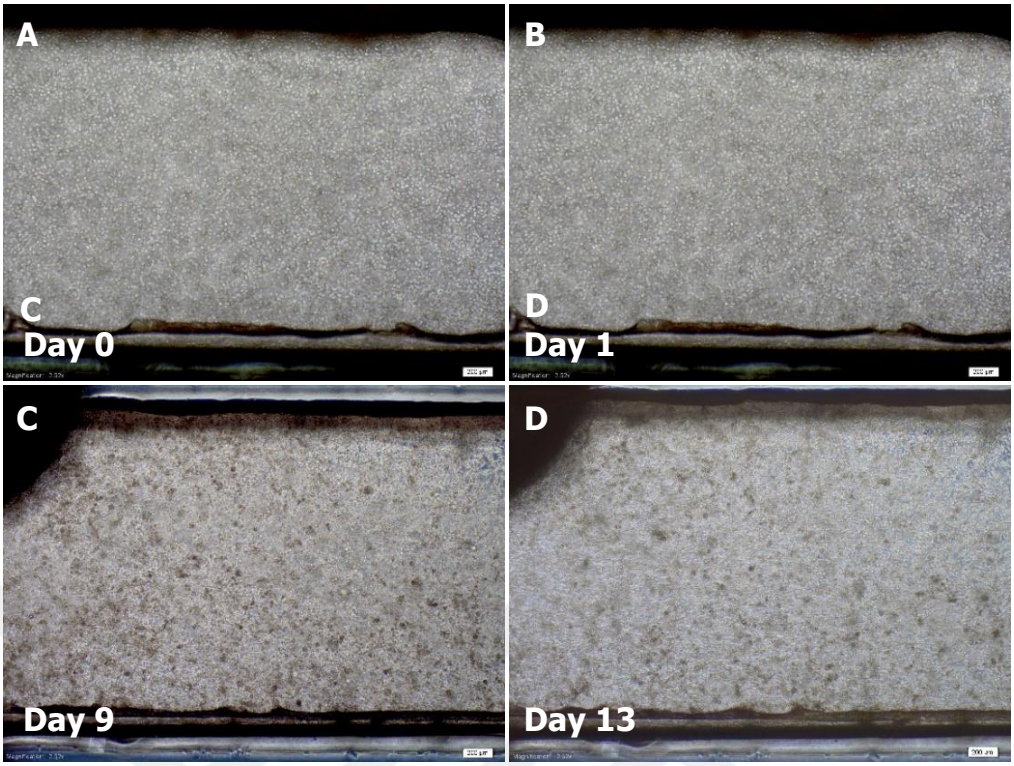

Figure 41: Encapsulation of U251 cells in GelMA into the single channel microfluidic chip time laps 4X images. Flow rate: 2 µl/min. Scale bar: 200 µm.

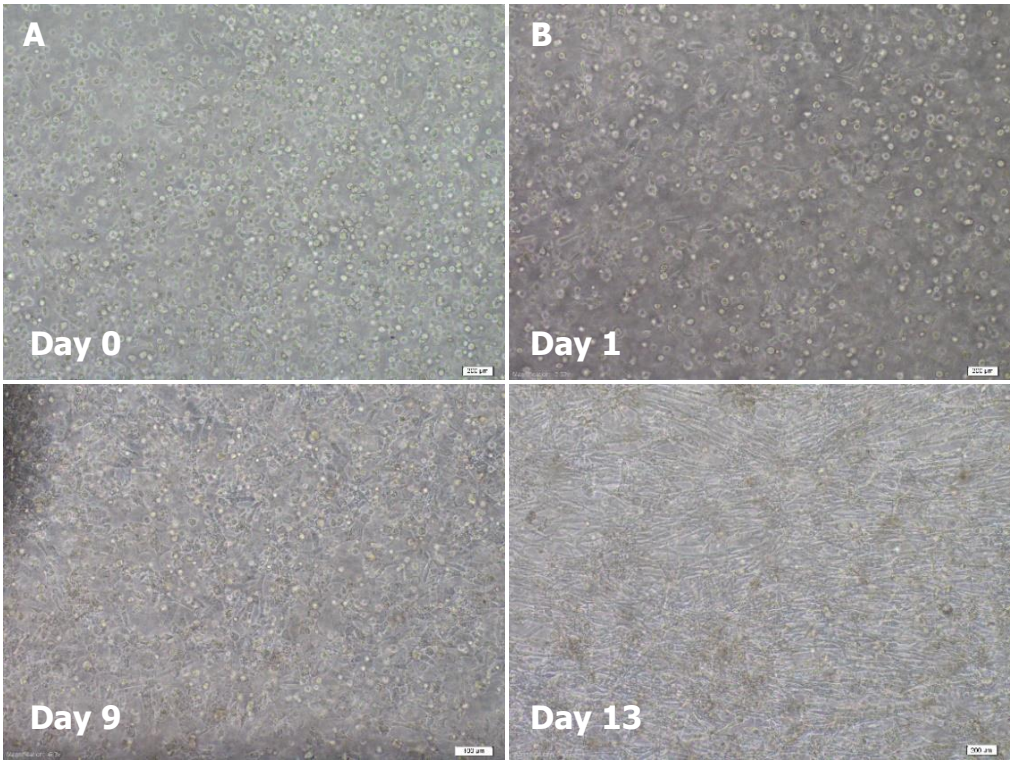

Figure 42: Encapsulation of U251 cells in GelMA into the single channel microfluidic chip time laps 10X images. Flow rate: 2 µl/min. Scale bar: 100 µm.

U87 Cell Line

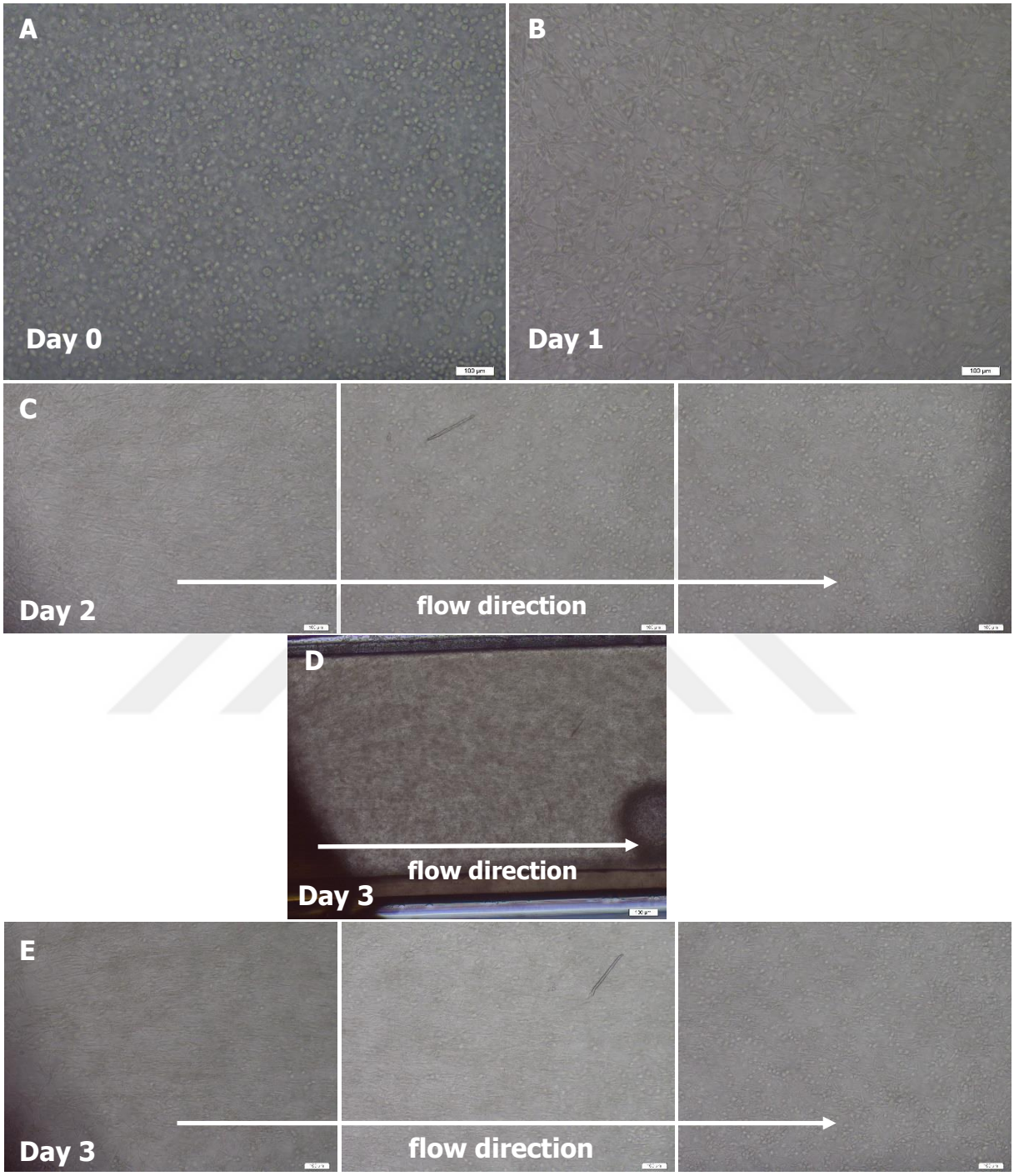

Figure 43: Encapsulation of U87 cells in GelMA into the single channel microfluidic chip time laps images. A) Day 0 10X image, B) Day 1 10X image, C) Day 2 10 X image from inlet to outlet of microfluidic channel, D) Day 3 4X image, E) Day 3 10 X image from inlet.

N9 Cell Line

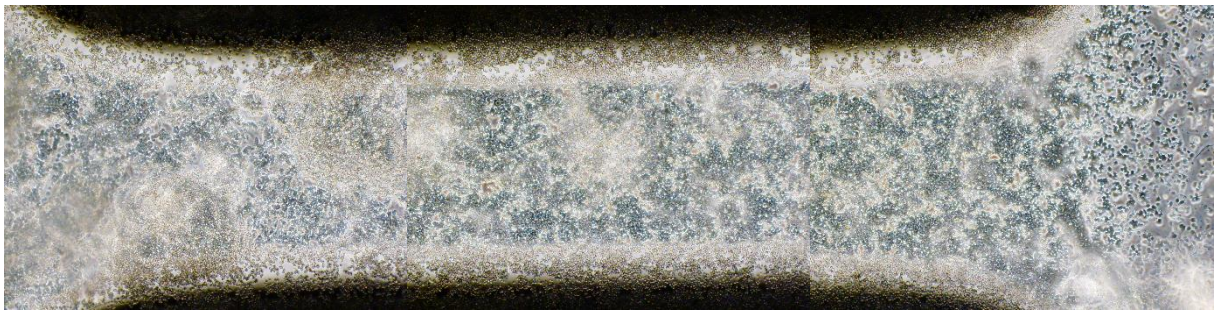

Figure 44: Encapsulation of N9 cells in GelMA into the single channel microfluidic chip and bubble formation in the microchannel 4X images. Flow rate: 2 µl/min

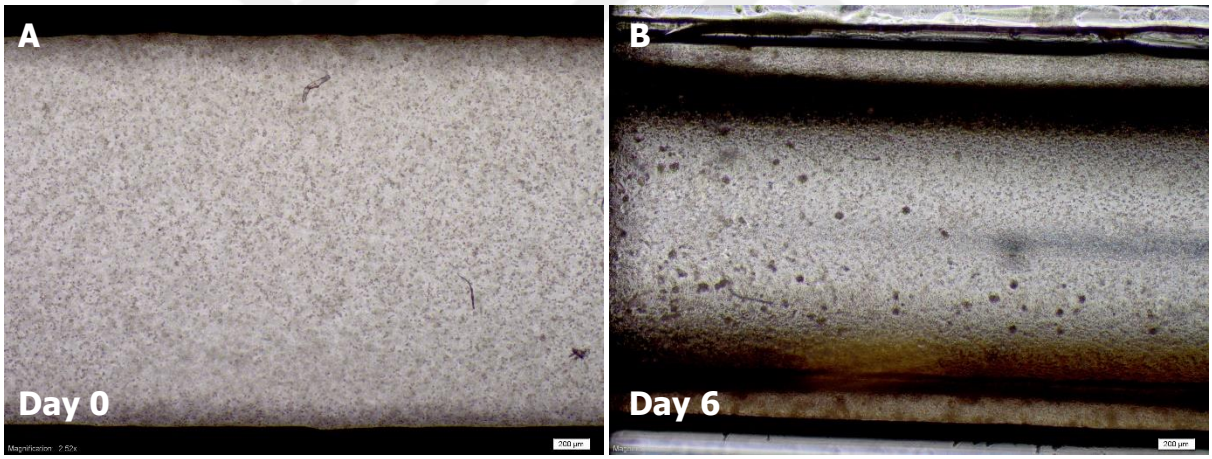

Figure 45: Encapsulation of N9 cells in GelMA into the single channel microfluidic chip 4X images. A) Day 0, B) Day 6 image. Flow rate: 2 µl/min.

THP-1 Cell Line

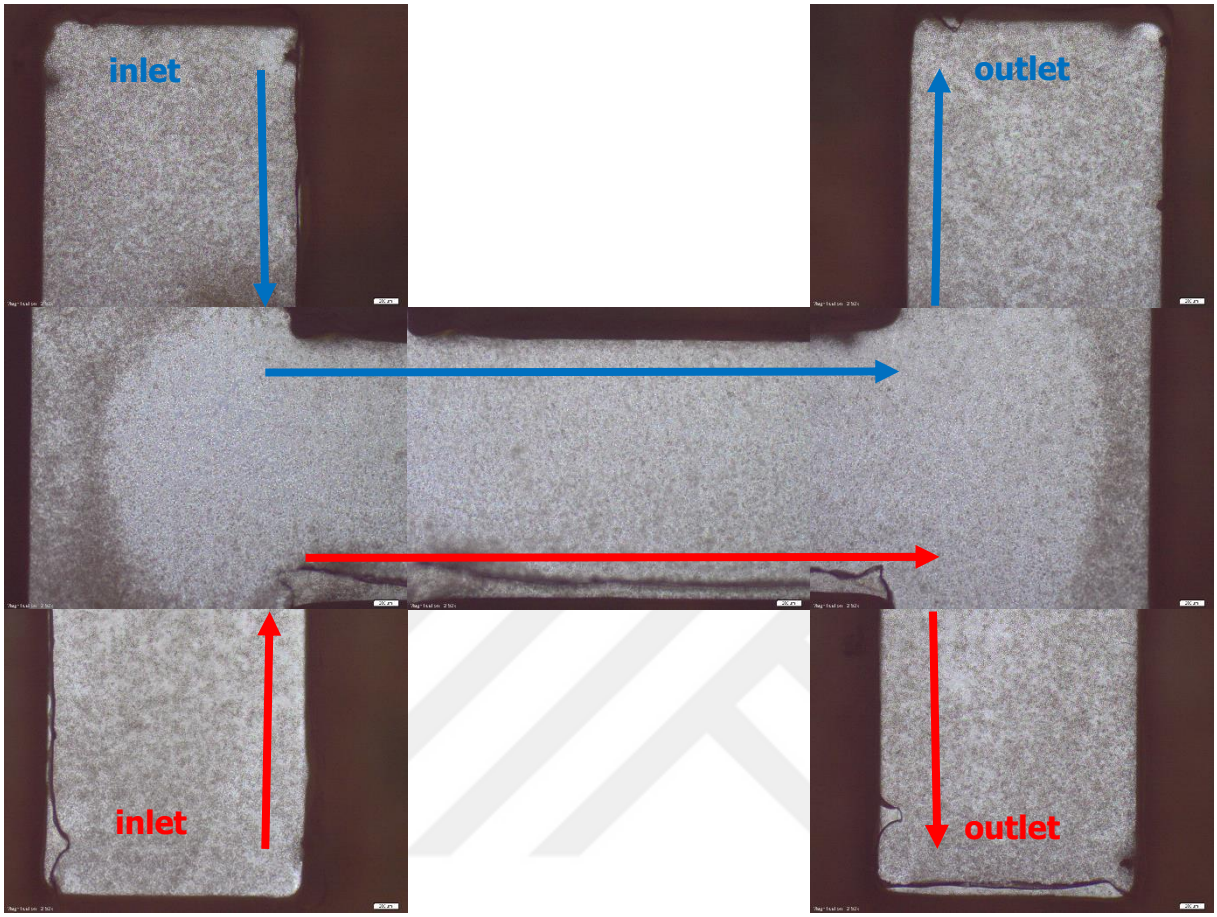

Figure 46: Encapsulation of THP-1 cells in GelMA into the H-filter microfluidic chip 4X images. Flow rate: 0,5 µl/min for 24 h.

Figure 47: Encapsulation of THP-1 cells in GelMA into the single channel microfluidic chip 4X images. Flow rate: 10 µl/min for 4 h.

4.5. Differentiation of THP-1 Cells with Various PMA Concentration

We used different concentrations (10, 50, 150, and 200 ng/ml) of PMA to differentiate suspended monocytic THP-1 cells into the adherent macrophage-like state. Figure 49 shows the phase-contrast image of the suspended, untreated THP-1 cells. Phase-contrast microscope images of differentiated THP-1 cells with PMA at various concentrations in 2D for 24 hours are shown in Figure 50.

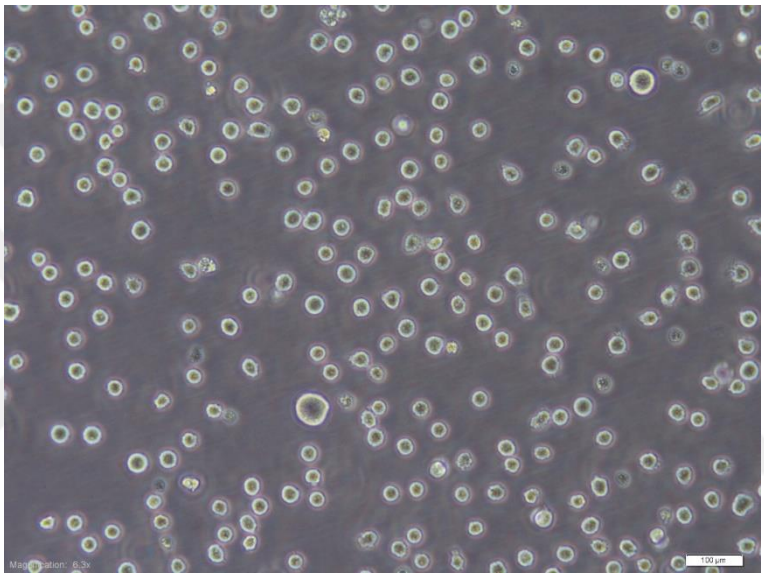

Figure 48: Suspended monocytic THP-1 cells 20X image. Scale bar: 50 µm.

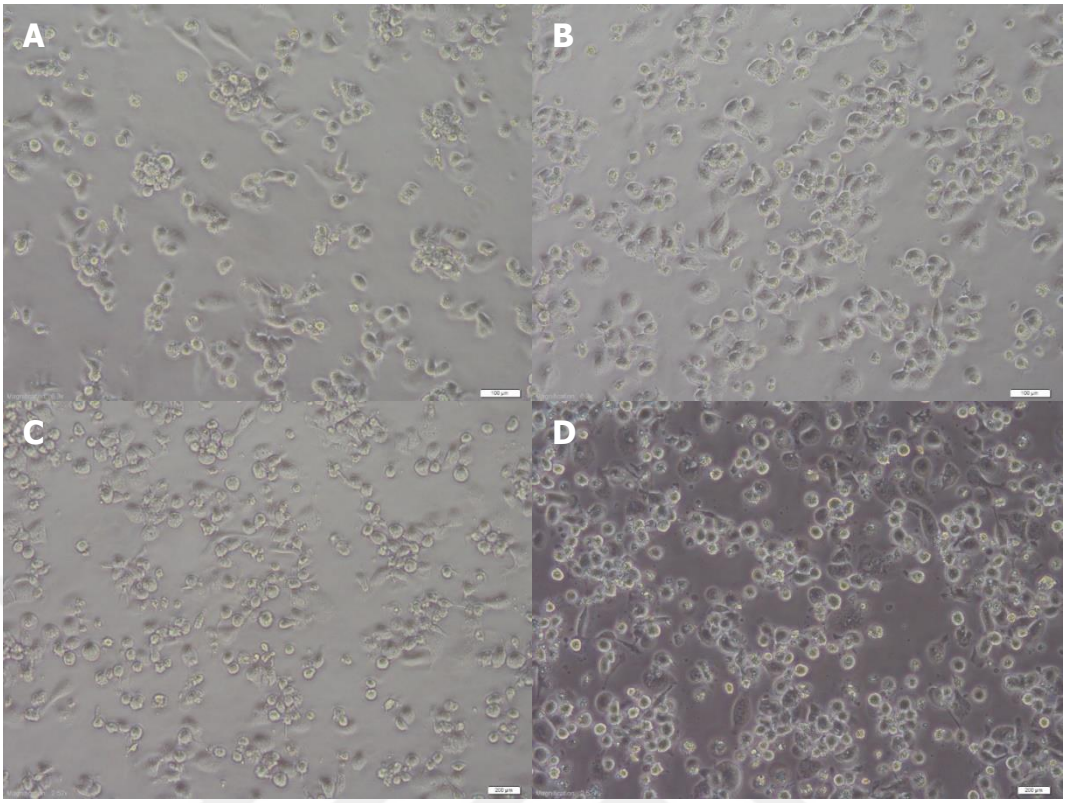

Figure 49: Differentiated THP-1 cells after 24h stimulation with PMA in 2D, 20X images. A) 10 ng/ml concentration. B) 50 ng/ml concentration. C) 150 ng/ml concentration. D) 200 ng/ml concentration. Scale bar: 50 µm.

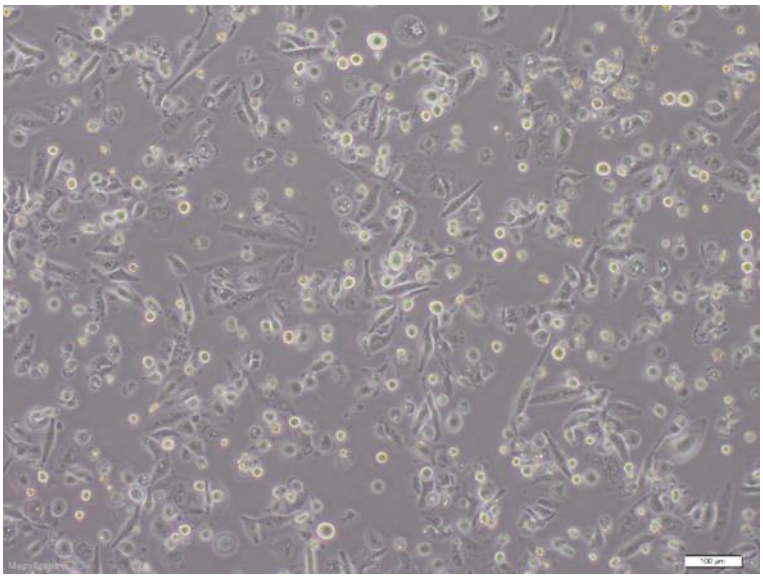

Figure 50: 10X image of THP-1 cells incubated in complete medium for 48 hours after 24 hours of differentiation with 10 ng/ml PMA. Scale bar: 100 µm.

We used various PMA concentrations as in 2D culture, THP-1 cells differentiation to macrophage-like state with PMA for 3D culture. Firstly, we have encapsulated the cells into the GelMA, then we have added the medium onto cells containing various concentrations of PMA as shown in Figure 52.

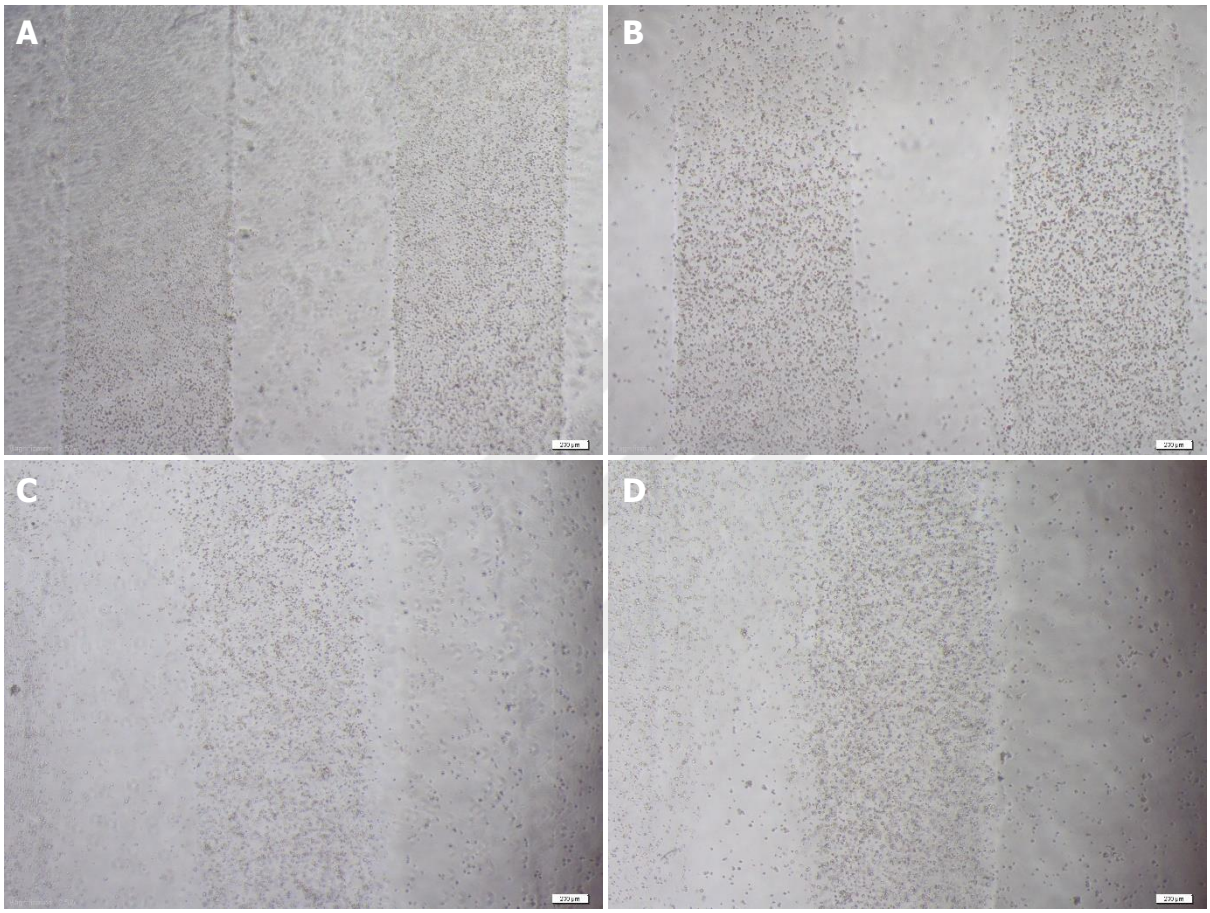

Figure 51: Differentiated THP-1 cells after 24h stimulation with PMA in 3D static culture, 4X images. A) Control group. B) 10 ng/ml concentration. C) 50 ng/ml concentration. D) 150 ng/ml concentration. Scale bar: 200 µm.

4.6. Polarization of Cells

We have polarized various cell lines as in *in vitro* 2D static culture, 3D static culture and 3D dynamic culture as described in Section 3.6.6.

4.6.1. Polarization of the Cells in 2D Static Culture

N9 Cell Line

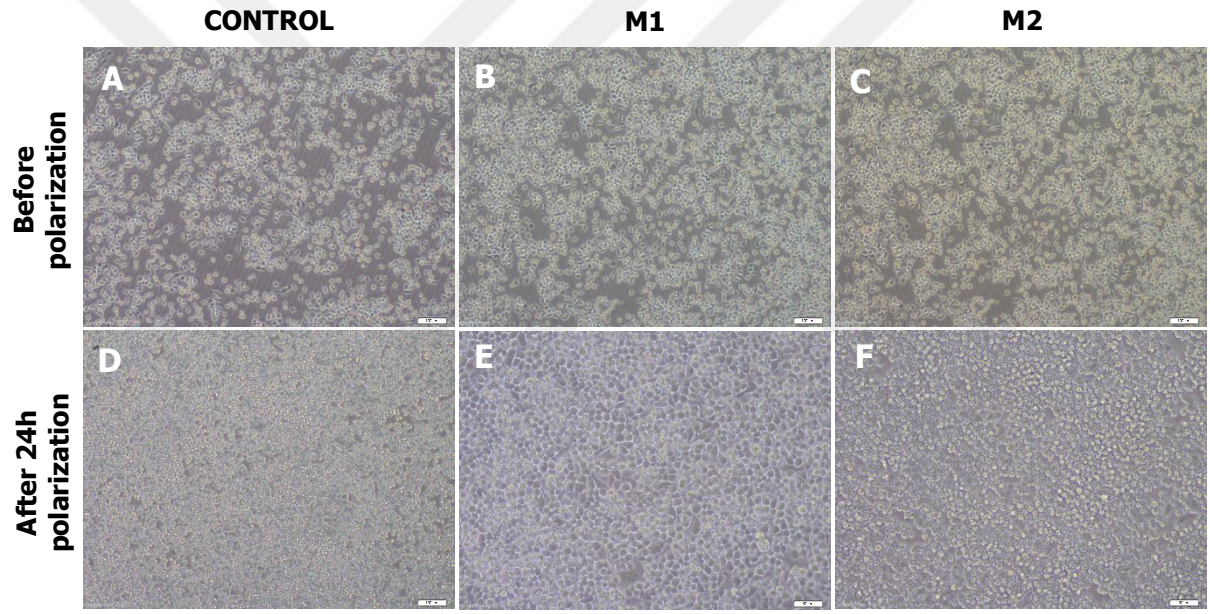

Figure 52: Polarization of N9 cells in 2D static culture in 6 well-plate. A-C) N9 cells 10X images before polarization. D-F) N9 cells 20X images after 24h polarization.

4.6.2. Polarization of the Cells in 3D Static Culture

N9 Cell Line

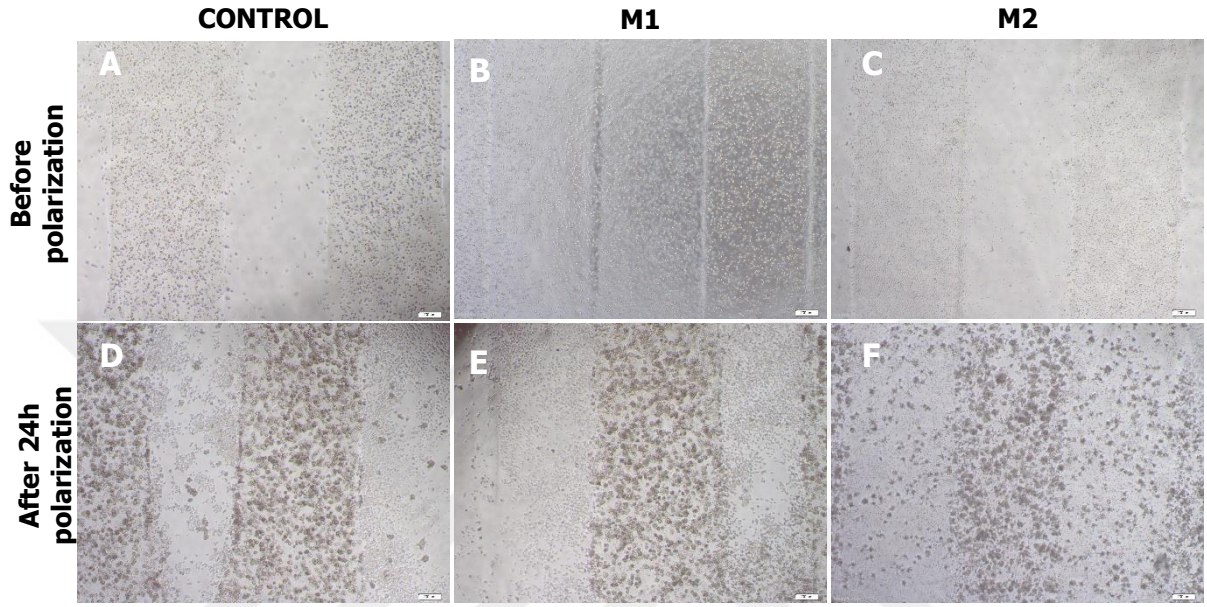

Figure 53: Polarization of N9 cells in 3D static culture onto the coverslip in 6 well-plate. A-C) N9 cells 4X images before polarization. D-F) N9 cells 10X images after 24h polarization.

THP-1 Cell Line

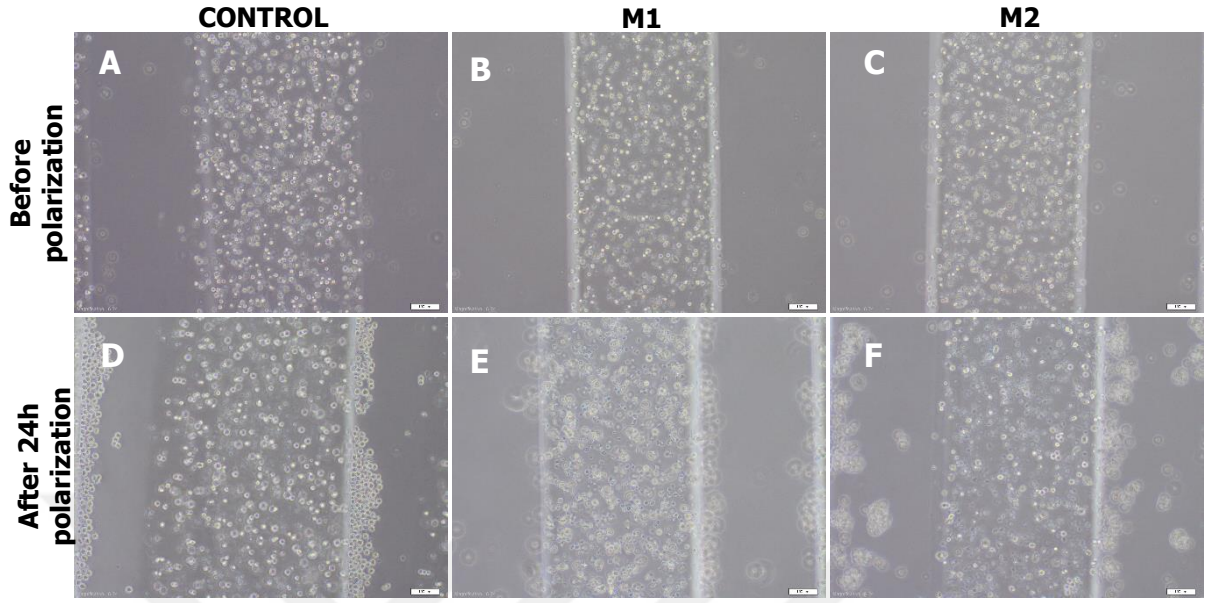

Figure 54: Polarization of THP-1 cells in 3D static culture onto the coverslip. A-C) THP-1 cells 10X images before polarization. D-F) THP-1 cells 10X images after 24h polarization.

4.6.3. Polarization of the Cells in 3D Dynamic Culture

N9 Cell Line

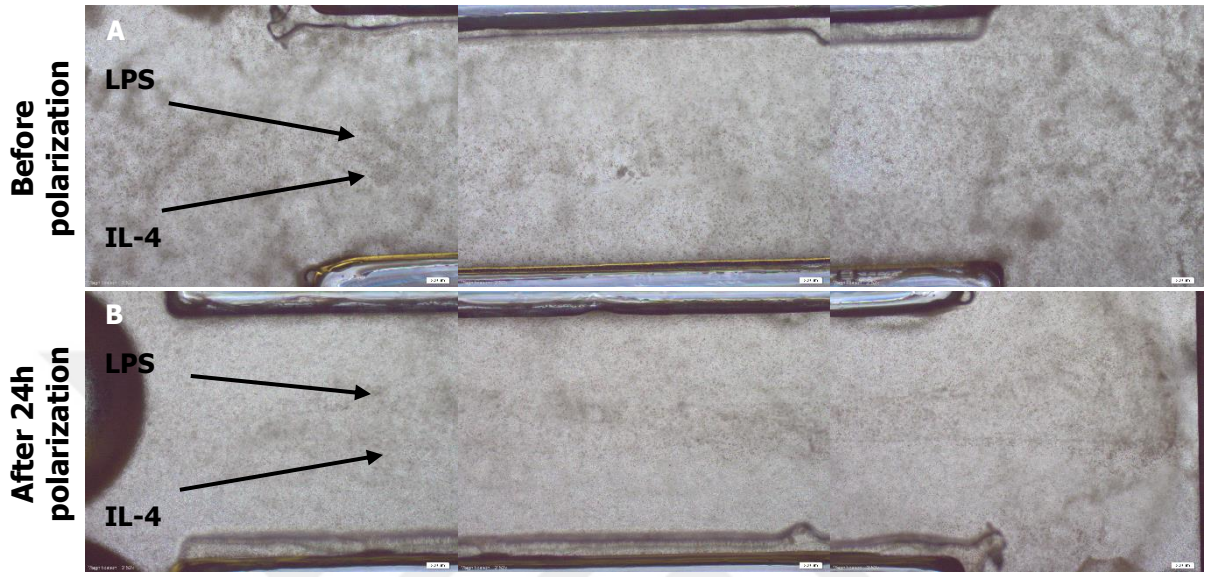

Figure 55: Polarization of N9 cells in 3D dynamic culture H-filter microfluidic chip. A) N9 cells images before the polarization. B) N9 cells images after the 24h polarization

The polarization of THP-1 cells was done in the same manner as the polarization of N9 cells in the H-filter and single channel.

4.7. Characterization of the Cells

We used the immunocytochemistry (ICC) and qPCR methods as described in section 3.6.7.2 to characterize polarized cells.

4.7.1. Fluorescence image of U87 Cells in 3D Static Culture

After encapsulating U87 cells into GelMA, we performed Phalloidin/DAPI fluorescence staining.

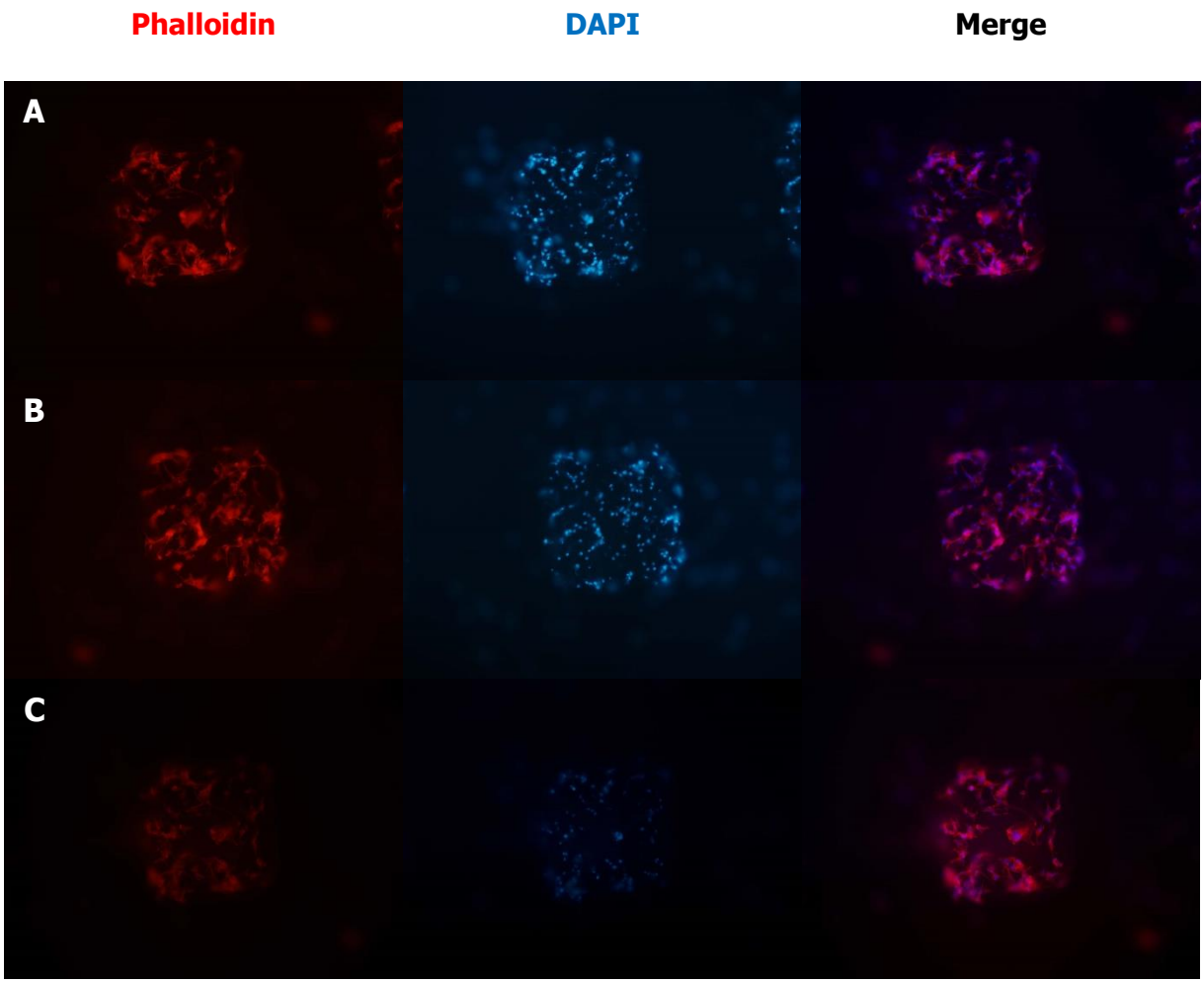

Figure 56: Encapsulation of U87 cells in 3D static culture onto the coverslip and Phalloidin/DAPI staining images.

4.7.3. qPCR Results

4.7.3.2. N9 Cell Line 24h Polarization qPCR Results

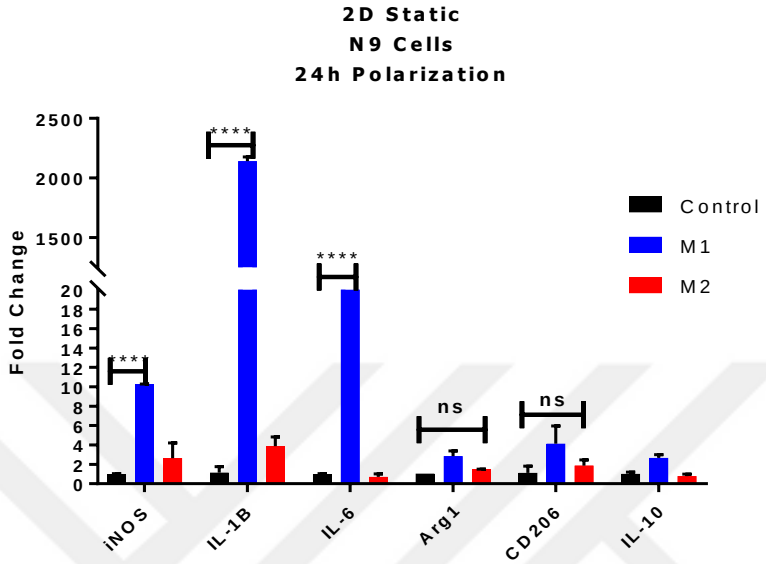

Figure 57: 2D static N9 cells 24h polarization result. M1 markers: iNOS, IL-1B, and IL-6. M2 Markers: Arg1, CD206, and IL-10.

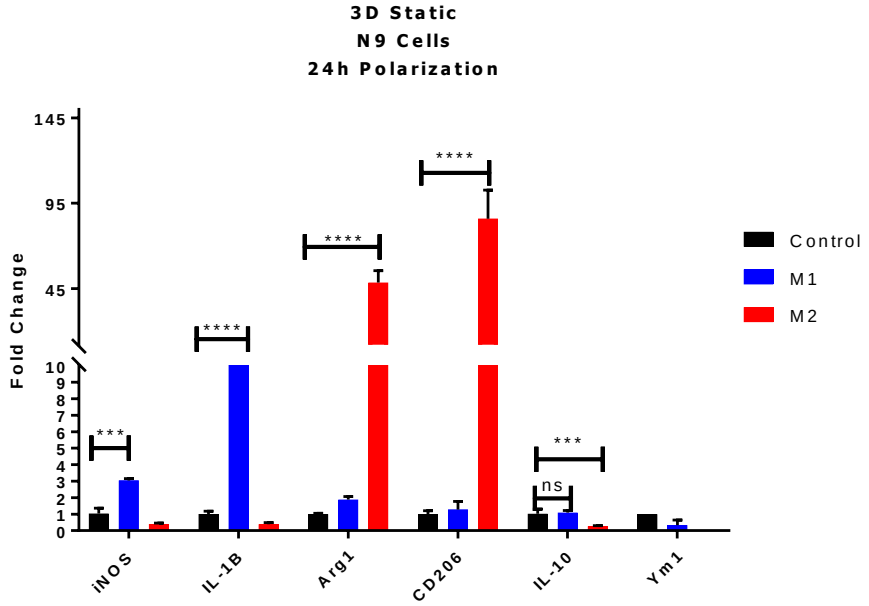

Figure 58: 3D Static N9 cells 24h polarization qPCR result. M1 markers: iNOS, IL-1B, M2 Markers: Arg1, CD206, IL-10, and Ym1.

4.7.3.3. N9 Cell Line 4h Polarization qPCR Results

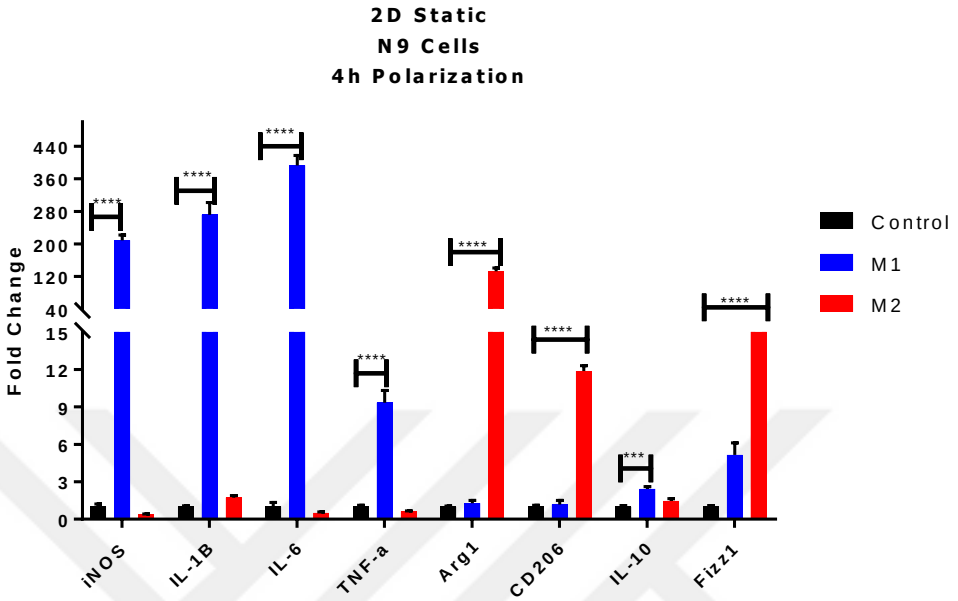

Figure 59: 2D static N9 cells 4h polarization qPCR result. M1 markers: iNOS, IL-1B, IL-6, and TNF-a. M2 Markers: Arg1, CD206, IL-10, and Fizz1.

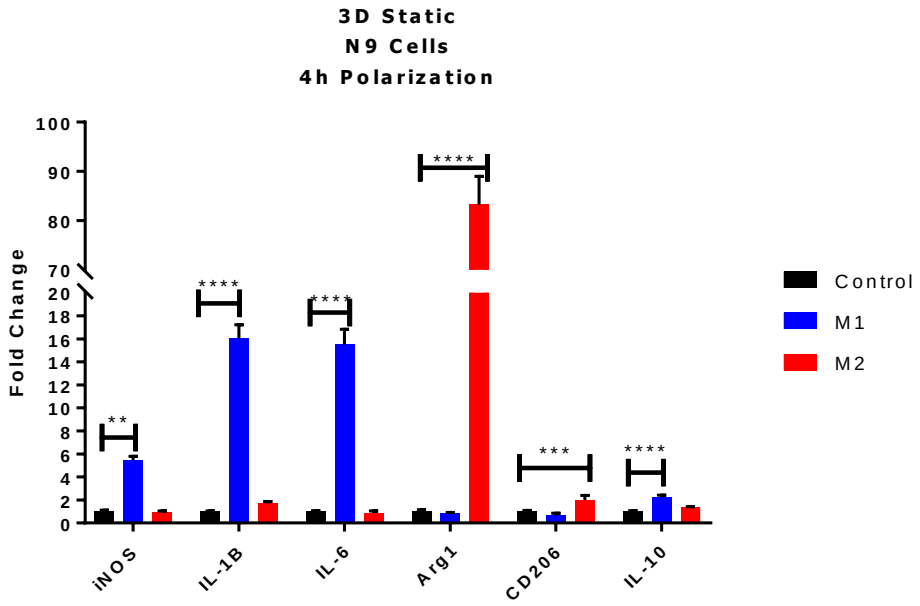

Figure 60: 3D static N9 cells 4h polarization qPCR result. M1 markers: iNOS, IL-1B, and IL-6. M2 Markers: Arg1, CD206, and IL-10.

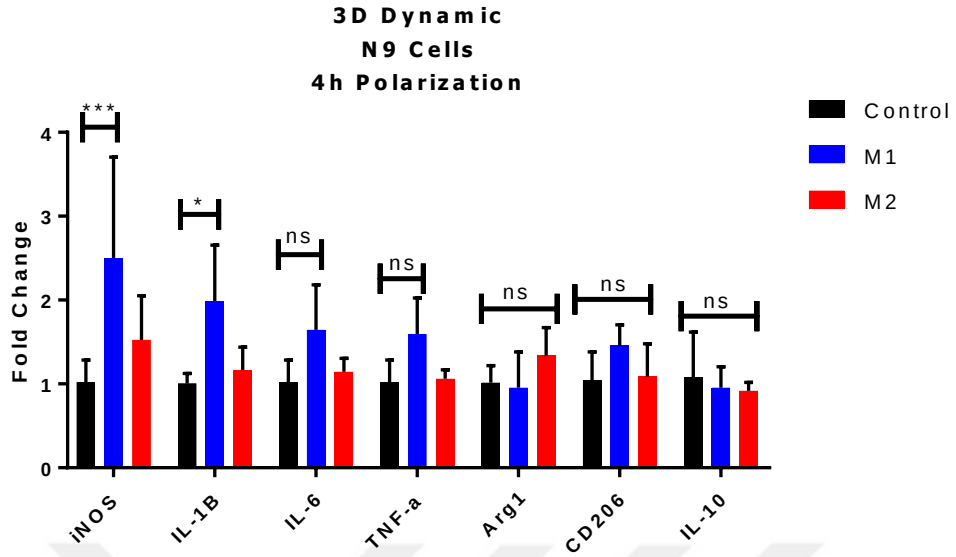

Figure 61: 3D dynamic N9 cells 4h polarization qPCR result. M1 markers: iNOS, IL-1B, IL-6, and TNF-a. M2 Markers: Arg1, CD206, and IL-10.

4.7.3.4. THP-1 Cell Line 4h Polarization qPCR Results

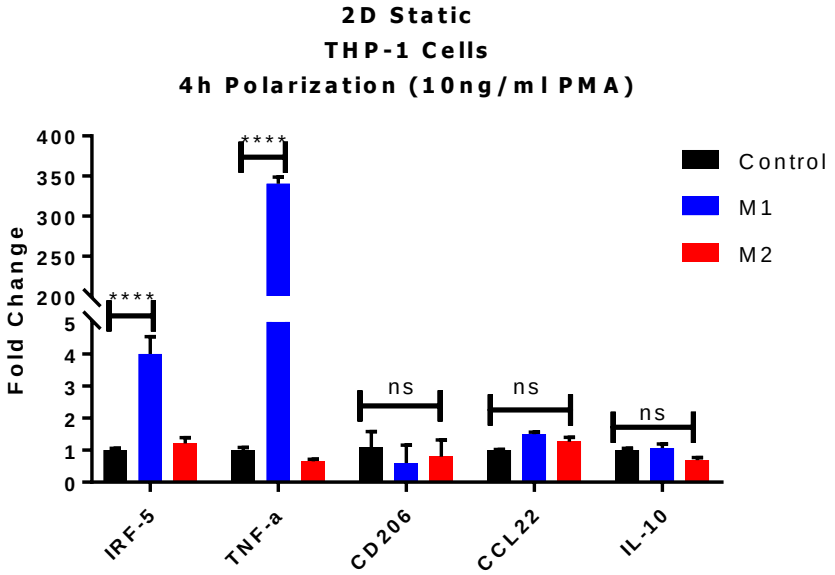

Figure 62: 2D Static THP-1 cells (treated with 10 ng/ml PMA) 4h Polarization qPCR result. M1 Markers: IRF-5 and TNF-a. M2 Markers: CCL22 and IL-10.

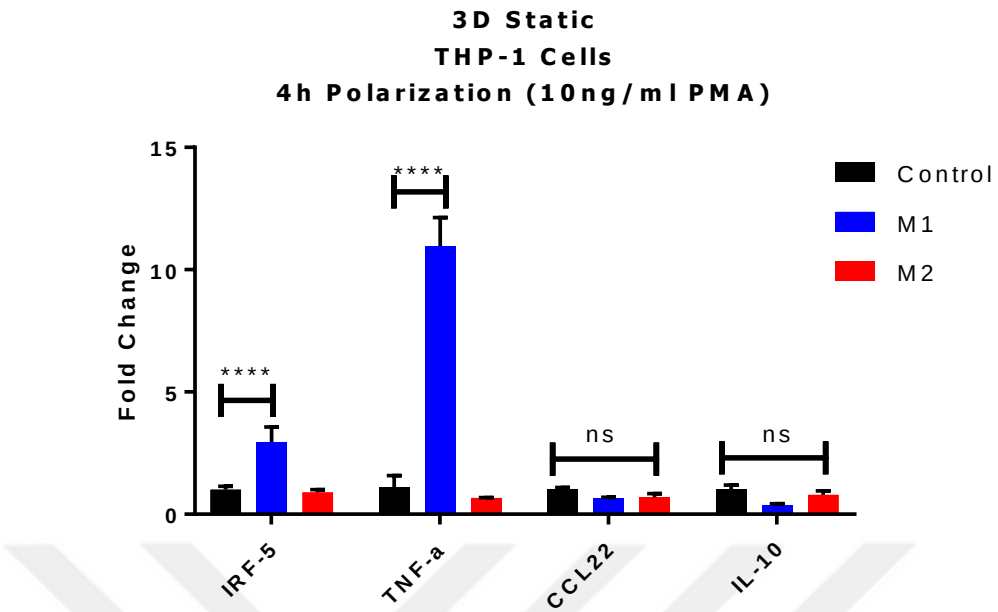

Figure 63: 3D Static THP-1 cells (treated with 10 ng/ml PMA) 4h Polarization qPCR result. M1 Markers: IRF-5 and TNF-a. M2 Markers: CCL22 and IL-10.

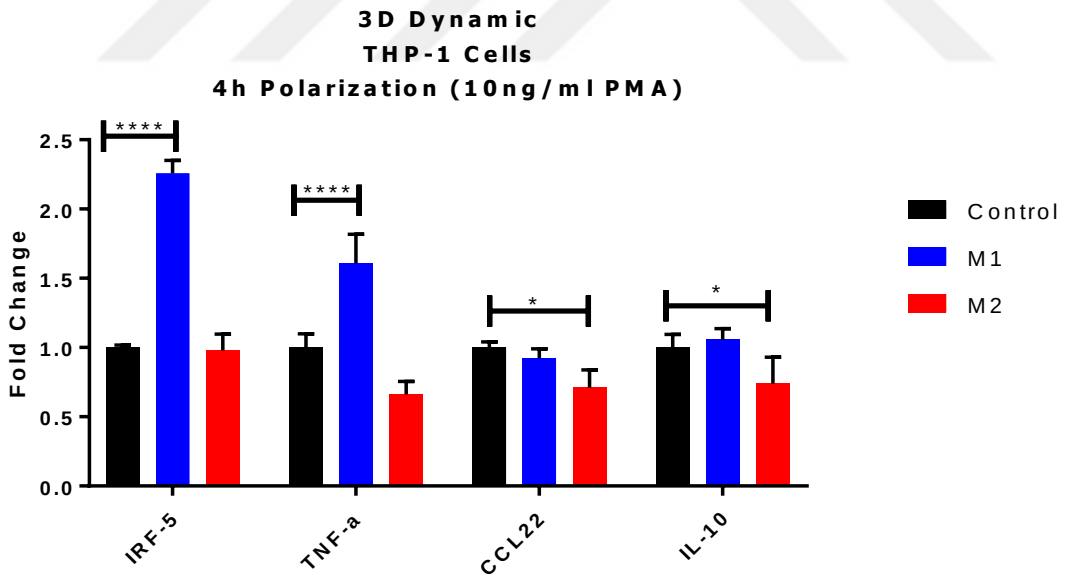

Figure 64: 3D Dynamic THP-1 cells (treated with 10 ng/ml PMA) 4h Polarization qPCR result. M1 Markers: IRF-5 and TNF-a. M2 Markers: CCL22 and IL-10.

4.7.3.5. Control Groups (Unstimulated Groups) qPCR Results

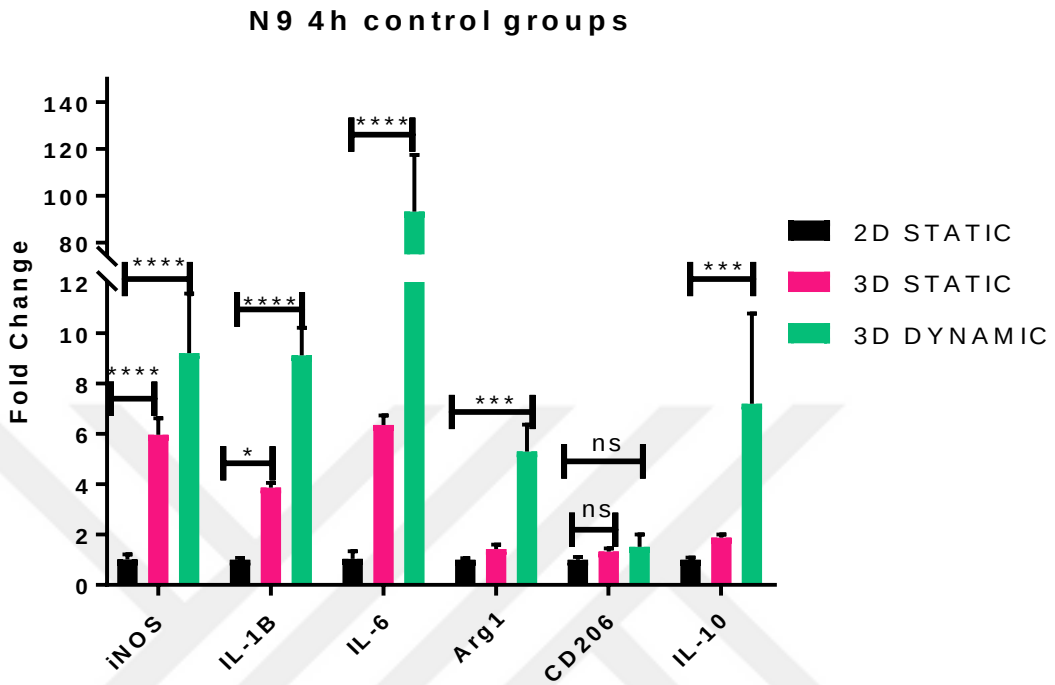

Figure 65: N9 cell line unstimulated control groups for 4h culture in complete medium qPCR results.

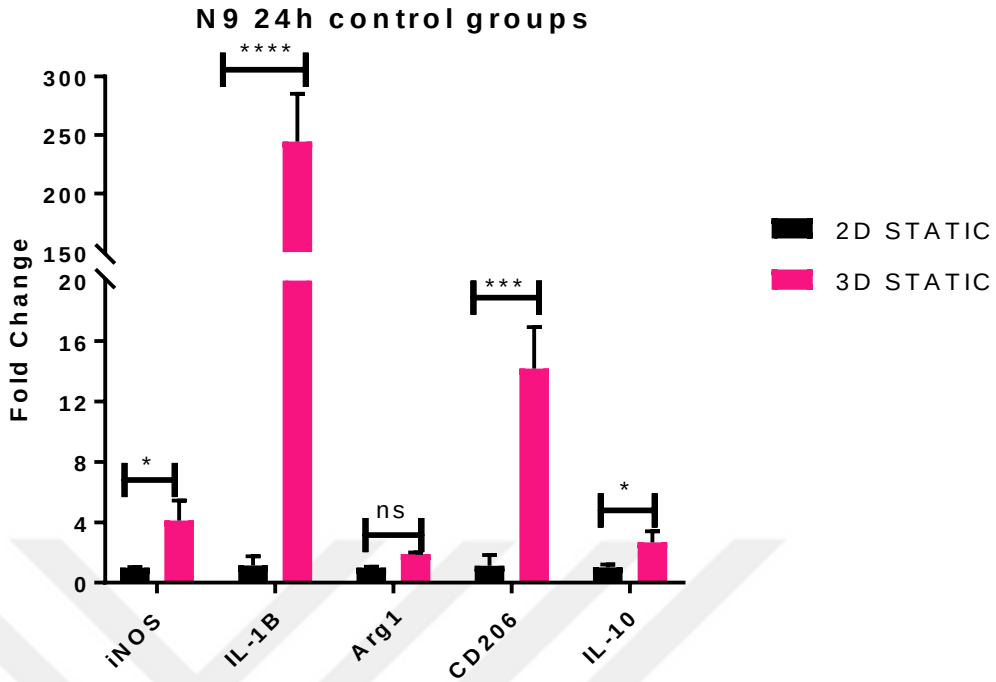

Figure 66: N9 cell line unstimulated control groups for 24h culture in complete medium qPCR results.

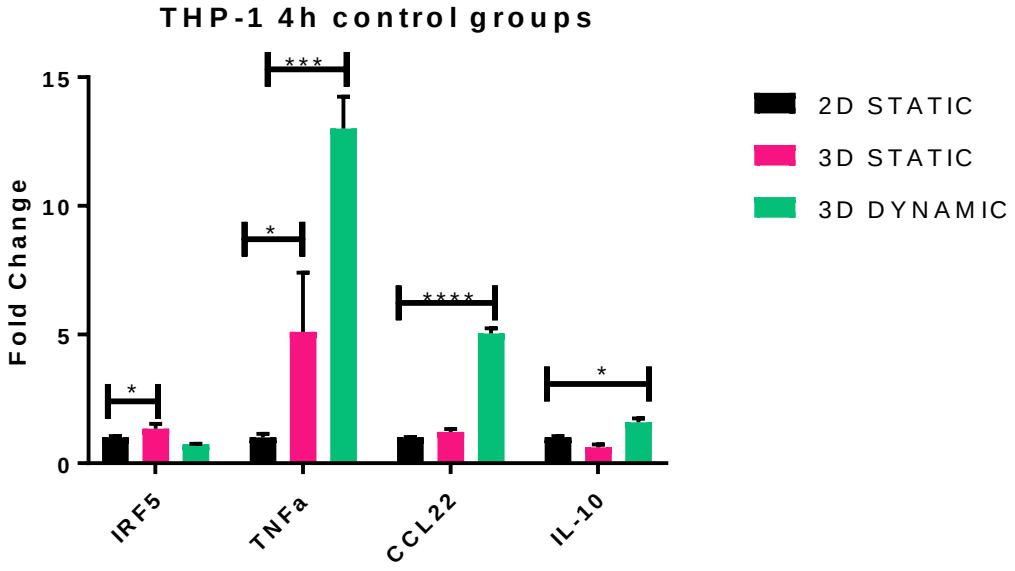

Figure 67: THP-1 cell line unstimulated control groups for 4h culture in complete medium qPCR results.

5. DISCUSSION

In the implantation of biomaterials and in tissue engineering studies, inflammation and foreign body response (FBR) formation are very important in terms of regeneration of target tissue. The aim of our study is to *in vitro* model the 3D natural, complex and dynamic structure of immune cells using microfluidic platforms. For this, we first synthesized biocompatible, biodegradable, gelatin-based hydrogel. During the synthesis of GelMA, we first used a 0.6 ml MAA per 1 gram of gelatin ratio suggested by Loessner et al. (Loessner et al., 2016), however, this amount did not yield for cross-linking GelMA. Then we adjusted this ratio to 0.8 ml MAA per 1 g of gelatin and finally optimized 1 ml MAA per 1 g of gelatin. The most important point to be considered during the synthesis stage is the stabilization of the temperature. As mentioned in Section 3.6.3, the gelatin and MAA reaction should be at 40 °C and the dialysis step should be at 40 °C. Another point to note is that in the reaction step MAA is added slowly to the gelatin solution and mixed properly. MAA is toxic for cells, therefore the excess MAA has been removed by discarding the supernatant after reaction and through the dialysis steps, which were carried out regularly for couple days.

We performed FTIR analysis to characterize the formation of methacrylate group and methacrylamide groups in GelMA which we synthesized. The peak O-H or N-H group formed between 3200-3400 cm^{-1}, peak C stretching between 2900-3000 cm^{-1}, peak C=O (amide I) formed between 1600-1650 cm^{-1} and 1230-1240 cm^{-1} peak N-H (amide II) group as shown in Figures 16 and 17 in section 4.2. We also performed SEM analysis to demonstrate that the GelMA has a porous structure and Figure 15 shows that the heterogeneous porous structure of GelMA. We calculated the average pore size as 37.8 µm.

After the synthesis of GelMA, we encapsulated with GelMA to give cells a 3D structure and incubated them for days. We used various cell lines as shown in section 4.4.1 and showed that they proliferated during the incubation period.

We designed the microfluidic systems to see the behavior of the cells in a dynamic environment. We used these systems which are optically transparent, easy to produce and cost-effective. We fabricated the Single channel and H-filter microfluidic systems according to the designs shown in section 4.3. We used double-sided adhesive tape to assemble the parts of the microfluidic system. We have tried many brands of double-sided adhesive tape, but all tapes have leakage problems. Finally, we eliminated the problem of leaking using 3M ™ High-Performance Acrylic Adhesive Transfer Tape 468MP tape. We used red and blue food dyes to test for non-leakage of microfluidic systems and also to show that fluids do not mix with each other in H-filter chips. After all, we encapsulated the cells into the chip and stimulated with continuous flow.

The amount of RNA from 3D static and 3D dynamic encapsulated and polarized cells were less than the amount of RNA obtained from 2D cells. In order to obtain the cells in the gel, we first used the Trizol but the gel became the solid part and even if we tried to pass through a 19-gauge needle with a 3 mL syringe 15–20 times the gel did not fragmentize and we could not obtain the RNA of the cells. Then we used the collagenase to the digestion of the GelMA, but we still couldn't get enough RNA. Finally, we got the encapsulated cells in a 3D static culture group using a cell scraper and added Trizol to the cells and transferred them to the eppendorf. Likewise, we removed the encapsulated cells in the 3D dynamic culture group by opening the microfluidic chips and added Trizol to the cells and transferred them to the eppendorf. We thoroughly digested these mixtures with the homogenizer and obtained a higher amount of RNA. After RNA isolation, we synthesized cDNA and then indicated at changes in gene expression at mRNA level by qPCR.

We have observed that some of the primers given in Table 3 are not working in our qPCR protocol at 60 degrees and we have not added these genes in the qPCR results in section 4.6.2. Non-working primer sequences; mouse TNF-α, mouse Ym1, human iNOS, human CD206, human IL-6, and human CCL17.

N9 Cell Line 24h Polarization qPCR Results

When we look at the qPCR results of 24h polarization of N9 cells in Section 4.7.3.2 (Fig. 65 and 66), we found that polarization of M1 occurred in the 2D static culture group but the polarization of M2 gave a non-significant result. However, in the 3D static culture group, we found that the polarization of M1 and M2 was significant. We also decided that for 24h the polarization was not suitable for looking at the mRNA level by qPCR and we changed the polarization time to 4h.

N9 Cell Line 4h Polarization qPCR Results

According to the results of the 4h polarization of N9 cells in Section 4.7.3.3, we observed that the polarization of M1 and M2 was performed significantly in the 2D static culture group (Fig. 67) and 3D static group (Fig.68). However, in the 3D dynamic group (Fig.69) we found that significant results were obtained for M1 polarization and non-significant results for M2 polarization.

THP-1 Cell Line 4h Polarization qPCR Results

We first differentiated THP-1 cells with 10 ng/ml PMA for 24h and then incubated in complete medium for 48h. Polarization of the cells was then carried out for 4h.

According to the qPCR results shown in Section 4.7.3.4, there was a significant change in the polarization of M1 in 2D static group (Fig.70), 3D static group (Fig.71) and 3D dynamic group (Fig.72), while we obtained ns results for M2 polarization.

N9 Cell Line Unstimulated Control Groups 24h qPCR Results

After 24h incubation of mouse N9 cells (unstimulated control groups) with complete medium under 2D static, 3D static and 3D dynamic conditions, according to qPCR results, we observed that GelMA hydrogel directions cells towards both the pro-inflammatory phenotype and anti-inflammatory phenotype.

N9 Cell Line Unstimulated Control Groups 4h qPCR Results

Similar to N9 cells unstimulated control groups 24h qPCR results, we observed that GelMA hydrogel directions cells towards both the pro-inflammatory phenotype and anti-inflammatory phenotype.

THP-1 Cell Line Unstimulated Control Groups 4h qPCR Results

Similar to N9 cells unstimulated control groups 4h and 24h qPCR results, we observed that GelMA hydrogel directions cells towards both the pro-inflammatory phenotype and anti-inflammatory phenotype.

6. CONCLUSION AND FUTURE DIRECTIONS

As a conclusion, in this thesis study, we have developed various microfluidic systems for the polarization of the cells in the dynamic environment of immune cells and developed the scaffold similar to the 3D natural microenvironment of the cells. We demonstrated the polarization of the cells in 3D static and 3D dynamic environments at the level of mRNA using M1 and M2 specific markers. But we couldn't get the ICC images of the cells in the H-filter as expected. We can obtain images in the H-filter using specific IF markers. The effect of scaffold material on the polarization of cells will be examined in the future studies by using other biomaterials besides the GelMA hydrogel which we synthesize. In addition, these microfluidic systems can be used for in various drug testing, immunomodulation, the modeling of FBR using the patient's own cells and polarization can be directed by adjusting the flow rate.

7. REFERENCES

Alvarez Moisés, M., Liu, J. C., Santiago, G. T., Cha, B., Vishwakarma, A., Ghaemmaghami, A. M., & Khademhosseini, A. (2016). Delivery strategies to control inflammatory response : Modulating M1 – M2 polarization in tissue engineering applications. *Journal of Controlled Release*, *240*, 349–363. https://doi.org/10.1016/j.jconrel.2016.01.026

Amadio, S., Ninno, A. De, Montilli, C., Businaro, L., & Gerardino, A. (2013). Plasticity of primary microglia on micropatterned geometries and spontaneous long-distance migration in microfluidic channels Plasticity of primary microglia on micropatterned geometries and spontaneous long-distance migration in microfluidic channels. https://doi.org/10.1186/1471-2202-14-121

Asghari, F., Samiei, M., Adibkia, K., Akbarzadeh, A., & Davaran, S. (2017). Biodegradable and biocompatible polymers for tissue engineering application: a review. *Artificial Cells, Nanomedicine and Biotechnology*, *45*(2), 185–192. https://doi.org/10.3109/21691401.2016.1146731

Bang, S., Na, S., Jang, J. M., Kim, J., & Jeon, N. L. (2016). Engineering-Aligned 3D Neural Circuit in Microfluidic Device, 159–166. https://doi.org/10.1002/adhm.201500397

Barthes, J., Dollinger, C., Muller, C. B., Liivas, U., & Griffith, M. (2018). Immune Assisted Tissue Engineering via Incorporation of Macrophages in Cell-Laden Hydrogels Under Cytokine Stimulation, *6*(August), 1–17. https://doi.org/10.3389/fbioe.2018.00108

Barthes, J., Ozcelik, H., Hindie, M., Hasan, A., Engin, N., Cell, V., … Vrana, N. E. (2014). Cell Microenvironment Engineering and Monitoring for Tissue Engineering and Regenerative Medicine : The Citation Accessed Citable Link Cell Microenvironment Engineering and Monitoring for Tissue Engineering and Regenerative Medicine : The Recent Advances. *BioMed Research International*, *2014*(i), 18.

Bassler, BL. The Cell. In: Reece, JB., Urry, LA., Cain, ML., Wasserman, SA., Minorsky, PV., and Jackson, RB., editors. Biology, 6th edition, Pearson Education, 2011. p. 92-245.

Bosshart, H., & Heinzelmann, M. (2016). THP-1 cells as a model for human monocytes. *Annals of Translational Medicine*, *4*(21), 438–438. https://doi.org/10.21037/atm.2016.08.53

Bouyer, C., Chen, P., Güven, S., Demirtaş, T. T., Nieland, T. J. F., Padilla, F., & Demirci, U. (2016). A Bio-Acoustic Levitational (BAL) Assembly Method for Engineering of Multilayered, 3D Brain-Like Constructs, Using Human Embryonic Stem Cell Derived Neuro-Progenitors. *Advanced Materials*, *28*(1), 161–167. https://doi.org/10.1002/adma.201503916

Breslauer, D. N., Lee, P. J., & Lee, L. P. (2006). Microfluidics-based systems biology. *Molecular BioSystems*, *2*(2), 97. https://doi.org/10.1039/b515632g

Bulcke, A. I. Van Den, Bogdanov, B., Rooze, N. De, Schacht, E. H., Cornelissen, M., & Berghmans, H. (2000). Structural and Rheological Properties of Methacrylamide Modified Gelatin Hydrogels, 31–38.

Calibasi Kocal, G., Güven, S., Foygel, K., Goldman, A., Chen, P., Sengupta, S., … Demirci, U. (2016). Dynamic Microenvironment Induces Phenotypic Plasticity of Esophageal Cancer Cells Under Flow. *Scientific Reports*, *6*(1), 38221. https://doi.org/10.1038/srep38221

Calvo, J. R., Gonzalez-Yanes, C., & Maldonado, M. D. (2013). The role of melatonin in the cells of the innate immunity: A review. *Journal of Pineal Research*, *55*(2), 103–120. https://doi.org/10.1111/jpi.12075

Cha, B. H., Shin, S. R., Leijten, J., Li, Y. C., Singh, S., Liu, J. C., … Khademhosseini, A. (2017). Integrin-Mediated Interactions Control Macrophage Polarization in 3D Hydrogels. *Advanced Healthcare Materials*, *6*(21), 1–12. https://doi.org/10.1002/adhm.201700289

Cha, B., Shin, S. R., Leijten, J., Li, Y., Singh, S., Liu, J. C., … Khademhosseini, A.

(2017). Integrin-Mediated Interactions Control Macrophage Polarization in 3D Hydrogels. https://doi.org/10.1002/adhm.201700289

Chanput, W., Mes, J. J., Savelkoul, F. J., & Wichers, H. J. (2013). Characterization of polarized THP-1 macrophages and polarizing ability of LPS and food compounds. *Food & Function*, *4*, 266–276. https://doi.org/10.1039/c2fo30156c

Chanput, W., Mes, J. J., & Wichers, H. J. (2014). THP-1 cell line: An in vitro cell model for immune modulation approach. *International Immunopharmacology*, (2013), 1–9. https://doi.org/10.1016/j.intimp.2014.08.002

Chaubaroux, C., Vrana, E., Debry, C., Schaaf, P., Senger, B., Voegel, J., … Lavalle, P. (2012). Collagen-Based Fibrillar Multilayer Films Cross-Linked by a Natural Agent, *16*.

Chhor, V., Le Charpentier, T., Lebon, S., Oré, M. V., Celador, I. L., Josserand, J., … Fleiss, B. (2013). Characterization of phenotype markers and neuronotoxic potential of polarised primary microglia In vitro. *Brain, Behavior, and Immunity*, *32*, 70–85. https://doi.org/10.1016/j.bbi.2013.02.005

CHo, H. Y. J. O. O. N. C., Erbridge, S. C. S. V, Avalos, R. A. V. D., & Ee, Y. O. N. G. W. L. (2018). Development of an In Vitro 3D Brain Tissue Model Mimicking In Vivo - Like Pro-inflammatory and Pro-oxidative Responses. https://doi.org/10.1007/s10439-018-2004-z

Choi, J. R., Yong, K. W., Choi, J. Y., & Cowie, A. C. (2019). Recent advances in photo-crosslinkable hydrogels for biomedical applications, 40–53.

Chung, L., Maestas, D. R., Housseau, F., & Elisseeff, J. H. (2017). Key players in the immune response to biomaterial scaffolds for regenerative medicine ☆. *Advanced Drug Delivery Reviews*, *114*, 184–192. https://doi.org/10.1016/j.addr.2017.07.006

Colton, C. A., & Wilcock, D. M. (2012). Assessing Activation States in Microglia. *CNS & Neurological Disorders - Drug Targets*, *9*(2), 174–191. https://doi.org/10.2174/187152710791012053

Convery, N., & Gadegaard, N. (2019). Micro and Nano Engineering 30 years of microfluidics, *2* (November 2018), 76–91. https://doi.org/10.1016/j.mne.2019.01.003

Cunha, C., Gomes, C., Vaz, A. R., & Brites, D. (2016). Exploring New Inflammatory Biomarkers and Pathways during LPS-Induced M1 Polarization, *2016*.

Daigneault, M., Preston, J. A., Marriott, H. M., Whyte, M. K. B., & Dockrell, D. H. (2010). The identification of markers of macrophage differentiation in PMA-stimulated THP-1 cells and monocyte-derived macrophages. *PLoS ONE*, *5*(1). https://doi.org/10.1371/journal.pone.0008668

Dempsey, P. W., Vaidya, S. A., & Cheng, G. (2003). The Art of War: Innate and adaptive immune responses. *Cellular and Molecular Life Sciences*, *60*(12), 2604–2621. https://doi.org/10.1007/s00018-003-3180-y

Dollinger, C., Vrana, N. E., Ghaemmaghami, A. M., Guner, R., Barthes, J., Knopf-Marques, H., … Ciftci, S. (2017). Incorporation of resident macrophages in engineered tissues: Multiple cell type response to microenvironment controlled macrophage-laden gelatine hydrogels. *Journal of Tissue Engineering and Regenerative Medicine*, *12*(2), 330–340. https://doi.org/10.1002/term.2458

Duinen, V. Van, Trietsch, S. J., Joore, J., Vulto, P., & Hankemeier, T. (2015). Microfluidic 3D cell culture : from tools to tissue models. *Current Opinion in Biotechnology*, *35*, 118–126. https://doi.org/10.1016/j.copbio.2015.05.002

Dziki, J. L., & Badylak, S. F. (2018). ScienceDirect Immunomodulatory biomaterials. *Current Opinion in Biomedical Engineering*, *6*, 51–57. https://doi.org/10.1016/j.cobme.2018.02.005

Ekdahl, C. T. (2012). Microglial activation-tuning and pruning adult neurogenesis. *Frontiers in Pharmacology*, *3 MAR*(March), 1–9. https://doi.org/10.3389/fphar.2012.00041

Forrester, M. A., Wassall, H. J., Hall, L. S., Cao, H., Heather, M., Barker, R. N., & Vickers, M. A. (2018). Similarities and differences in surface receptor expression

by THP-1 monocytes and differentiated macrophages polarized using seven different conditioning regimens Authors : *Cellular Immunology*. https://doi.org/10.1016/j.cellimm.2018.07.008

Forrester, M. A., Wassall, H. J., Hall, L. S., Cao, H., Wilson, H. M., Barker, R. N., & Vickers, M. A. (2018). Similarities and differences in surface receptor expression by THP-1 monocytes and differentiated macrophages polarized using seven different conditioning regimens. *Cellular Immunology*, *332*(April), 58–76. https://doi.org/10.1016/j.cellimm.2018.07.008

Geckil H, Xu F, Zhang X, Moon S, D. U. (2010). Engineering hydrogels as extracellular matrix mimics, *5*(3), 469–484. https://doi.org/10.2217/nnm.10.12.Engineering

Geissmann, F., Manz, M. G., Jung, S., Sieweke, M. H., & Ley, K. (2011). Development of monocytes, macrophages and dendritic cells Frederic. *Science*, *327*(5966), 656–661. https://doi.org/10.1126/science.1178331.Development

Genin, M., Clement, F., Fattaccioli, A., Raes, M., & Michiels, C. (2015). M1 and M2 macrophages derived from THP-1 cells differentially modulate the response of cancer cells to etoposide, 1–14. https://doi.org/10.1186/s12885-015-1546-9

Graeber, M. B., & Streit, W. J. (2009). Microglia: Biology and pathology. *Acta Neuropathologica*, *119*(1), 89–105. https://doi.org/10.1007/s00401-009-0622-0

Güven, S., Mehrkens, A., Saxer, F., Schaefer, D. J., Martinetti, R., Martin, I., & Scherberich, A. (2011). Engineering of large osteogenic grafts with rapid engraftment capacity using mesenchymal and endothelial progenitors from human adipose tissue. *Biomaterials*, *32*(25), 5801–5809. https://doi.org/10.1016/j.biomaterials.2011.04.064

Harink, B., Gac, S. Le, Truckenmüller, R., Blitterswijk, C., & Habibovic, P. (2013). Regeneration-on-a-chip ? The perspectives on use of microfluidics in regenerative medicine. *Lab on a Chip*, 3512–3528. https://doi.org/10.1039/c3lc50293g

He, C., & Carter, A. B. (2016). The Metabolic Prospective and Redox Regulation of Macrophage Polarization. *Journal of Clinical & Cellular Immunology*, *6*(6).

https://doi.org/10.4172/2155-9899.1000371

Helton, K. L., Nelson, K. E., Fu, E., & Yager, P. (2008). Conditioning saliva for use in a microfluidic biosensor. *Lab on a Chip*, *8*(11), 1847–1851. https://doi.org/10.1039/b811150b

Helton, K. L., & Yager, P. (2007). Interfacial instabilities affect microfluidic extraction of small molecules from non-Newtonian fluids. *Lab on a Chip*, *7*(11), 1581. https://doi.org/10.1039/b709585f

Hickman, S. E., Kingery, N. D., Ohsumi, T. K., Borowsky, M. L., Wang, L. C., Means, T. K., & El Khoury, J. (2013). The microglial sensome revealed by direct RNA sequencing. *Nature Neuroscience*, *16*(12), 1896–1905. https://doi.org/10.1038/nn.3554

Hickman, S., Izzy, S., Sen, P., Morsett, L., & Khoury, J. El. (2018). Microglia in neurodegeneration. *Nature Neuroscience*, *21*(October). https://doi.org/10.1038/s41593-018-0242-x

Holleran, GrainneLopetuso, L., Gasbarrini, A., Graziani, C., Petito, V., Ianiro, G., McNamara, D., & Scaldaferri, F. (2017). The Innate and Adaptive Immune System as Targets for Biologic Therapies in Inflammatory Bowel Disease. *International Journal of Molecular Sciences*, *18*(10), 2020. https://doi.org/10.3390/ijms18102020

Hu, X., Leak, R. K., Shi, Y., Suenaga, J., Gao, Y., & Zheng, P. (2014). Microglial and macrophage polarization—new prospects for brain repair. *Nature Publishing Group*, 1–9. https://doi.org/10.1038/nrneurol.2014.207

Huh, D. (2010). Reconstituting Organ-Level Lung Functions on a Chip, *1662*. https://doi.org/10.1126/science.1188302

Hutson, C. B., Tunable, C., Liebert, M. A., & Link, C. (2019). Synthesis and Characterization of Tunable PEG - Gelatin Methacrylate Hydrogels. https://doi.org/10.1089/ten.tea.2010.0666

Jablonski, K. A., Amici, S. A., Webb, L. M., Ruiz-rosado, J. D. D., Popovich, P. G., Partida-sanchez, S., & Guerau-de-arellano, M. (2015). Novel Markers to Delineate Murine M1 and M2 Macrophages, 5–11. https://doi.org/10.1371/journal.pone.0145342

Journal, A. I., Modaresifar, K., Hadjizadeh, A., & Niknejad, H. (2018). Design and fabrication of GelMA / chitosan nanoparticles composite hydrogel for angiogenic growth factor delivery. *Artificial Cells, Nanomedicine, and Biotechnology*, *46*(8), 1799–1808. https://doi.org/10.1080/21691401.2017.1392970

Kettenmann, H., Hanisch, U.-K., Noda, M., & Verkhratsky, A. (2011). Physiology of Microglia. *Physiological Reviews*, *91*(2), 461–553. https://doi.org/10.1152/physrev.00011.2010

Khademhosseini, A., & Langer, R. (2016). A decade of progress in tissue engineering. *Nature Protocols*, *11*(10), 1775–1781. https://doi.org/10.1038/nprot.2016.123

Knopf-Marques, H., Singh, S., Htwe, S. S., Wolfova, L., Buffa, R., Bacharouche, J., … Lavalle, P. (2016). Immunomodulation with Self-Crosslinked Polyelectrolyte Multilayer-Based Coatings. *Biomacromolecules*, *17*(6), 2189–2198. https://doi.org/10.1021/acs.biomac.6b00429

Kong, D. S., Thorsen, T. A., Babb, J., Wick, S. T., Gam, J. J., Weiss, R., & Carr, P. A. (2017). Open-source, community-driven microfluidics with Metafluidics, *35*(6), 523–529. https://doi.org/10.1038/nbt.3873

Kzhyshkowska, J., Vrana, N. E., Riabov, V., Lavalle, P., Dollinger, C., & Gudima, A. (2015). Macrophage responses to implants: prospects for personalized medicine. *Journal of Leukocyte Biology*, *98*(6), 953–962. https://doi.org/10.1189/jlb.5vmr0415-166r

Langer, R., & Vacanti, J. P. (1993). Tissue Engineering. *Science*, *260*(5110), 920–926. https://doi.org/10.1126/science.8493529

Lee, D., Ji, E., Eun, S., Lhi, K., Moon, H., Jun, H., … Lee, Y. (2019). Injectable biodegradable gelatin-methacrylate / β - tricalcium phosphate composite for the

repair of bone defects. *Chemical Engineering Journal*, *365*(November 2018), 30–39. https://doi.org/10.1016/j.cej.2019.02.020

Li, C., Levin, M., & Kaplan, D. L. (2016). Bioelectric modulation of macrophage polarization. *Nature Publishing Group*, (February 2015), 1–12. https://doi.org/10.1038/srep21044

Littlefield, M. J., Teboul, I., Voloshyna, I., Reiss, A. B., Reiss, A. B., Hospital, W., & Plaza, S. (2014). Immunology and Immunotherapy ClinMed, 1–8.

LOCATI, M., SICA, A., ALLAVENA, P., SOZZANI, S., MANTOVANI, A., & VECCHI, A. (2004). The chemokine system in diverse forms of macrophage activation and polarization. *Trends in Immunology*, *25*(12), 677–686. https://doi.org/10.1016/j.it.2004.09.015

Loessner, D., Meinert, C., Kaemmerer, E., Martine, L. C., Yue, K., Levett, P. A., … Hutmacher, D. W. (2016). Functionalization, preparation and use of cell-laden gelatin methacryloyl-based hydrogels as modular tissue culture platforms. *Nature Protocols*, *11*(4), 727–746. https://doi.org/10.1038/nprot.2016.037

Lund, M. E., To, J., Brien, B. A. O., & Donnelly, S. (2016). The choice of phorbol 12-myristate 13-acetate differentiation protocol influences the response of THP-1 macrophages to a pro-inflammatory stimulus. *Journal of Immunological Methods*, 6–12. https://doi.org/10.1016/j.jim.2016.01.012

Macrophages, M., Daigneault, M., Preston, J. A., Marriott, H. M., Whyte, M. K. B., & Dockrell, D. H. (2010). The Identification of Markers of Macrophage Differentiation in PMA-Stimulated THP-1 Cells and, *5*(1). https://doi.org/10.1371/journal.pone.0008668

Maeß, M. B., Wittig, B., Cignarella, A., & Lorkowski, S. (2014). Reduced PMA enhances the responsiveness of transfected THP-1 macrophages to polarizing stimuli. *Journal of Immunological Methods*, *402*(1–2), 76–81. https://doi.org/10.1016/j.jim.2013.11.006

Mantovani, A., Martinez, F. O., & Gordon, S. (2004). The M1 and M2 paradigm of

macrophage activation : time for reassessment, *13*(March), 1–13. https://doi.org/10.12703/P6-13

Mantovani, A., Sica, A., & Locati, M. (2007). New vistas on macrophage differentiation and activation. *European Journal of Immunology*, *37*(1), 14–16. https://doi.org/10.1002/eji.200636910

Martinez, F. O., Gordon, S., Locati, M., & Mantovani, A. (2006). Transcriptional Profiling of the Human Monocyte-to-Macrophage Differentiation and Polarization: New Molecules and Patterns of Gene Expression. *The Journal of Immunology*, *177*(10), 7303–7311. https://doi.org/10.4049/jimmunol.177.10.7303

Matias, D., Predes, D., Filho, P. N., Lopes, M. C., Abreu, J. G., Lima, F. R. S., & Neto, V. M. (2017). BBA - Reviews on Cancer Microglia-glioblastoma interactions : New role for Wnt signaling, *1868*(October 2016), 333–340. https://doi.org/10.1016/j.bbcan.2017.05.007

Min, B., Brown, M. A., & Legros, G. (2012). Understanding the roles of basophils: Breaking dawn. *Immunology*, *135*(3), 192–197. https://doi.org/10.1111/j.1365-2567.2011.03530.x

Mogosanu, D., Verplancke, R., Dubruel, P., & Van, J. (2016). Fabrication of 3-dimensional biodegradable microfluidic environments for tissue engineering applications, *89*, 1315–1324. https://doi.org/10.1016/j.matdes.2015.10.046

Mosser, D. M., & Edwards, J. P. (2008). Exploring the full spectrum of macrophage activation. *Nature Reviews Immunology*, *8*(12), 958–969. https://doi.org/10.1038/nri2448

Nakagawa, Y., & Chiba, K. (2015). Pharmacology & Therapeutics Diversity and plasticity of microglial cells in psychiatric and neurological disorders. *Pharmacology and Therapeutics*. https://doi.org/10.1016/j.pharmthera.2015.06.010

Namkoong, B., Güven, S., Ramesan, S., Liaudanskaya, V., Abzhanov, A., & Demirci, U. (2016). Recapitulating cranial osteogenesis with neural crest cells in 3-D microenvironments. *Acta Biomaterialia*, *31*, 301–311.

https://doi.org/10.1016/j.actbio.2015.12.004

Nichol, J. W., Koshy, S. T., Bae, H., Hwang, C. M., Yamanlar, S., & Khademhosseini, A. (2010). Biomaterials Cell-laden microengineered gelatin methacrylate hydrogels. *Biomaterials*, *31*(21), 5536–5544. https://doi.org/10.1016/j.biomaterials.2010.03.064

Nos, S., Myung, N., Park, M., Kim, S., Zhang, SU., and Kang, HW. 3D Bioprinting for Tissue Engineering. In: Kim, BW., editor. Clinical Regenerative Medicine in Urology. Springer, 2018. p.105-123.

Oktay, S., & Alemdar, N. (2019). Electrically controlled release of 5- fluorouracil from conductive gelatin methacryloyl-based hydrogels, *46914*, 1–8. https://doi.org/10.1002/app.46914

Orihuela, R., McPherson, C. A., & Harry, G. J. (2016). Microglial M1/M2 polarization and metabolic states. *British Journal of Pharmacology*, *173*(4), 649–665. https://doi.org/10.1111/bph.13139

Osborn, J. L., Lutz, B., Fu, E., Kauffman, P., Stevens, D. Y., & Yager, P. (2010). Microfluidics without pumps: reinventing the T-sensor and H-filter in paper networks. *Lab on a Chip*, *10*(20), 2659. https://doi.org/10.1039/c004821f

Park, E. K., Jung, H. S., Yang, H. I., Yoo, M. C., Kim, C., & Kim, K. S. (2007). Optimized THP-1 differentiation is required for the detection of responses to weak stimuli, *56*, 45–50. https://doi.org/10.1007/s00011-007-6115-5

Paula, M. De, Michelle, M., Bassous, N. J., Id, S. A., Harb, S. V., Ghannadian, P., … Id, L. (2018). Understanding the impact of crosslinked PCL / PEG / GelMA electrospun nanofibers on bactericidal activity, 1–19.

Perry, V. H., Nicoll, J. A. R., & Holmes, C. (2010). Microglia in neurodegenerative disease. *Nature Reviews Neurology*, *6*(4), 193–201. https://doi.org/10.1038/nrneurol.2010.17

Ransohoff, R. M., & Perry, V. H. (2009). Microglial Physiology: Unique Stimuli,

Specialized Responses. *Annual Review of Immunology*, *27*(1), 119–145. https://doi.org/10.1146/annurev.immunol.021908.132528

Righi, M., Mori, L., Libero, G. De, Sironi, M., Biondi, A., Mantovani, A., … Ricciardi-Castagnoli, P. (1989). Monokine production by microglial cell clones. *European Journal of Immunology*, *19*(8), 1443–1448. https://doi.org/10.1002/eji.1830190815

Rivera, A., Siracusa, M. C., Yap, G. S., Gause, W. C., Biomedical, R., Sciences, H., … Sciences, H. (2016). Innate cell communication kick-starts pathogen-specific immunity, *17*(4), 356–363. https://doi.org/10.1038/ni.3375.Innate

Saijo, K., & Glass, C. K. (2011). Microglial cell origin and phenotypes in health and disease. *Nature Reviews Immunology*, *11*(11), 775–787. https://doi.org/10.1038/nri3086

Saleh, L. S., & Bryant, S. J. (2017). In vitro and in vivo models for assessing the host response to biomaterials. *Drug Discovery Today: Disease Models*, *24*, 13–21. https://doi.org/10.1016/j.ddmod.2018.04.002

Sharifi, F., Htwe, S. S., Righi, M., Liu, H., Pietralunga, A., Yesil-celiktas, O., … Zhang, Y. S. (2019). A Foreign Body Response-on-a-Chip Platform, *1801425*, 1–10. https://doi.org/10.1002/adhm.201801425

Shirahama, H., Lee, B. H., Tan, L. P., & Cho, N. (2016). Precise Tuning of Facile One-Pot Gelatin Methacryloyl (GelMA) Synthesis. *Nature Publishing Group*, (August), 1–11. https://doi.org/10.1038/srep31036

Shiratori, H., Feinweber, C., Luckhardt, S., Linke, B., Resch, E., Geisslinger, G., … Parnham, M. J. (2017). THP-1 and human peripheral blood mononuclear cell-derived macrophages differ in their capacity to polarize in vitro. *Molecular Immunology*, *88*(June), 58–68. https://doi.org/10.1016/j.molimm.2017.05.027

Stansley, B., Post, J., & Hensley, K. (2012). A comparative review of cell culture systems for the study of microglial biology in Alzheimer ' s disease, 1–8.

Tarique, A. A., Logan, J., Thomas, E., Holt, P. G., Sly, P. D., & Fantino, E. (2015). Phenotypic, functional, and plasticity features of classical and alternatively activated human macrophages. *American Journal of Respiratory Cell and Molecular Biology*, *53*(5), 676–688. https://doi.org/10.1165/rcmb.2015-0012OC

Tedesco, S., Majo, F. De, Kim, J., Trenti, A., Trevisi, L., Fadini, G. P., … Vitiello, L. (2018). Convenience versus Biological Significance : Are PMA-Differentiated THP-1 Cells a Reliable Substitute for Blood-Derived Macrophages When Studying in Vitro Polarization ?, *9*(February), 1–13. https://doi.org/10.3389/fphar.2018.00071

Vrana, N. E. (2016). Immunomodulatory biomaterials and regenerative immunology. *Future Science OA*, *2*(4), FSO146. https://doi.org/10.4155/fsoa-2016-0060

wang, J. (2018). Treatment targets for M2 microglia polarization in ischemic stroke, *105*(March), 518–525. https://doi.org/10.1016/j.biopha.2018.05.143

Wang, Y., Ma, M., Wang, J., & Zhang, W. (n.d.). Development of a Photo-Crosslinking, Biodegradable, 6–8. https://doi.org/10.3390/ma11081345

Warrington, R., Watson, W., Kim, H. L., & Antonetti, F. R. (2011). An introduction to immunology and immunopathology. *Allergy, Asthma & Clinical Immunology*, *7*(S1), 1–8. https://doi.org/10.1186/1710-1492-7-s1-s1

Wen, T., & Rothenberg, E. (2017). The Regulatory Function of Eosinophils, *4*(11), 1–19. https://doi.org/10.1016/S2214-109X(16)30265-0.Cost-effectiveness

Xiong, X., Liu, L., & Yang, Q. (2016). Progress in Neurobiology Functions and mechanisms of microglia/macrophages in neuroinflammation and neurogenesis after stroke. *Progress in Neurobiology*, *142*, 23–44. https://doi.org/10.1016/j.pneurobio.2016.05.001

Yanagawa, F., Sugiura, S., & Kanamori, T. (2016). Hydrogel microfabrication technology toward three dimensional tissue engineering. *Regenerative Therapy*, *3*, 45–57. https://doi.org/10.1016/j.reth.2016.02.007

Zhang, H., Wang, G., Ding, H., Xu, K., Wu, X., Tang, H., … Ji, F. (2018). Macrophage

polarization, inflammatory signaling, and NF-κB activation in response to chemically modified titanium surfaces. *Colloids and Surfaces B: Biointerfaces*, *166*, 269–276. https://doi.org/10.1016/j.colsurfb.2018.03.029

Zhou, T., Huang, Z., Sun, X., Zhu, X., Zhou, L., Li, M., & Cheng, B. (2017). Microglia Polarization with M1 / M2 Phenotype Changes in rd1 Mouse Model of Retinal Degeneration, *11*(September), 1–11. https://doi.org/10.3389/fnana.2017.00077

8. APPENDIX

8.1. Curriculum Vitae

Olcay Burçin AKBULUD

ID No / Pasaport No:	28280152356
Date of Birth:	11.05.1991
Contact Address:	1403 sokak No:9 D:10 Nilüfer Apartmanı Erkent 1 Sitesi Bucakoop Buca/İZMİR
Phone :	05058095174
Faks :	
e-mail:	olcay.akbulud@hotmail.com

EDUCATIONAL BACKGROUND

Country	University	Faculty/Institute	Department	Degree	Year of Graduation
T.C	Ege University	Engineering	Bioengineering	Bachelor	2015
T.C	Dokuz Eylul University	Izmir Biomedicine and Genome Institute	Molecular Biology and Genetics	Master of Science	2019

ACADEMIC / PROFESSIONAL EXPERIENCE

Kurum/Kuruluş	Country	City	Bölüm/Birim	Görev Türü	Görev Dönemi
Dokuz Eylul University	T.C	Izmir	Medical Biology	Internship	July-Agust 2014
Izmir Biomedicine and Genome Center	T.C	Izmir	Molecular Biology and Genetic	Internship	August-September 2014

Specialist Fields
Tissue Engineering Biomaterial Microfluidic Systems Molecular Biology and Genetics Immunology

CONFERENCES and ABSTRACT BOOKS

Poster Presentation:”3 Boyutlu Dinamik Kültürde M1-M2 Makrofaj Polarizasyonu, 23. Biyomedikal ve Teknoloji Sempozyumu”, Acıbadem University, Istanbul
Poster Presentation:” Lacrimal Tissue Engineering, 23. Biyomedikal Bilimler ve Teknoloji Sempozyumu”, Acıbadem Universtiy, Istanbul
Poster Presentation:”Engineering Bone-Cartilage Interface in Microfluidic System, 23. Biyomedikal ve Teknoloji Sempozyumu”, Acıbadem University, Istanbul
Poster Presentation:” Tissue Engineering of Lacrimal Gland, 5. Biyomalzeme Günleri”, Yıldız Technical University, Istanbul
Poster Presentation:” Mikroakışkan Sistemler ile 3D Makrofaj Polarizasyonu, 5. Biyomalzeme Günleri”, Yıldız Technical University, Istanbul
Poster Presentation: ”3 Boyutlu Mikroakışkan Sistemlerde Nörodejeneratif Hastalık Modellemesi, 3. Novel Fluidic Technologies Workshop with an Emphasis on Tissue Engineering,” Ege University, Izmir
Poster Presentation:” Mikroakışkan Sisteminde Kemik Kıkırdak Arayüzü Modellemesi, 4. Biyomateryal Günleri”, Yalova
Poster Presentation:” 3 Boyutlu Mikroakışkan Sistemlerde Nörodejeneratif Hastalık Modellemesi, 4. Biyomateryal Günleri”, Yalova
Poster Presentation:” Mikroakışkan Sisteminde Kemik Kıkırdak Arayüzü Modellemesi, 22. International Symposium on Biomedical Science and Technology”, Ankara
Poster Presentation:”3 Boyutlu Mikroakışkan Sistemlerde Nörodejeneratif Hastalık Modellemesi, 22. International Symposium on Biomedical Science and Technology”, Ankara